Doctoral Dissertation

Study of silk and cellulose materials for bone tissue engineering and environment friendly production of functional cellulose nanofibers

BURGER DENNIS EUGEN

March 2021

Shinshu University

Department of Medicine, Science and Technology

Table of Contents

Abstract

Current methods employed for healing problematic bone fractures strongly rely on the use of autologous bone grafts, whereas bone matrix is harvested from the patient and implanted at the critical bone fracture site. As the harvest itself can lead to chronic pain at the donor site, other materials are investigated for application as bone grafts; this is done in the field of bone tissue engineering. Scaffolds used for bone tissue engineering need to have a variety of features to accommodate bone cells. The scaffold should mimic natural bone, it should have appropriate mechanical strength, support cell differentiation to the osteogenic lineage and offer adequate porosity to allow vascularization and bone in-growth. Silk fibroin is a desirable material for many tissue engineering applications due to its superior moldability and beneficial effect on cells. As silk fibroin is obtained from the silkworm, it has also great possibilities for improvement by genetic engineering of the silkworm. Cellulose is also of interest for tissue engineering application, as the strong mechanical properties and biocompatibility are desirable for use of cellulose as structural bone tissue engineering scaffold component.

In the first part of this dissertation the aim was to develop a new process to fabricate a bone tissue engineering scaffold by creating a porous composite material made of silk fibroin and cellulose. Silk fibroin and cellulose were both dissolved together in *N*,*N*-dimethylacetamide/LiCl and molded to a porous structure using NaCl powder. The hydrogels were prepared by a sequential regeneration process: Cellulose was solidified by water vapor treatment, while remaining silk fibroin in the hydrogel was insolubilized by methanol, which lead to a cellulose framework structure embedded in a silk fibroin matrix. Finally the hydrogels were soaked in water to dissolve the NaCl for making a porous structure. The cellulose composition resulted in improving mechanical properties for the hydrogels in comparison to the silk fibroin control material. The pore size and porosity were estimated at around 350 µm and 70 % respectively. The hydrogels supported differentiation of MC3T3 cells to osteoblasts and are expected to be a good scaffold for bone tissue engineering.

The second part of the dissertation addresses the project of developing basic fibroblast growth factor-binding recombinant silk fibroin by expression with transgenic silkworms, *Bombyx mori*. Basic fibroblast growth factor application leads to enhanced osteoblast adhesion and promotion of angiogenesis, which is vital for malnourished bone defects. In preparation, a transgenic SF L-chain sequence which codes for a basic fibroblast growth factor-binding peptide, called P7, in the C-terminal region was prepared and subsequently introduced into the genome of silkworms via the *piggyBac* Transposon system. This led to 22 % of all expressed SF L-chains to be recombinant. Enhancement of basic fibroblast growth factor binding affinity of recombinant silk fibroin compared to that of the control, non-transgenic silkworm, was also confirmed.

The final part of the dissertation initially aimed at making silk fibroin/cellulose composites for bone tissue engineering via dissolution in $ZnCl_2$ hydrate solution. While this approach was unfortunately difficult due to a lack of an appropriate coprecipitation mechanism, a very small fiber size cellulose was found in the precipitation yielded by the process. From this new finding, the project goal was changed to the development of an energy-saving and straightforward treatment of cellulosic pulp to obtain functional cellulose nanofibers with catalytic activity and flame-retardant properties. For this purpose, dried cellulose pulp was mixed with the recyclable swelling agent, $ZnCl_2$ hydrate, at room temperature. The mild treatment affected the crystal structure through a partial amorphization, yielding a mix of native cellulose I and regenerated cellulose II. This treatment tremendously facilitated the fibrillation into a cellulose nanofiber (CNF) network. In comparison to fibrillated cellulose from non-treated pulp, the $ZnCl_2$-treated counterpart featured higher viscosity, film transparency, better mechanical properties and higher heat stability. Films produced from these nanofibers showed flame-retardant properties without any further modification. The $ZnCl_2$-CNF showed high reactivity in fiber surface acetylation and allowed a fast and efficient reaction while using very mild conditions. The cellulose nanofibers obtained by this process will also be useful for application as structural compound in BTE composite scaffolds.

1. Chapter
General Introduction

1. Chapter - General Introduction

1.1. Background

Bone fractures that do not heal in adequate time are considered as “delayed union”, whereas the healing process is slow, but healing without surgical intervention is still possible. On the other side, for so called “non-unions” healing cannot be expected without the use of surgical means [1]. According to the American Food and Drug Administration FDA, a non-union is established 9 months after trauma with no visible signs of healing for 3 months [2]. When considering non-union rates of all fractures, estimates are around 1.9 %, whereas certain fractures, such as tibia (lower leg) and clavicular (collarbone) fractures in the group of young and middle-aged adults show a risk of 9 % [3]. In a scottish study, non-union incidence was determined at 18.94 in a population of 100 000 per annum [4]. The rate of non-unions varies with different anatomic regions, soft-tissue injuries and fracture fixation principles applied for surgical treatment. Biological reasons for non-unions are severe soft-tissue and bone damage such as infections and large bone defects. Biomechanical reasons are shear stress and instability at the fracture site [1]. Significantly decreased healing was confirmed for fracture gaps larger than 10 mm, compared to fracture gaps smaller than 3 mm [5], whereas other studies already showed a higher risk for delayed or non-union for tibia fracture gaps larger than 3 mm after surgical intervention [6,7]. Risk factors for non-union occurrence are: being male, smoking, a high BMI, diabetes I and II, osteoporosis, osteoarthritis with rheumatoid arthritis, renal insufficiency, vitamin D deficiency, and the use of benzodiazepine, anticoagulants, antibiotics, diuretics, opioids and NSAID painkillers [8].

The applicable methods for restoration of damaged bone depend on the condition of the tissue. Non-unions can be grouped into biologically viable and biologically non-reactive, non-viable non-unions. Biological non-reactivity is typically caused by insufficient vascular supply to fracture or non-union site, absence of healing between non-viable bone fragments while main fragments are viable (necrotic fragments between viable main fragments, comminuted fracture), bone loss by trauma or infection which results in sequester formation and finally atrophic (breakdown involving programmed cell death) non-unions with scar tissue in

former fracture gaps with atrophy and osteoporosis of main fragments close to the fracture site [1].

The “diamond concept” established the mechanical environment and the use of growth factors, mesenchymal stem cells (MSCs) and scaffolds as the four known factors that contribute to bone restoration [9]. Common procedures that supply the mechanical environment for bone restoration are intramedullary locking nails (with nail dynamization and exchange nailing), external fixation techniques and augmentation plating. Intramedullary locking nails were established as standard method for fixation of diaphyseal (long bone shaft) bone fractures, whereas a long nail (metal rod) is inserted into the medullary cavity (hollow area in long bone where bone marrow is located) of the long bone to fixate the fracture site [10]. This method further evolved to nail dynamization, as removal of interlocking screws at later healing stage allows telescopic movement of nail and tubular bone, which accelerates the bone healing process [1,11]. Another method based on intramedullary locking nails is exchange nailing, which comprises exchanging of nails by a nail that is at least 1 mm thicker than the one previously used. This leads to increased stabilization, possibility of locally increased blood supply, which supports the formation of new bone and supply of MSCs originating from bone marrow [12,13]. External fixation devices are located outside the body with screws reaching the bone. External fixation makes use of compression osteosynthesis and/or distraction osteogenesis. The former describes the process of bringing fracture sites in proximity to initiate fracture healing, whereas the later describes the method of applying longitudinal tension to the bone to force elongation by bone growth [14]. Augmentation plating entails the additional use of a plate, which is fixated with screws at the non-union site after failure of intramedullary nailing, whereas the nail remains [15].

Bone grafts address the scaffold aspect of the diamond concept. Currently autologous “Autografts” and allogeneic “Allografts” are used, whereas the former describes bone harvested from the patient and the latter describes bone harvested from a human cadaver. Autografts fulfill all required properties for bone formation, as they are osteogenic (promote synthesis of new bone at recipient site by donor cells), osteoconductive (promote attachment of osteoblastic cells) and osteoinductive (stimulate differentiation of host precursor cells to osteoblasts

for bone formation). Further, autografts have a low cost and have no risk for disease transmission or rejection [16]. Shortcomings of autografts are limited availability and donor site morbidity, such as chronic donor site pain, sensory loss, scarring and wound complications [17]. Allografts are available from many donor sites, but are primarily used as structural scaffold with osteoconductive and decreased osteoinductive potential, because all cells are removed during preparation which also removes the osteogenic ability [16,18]. Other drawbacks include the risks of transfer of viral diseases [19] and local infection due to contamination, with infection rates between 5% and 12.2% [20,21].

Stimulation of bone healing by use of bone morphogenetic proteins (BMPs) as growth factors has been confirmed in many case reports for non-unions of long bones of all extremities with good success rates [22–26]. This also led to clinical application. The FDA approved recombinant human BMP2 for acute tibia fractures in adults as an adjunct to standard care and recombinant human BMP7 was also approved by the FDA for treatment of tibia non-union in cases where autografts failed or were unfeasible [27].

Cell therapy based approaches to bone healing employ cells for healing of bone tissue. When a fracture occurs, the initial phase of bone healing is marked by the onset of inflammation. At this step, factors and cells from the surrounding tissue and bone marrow, in particular endothelial cells, immune cells and MSCs, migrate to the impaired bone region, which finally leads to the homing of osteoprogenitor cells and osteogenesis [28]. Cell therapy based approaches for healing bone non-unions successfully supplied autologous MSCs or osteoprogenitor cells harvested from bone marrow to bone defect sites, after case setup dependent *ex vivo* expansion of cells. The treatment showed performance comparable to autografts, but without any donor site morbidity, and even allowed regeneration of large bone defects [29–32]. Unfortunately no standards for optimum cell application, processing and harvest have been established until now [1].

Simplified, in summary current treatment recommendations for bone non-unions provide augmentation plating for humeral diaphyseal (upper arm, long bone) shaft non-unions, and nail dynamization for femoral and tibial diaphyseal (upper

and lower leg, long bone) shaft non-unions, while biological stimulation by grafts or BMPs is necessary in case of hypertrophic or atrophic (in the process of being degraded or degraded, biologically (almost) non-reactive) non-unions. External fixations are used for segmental defects [1].

As the use of autografts comes with the aforementioned donor site morbidity and allografts carry a high infection risk, alternative scaffold materials for cell homing are researched as part of bone tissue engineering (BTE) research; one such material being silk fibroin (SF) [33,34]. Apart from the already established biocompatibility, SF supports bone growth by down-regulating a suppressor of osteoblastogenesis [35]. Another particular benefit of using SF for BTE is that its surface amide groups interact with MSCs and were shown to induce expression of osteogenic mRNA [36]. Similarly the high β-sheet contents in SF have been shown to favor osteogenic differentiation of MSCs [37]. The β-sheet content varies with the processing method of SF [38,39] and a high content also coincides with an increase in degradation time *in vivo* [40]. Cellulose has also been researched for tissue engineering applications because of the wide availability, the ease of modification and as a structural component for scaffolds due to its favorable mechanical properties [41]. The composition of SF and cellulose allows them to complement each other, as mechanical strength of scaffold materials has been shown to increase with increasing cellulose content [42–44], whereas cell viability and adhesion were improved upon using SF and cellulose together rather than cellulose alone [45].

1.2. Silk

1.2.1. General

Silk from *Bombyx mori*, the domesticated silkworm, is a common fiber material that is composed of the two major proteins silk fibroin and sericin [46]. SF is also a widely known material and currently undergoes much research as a material for tissue engineering. SF consists of 3 parts, which are 6 subunits of disulfide-linked heavy and light chains and a central peptide called fibrohexamerin [47], which joins the other 6 subunits together by hydrophobic interactions [48].

1.2.2. Processing and fabrications

Before any further processing SF is normally degummed (cooked) in a Na_2CO_3 solution in order to remove sericin, which is immunogenic in connection with SF [49]. Then for further molding SF is dissolved, whereas mostly a highly concentrated LiBr solution is used. After dialysis SF is dissolved in water and processed into shape directly or regenerated and dissolved in organic solvents depending on the material properties aimed at [50–52]. Examples of SF before and after processing are shown in Figure 1.1. Silk cocoons as raw material, silk after degumming as “SF Fiber” and SF dissolved in water as “Solution” are shown in Figure 1.1. SF Powder is obtained through milling of degummed SF by chopping and grinding of fibers by a cutter and ball mill or from stirring regenerated SF aqueous solution. Potential applications include the reinforcement of SF materials or the production of resins by high-pressure and high-temperature treatment of SF powder [51,53]. SF films are commonly produced by coating a Petri dish with aqueous SF solution and subsequent drying. As films obtained at this stage are still water soluble and very amorphous, they are subjected to either methanol treatment for induction of β-sheets, leading to a silk II structure or treated with water vapor (water annealing), whereas α-helix and β-sheet content are tailorable [40,54]. SF can also be used to form sponges, which mainly relies on freezing of SF solution, which ultimately leads to a spongy, porous structure. As the pore size can be manipulated by controlling the freezing conditions, SF sponges have been further investigated for tissue engineering applications [55–57]. Another method to obtain porous SF materials works by making SF hydrogels via porogens such as NaCl. For this either an aqueous or HFIP solution of SF is added to an excess of NaCl in a mold. The SF in aqueous solution forms β-sheets and solidifies due to salt-induced precipitation, whereas SF in HFIP solution simply remains as a solid, while the HFIP evaporates; this also necessitates subsequent methanol treatment for induction of β-sheets [58]. Another form of processed SF currently under investigation is electrospun nanofiber SF. These fibers with diameters in the nanometer range are obtained by electrospinning, which relies on the generation of fibers through electric field-elicited attraction of a thread of SF solution from a charged dispenser onto a charged surface. For this method the viscosity of the SF solution can be adjusted

via removable additives to improve the homogeneity of fibers in the resulting nanofiber sheet [59].

Figure 1.1: SF before and after processing into various shapes (kindly provided by Y.Tamada [60])

1.2.3. Applications

The safety of SF for medical applications has been sufficiently investigated, as it has been approved by the FDA for clinical use [61]. For instance SF threads are used as suture material after surgeries [62] and SF is also researched as base material for tissue engineering scaffolds [45,63]. As SF is a very moldable material it allows great freedom in scaffold design. The material can be processed into films, fibers, foams and meshes, which enables the user to suit the scaffold to the target tissue. This in turn elicits favorable cellular responses [34,64]. SF has very appropriate properties for tissue engineering regarding mechanical stability, biological interactions, biocompatibility, tunable degradability and low inflammatory response, which is why it is used for targets such as blood vessels, bones, tendons, ligaments and cartilage tissue [34,38,63].

1.3. Cellulose

1.3.1. General

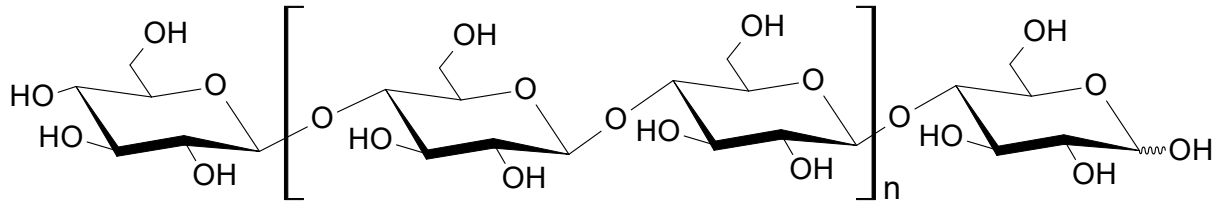

Figure 1.2: Structure of cellulose polymer with non-reducing end to the left and reducing end group to the right.

Cellulose is a widely available, renewable polymer that also naturally occurs in pure form (e.g. cotton fibers), but in most cases appears in combination with lignin and other non-cellulosic polysaccharides, so called hemicelluloses, as they are the main constituents of the cell walls of all wood species. Cellulose is a linear homopolymer consisting of β-1,4 glycosidic linked D-glucopyranose units, as shown in Figure 1.2 [65].

1.3.2. Processing of wood pulp to cellulose

In order to process the wood chip raw material into cellulose pulp, the raw material needs to be delignified. The principal procedure for this is the Kraft pulping process that was used for more than 90 % of worldwide pulp production in 2006 [66]. In the Kraft process the “white liquor”, containing hydroxide and hydrosulfide anions as active chemical agents, is cooked with wood chips for removal of lignin, with subsequent washing and bleaching of the pulp. During cooking in the white liquor the lignin is fragmented into fragments of lower molecular weight that are dissolved in the pulping liquor, resulting in the so called “black liquor”. The degradation of lignin mainly aims at cleavage of lignin ether-bonds and liberation of phenolic groups. During the Kraft pulping process hemicelluloses are also dissolved and chemically modified, as they are deacetylated and glycosidic bonds are cleaved. At a later stage in the process the hemicelluloses reprecipitate on the cellulose fibers resulting in an improvement of their strength properties [67]; therefore the Kraft process is utilized for production of most paper-grade pulps [66]. When aiming for dissolving pulp, which consists of more than 90 % pure cellulose with most hemicelluloses

removed [68], the standard Kraft process is not feasible due to the high amount of remaining hemicelluloses. In order to avoid this issue a pre-hydrolysis prior to cooking in white liquor is used to hydrolyze and solubilize the hemicelluloses in an acidic environment [69].

The main method for production of dissolving pulp is the acid-sulfite process, which is used for approximately 70 % of dissolving pulp production worldwide. This process has a higher pulp yield, higher reactivity and better bleachability compared to prehydrolysis Kraft pulp. During the cooking step the degradation of lignin mainly depends on two reaction types. One is sulfonation, which increases hydrophilicity of lignin and thereby solubility. The other is hydrolysis of lignin-lignin and lignin-carbohydrate bonds. During this process polysaccharides are also hydrolyzed, whereas this reaction favors hemicelluloses over cellulose to a feasible degree [66].

Finally for Kraft and sulfite pulps, after cooking the pulps are washed and subsequently bleached. Bleaching is performed with chlorine based chemicals or oxygen, hydrogen peroxide and ozone as an environmentally friendly alternative. The bleaching process is used for removal of color in pulps, due to residual lignin and other colored impurities [70].

1.3.3. Cellulose Processing

Cellulose is the raw material for the production of rayon or lyocell fibers, which are both produced by wet-spinning, whereas a cellulose solution is extruded into a coagulation bath to yield fibers. Both have wide application in the common textile industry. Rayon fibers are produced as viscose rayon. While viscose rayon uses wood pulp as raw material, the cellulose needs to be chemically modified for dissolution through xanthogenation and reacts back to cellulose during the fiber coagulation step. Lyocell fibers use wood pulp as raw material too, but only require dissolution of cellulose by a mixture of *N*-methylmorpholine-*N*-oxide (NMMO) and water without any chemical modification. The obtained cellulose solution is also extruded in a coagulation bath in order to produce fibers [71]. Cellulose has been processed into other shapes such as films, hydrogels or electrospun nanofibers. In all these cases, the basic mechanism is that cellulose is dissolved, shaped and regenerated in an anti-solvent [72,73] or it is chemically

modified for dissolution and after shaping it is reverted back to non-derivatized cellulose by a chemical reaction [74]. The regeneration of cellulose after dissolution occurs with a change of the allomorph from cellulose I to cellulose II. Cellulose I is the allomorph of native cellulose with a parallel chain arrangement, whereas the chain arrangement in cellulose II is anti-parallel [75,76]. This change can also be elicited through mercerization. In this process swelling of cellulose is caused by treatment with a sodium hydroxide solution, with the conversion to the more stable cellulose II occurring after removal of the base. This is a solid phase process in which the swelling allows the cellulose chains a sufficient degree of mobility for rearrangement to the anti-parallel chain orientation of the cellulose II allomorph [77].

1.3.4. Applications

Cellulose is the basis of the pulp and paper industries, being used for a great variety of applications [78], such as textiles, paper, green plastics [79], or also drug delivery [80]. Cellulose has been researched for tissue engineering applications as well as wound dressings [81–83] and its *in vivo* biodegradability has been confirmed [84]. For some applications, with further research ongoing, nano-structured cellulose is used, which designates cellulosic materials with the size of at least one dimension being in the nanometer range [85]; nanocrystalline and nanofibrillar cellulose being the two most prominent subforms. Commercial uses for nanocellulose include the use as absorbent in diapers and rheology modifier in pen inks (cellulose nanofibrils) [86,87], or as food product by the name “nata de coco” (cellulose of bacterial origin) [88]. The application of cellulose nanofibrils and nanocrystals is also considered for use in composites, whereas the high aspect ratio of nanofibrils [89,90] and the high crystallinity and strength of nanocrystals [91] are both useful for enhancing composite properties. An example for this is the use of nanocellulose together with brittle, silica-based materials for bone tissue engineering, with the nanocellulose component aiding the stability of the material [92]. Cellulose nanofibrils and nanocrystals also exhibit osteoconductive behavior in bone [93] and many methods have been established to form tissue engineering scaffolds with varying elastic modulus, pore size and interconnectivity [94]. Bacterial cellulose is a form of nanocellulose which occurs naturally. It consists of pure cellulose of bacterial origin produced as

nanofiber network, and with its natural, three dimensional structure it has been researched for its favorable characteristics for medical application as well [83]. Another form of such naturally occurring cellulose 3D structures are decellularized cellulose scaffolds of plant-origin, which have been investigated for their tissue engineering performance, since they are easily shapeable and their porous structure can be designed to offer a suitable foothold for cell attachment and vascularization [95].

1.4. Bone Tissue Engineering

1.4.1. General

Tissue engineering deals with the development of treatments for damaged tissue by making use of functional substitutes [64]. Bone tissue engineering (BTE) investigates methods to regenerate bone for clinical application and tissue models. Such grafts can be transplanted to alleviate and heal bone defects and thereby provide another option for current clinical treatments [96]. In general the bone structure is comprised of dense cortical bone and to some extent sponge-like cancellous bone that contains pores filled with bone marrow or fat [96]. The bone structure consists of approximately 20 % organic matter, 10 % water and 65 % inorganic matrix [97]. The organic and inorganic matrix is mainly made up of an elaborate arrangement of collagen I fibers with hydroxyapatite [98]. Bone tissue is renewed and remodeled constantly by formation and resorption, which is performed by osteoblasts (bone forming) and osteoclasts (bone resorbing) [96,99]. For this reason, the recruitment of mesenchymal stem cells (MSCs), which are the progenitors of osteoblasts, their homing and the ability of the surrounding tissue to elicit differentiation to the osteogenic lineage is of great importance for the repair of bone fractures [100]. Osteoblasts express alkaline phosphatase (ALP) which is an important enzyme involved in tissue matrix mineralization, and as they become encapsulated within their own matrix they are referred to as osteocytes [99,101,102]. These in turn produce substances that can modulate the recruitment, differentiation and activity of osteoblasts and osteoclasts upon mechanical stimulation [96]. This makes osteocytes an essential mediator in directing bone remodeling in response to mechanical stimulation [103].

1.4.2. Requirements

In general the scaffold matrices used as tissue substitutes need to fulfill several requirements. These are appropriate mechanical strength that can sustain cell attachment and proliferation and withstands load-bearing, good biocompatibility, biodegradability that matches tissue growth rate and an interconnected porous structure that allows flow of nutrients and waste to maintain cell viability [33,104]. To improve applicability, scaffold features such as molecular structure, embedding of cell signaling factors, surface treatment, mechanical properties and micro/nanometer scale topography are varied to positively influence adhesion, migration, proliferation, differentiation and cell signaling [105–112].

A BTE scaffold in particular should favor cell differentiation to the osteoblastic lineage, which largely depends on the extra cellular matrix (ECM) as regulator of stem cell fate [107,113,114]. Further tasks include guiding bone growth to desired areas and stimulating integration of nascent bone tissue into the surrounding bone matrix [115]. The choice of base material for the scaffold matrix mimicking mechanical and biological characteristics of natural bone matrix therefore presents the key challenge for BTE, which is why many materials have already been tested for BTE application [33,96,116]. Sponge-like scaffolds are favored as the pores have been shown to support cell adhesion, proliferation, migration and nutrient/waste flow. Pores are mostly induced by gas foaming, lyophilization or porogen leaching, whereas size can be adjustable [55,117]. Various authors have reported on the optimum pore size for BTE with different conclusions, some ranging from 96 µm to 400 µm [118–122]. A minimum pore size of 300 µm has been established though as minimum requirement for vascularization and bone ingrowth, which are imperative for success in tissue regeneration [121–123]. In addition to porosity, also stiffness is an important feature, which contributes to more than only mechanical stability. MSCs have been confirmed to show a varying degree of cell adhesion and different differentiation lineages depending on the elasticity of the substrate upon which they were cultured. A differentiation to neuronal lineage has been reported for soft matrices, whereas stiff matrices were shown to be osteogenic [107,124]. Nanoscale matrix surface has also been shown to govern stem cell fate, with disordered surfaces eliciting expression of calcifying proteins, while cells cultured on smooth surfaces failed to do so [106].

Summarized, the requirements are:

- Mechanical strength similar to bone, suitable for load bearing applications.
- Rough nanoscale surface topography, presence of cell signaling factors, appropriate surface functional groups and material stiffness similar to bone, which all influence adhesion, migration, proliferation, differentiation and cell signaling.
- Pores with minimum size of 300 µm for cell migration and nutrient/waste flow which allows vascularization and bone ingrowth.
- Biodegradability to match tissue growth rate.
- Biocompatibility to avoid immune response.

1.4.3. Scaffold Materials

Various materials were investigated for application in BTE. These include metals [125,126], ceramic and silica based materials [127,128] and natural polymers, such as collagen or silk fibroin [96,129]. Many materials on an exclusive polymer basis offer great biocompatibility, but face the drawback of being unable to match the load-bearing requirements of bone tissue. To ameliorate this shortcoming, composite materials are designed that allow the modulation of mechanical properties by controlling the composition [33]. By pursuing this approach many works have been published that successfully elaborate on different material compositions of composites for BTE scaffolds. The investigated materials include but are not limited to compositions of SF, (nano-)cellulose and its derivatives, hydroxyapatite, glass and gelatin [37,45,130–133]. A comparison of advantages and disadvantages of scaffold materials is provided in Figure 1.3.

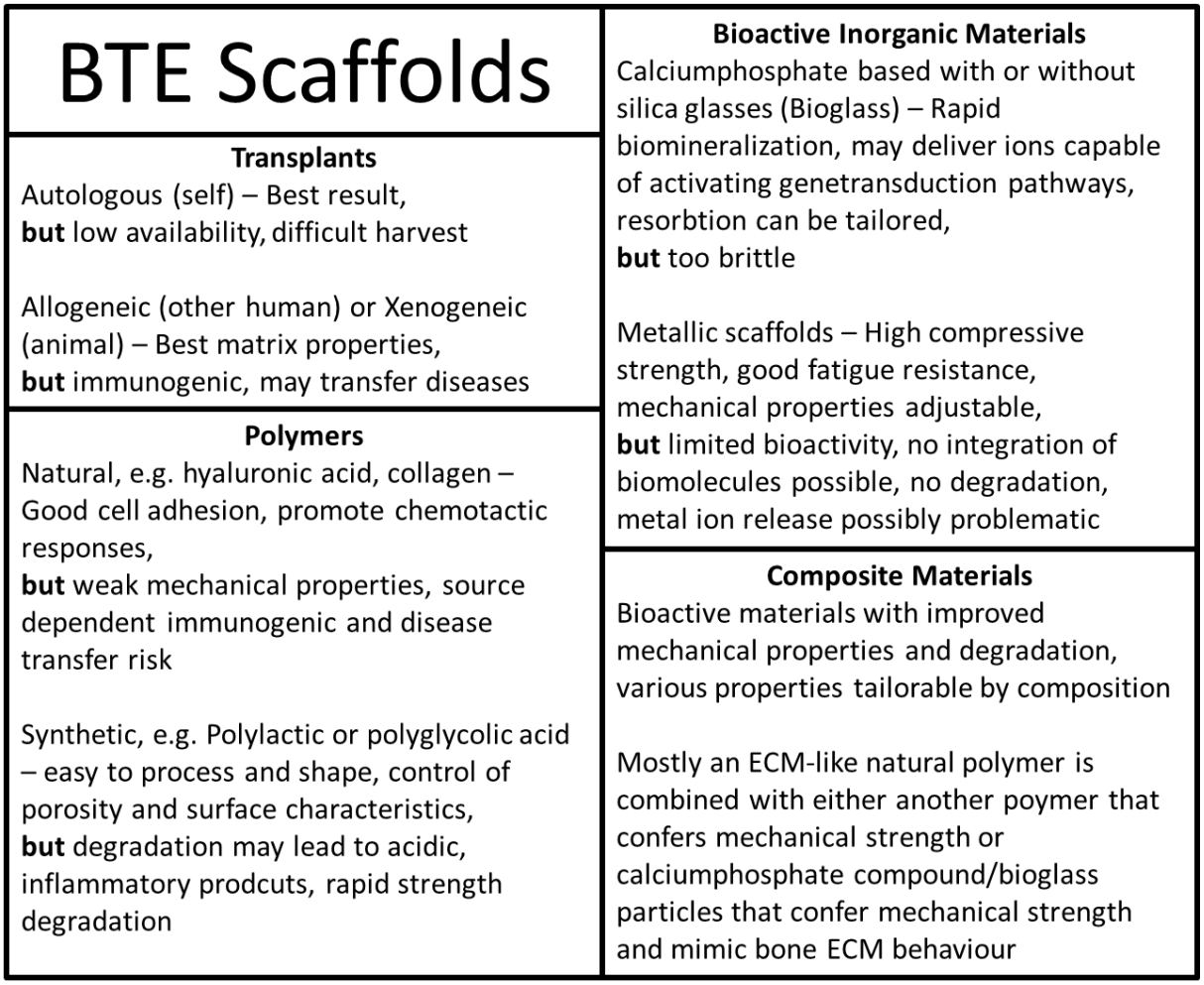

Figure 1.3: General overview of BTE scaffold materials in use, their advantages and drawbacks [33,116,134,135].

1.5. Transgenic Technology

1.5.1. Applications and Tools for Gene Editing

Transgenic animals are made for various reasons, such as models for particular diseases [136] or in order to study specific protein functions [137]. They are also made for economic reasons to aim for disease resistance in cattle [138], improved wool production performance [139,140] and to produce pharmaceuticals like human antibodies [141,142]. The term transgenic designates an animal with an altered genetic content. This is facilitated by introduction, inactivation or modification of a gene [143]. This change is performed in vitro and alters the genome of all cells, which causes the transmittance of this change to the litters after breeding [144]. Many methods

have been established to induce overexpression of a gene by introduction of one or more copies of that gene into the genome. The methods to achieve this include pronuclear microinjection (injection of genetic material into nucleus of fertilized oocyte) [145], embryo infection by retroviral vectors (introduction of genetic material by use of a retrovirus) [146], transfer of chromosome segments [147], sperm-mediated DNA transfer [148] and introduction of genetically modified embryonic stem cells, which leads to chimeras (organism composed of cells of more than one genotype) [149,150]. In addition to pronuclear microinjection that simply relies on random integration events of injected DNA, transposon based methods such as the *piggyBac* system are also used with microinjection [151]. Gene knock-outs and knock-ins depend on the introduction of double strand breaks in the genome that are repaired by the natural mechanisms non-homologous end-joining or homology directed repair respectively. This can be achieved by site-specific nucleases which are designed to target specific loci in the genome. The four nucleases currently employed for this purpose are meganucleases, zinc finger nucleases, transcription activator-like effector nucleases (TALEN) and the (clustered regularly interspaced palindromic repeats) CRISPR/Cas9 system (CRISPR associated 9 nuclease) [136].

1.5.2. *piggyBac* Transposon Method

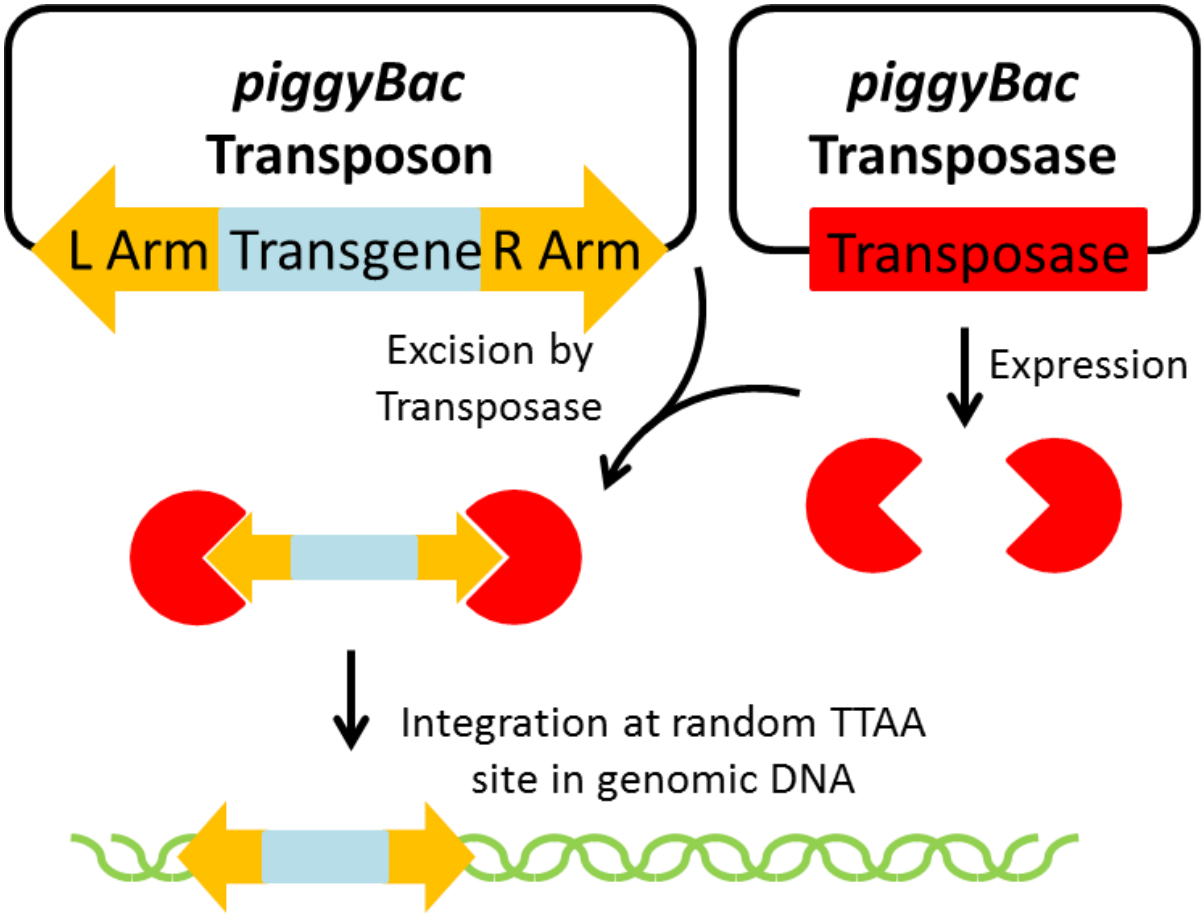

Figure 1.4: *piggyBac* Transposon system. A cell is transfected with a vector carrying the *piggyBac* transposon and another vector coding for the *piggBac* transposase. The transposase (red) is expressed and recognizes the inverted terminal repeat sequences (L arm and R arm, yellow arrow) of the transposon. The transposase transfers the transposon into a random TTAA site in the host genome.

The *piggyBac* transposon was initially discovered in mutant Baculovirus strains [152] and was later determined to work with the *piggyBac* transposase, which facilitates transposition of the *piggyBac* transposon into the genome. The transposase recognizes inverted repeat elements 5' and 3' of the transposon cassette (L arm and R arm in Figure 1.4) and transfers it into a random TTAA site in the genome [153–155]. The *piggyBac* transposon system has been used for establishing transgenic silkworm strains [151] and effectiveness was also shown for gene transfer into human cells [156] and in adult mice *in vivo* [157]. Footprint-free removal of the transposon is also possible, which was made use of by

generation of induced pluripotent stem cells by expression of reprogramming factors facilitated by the *piggyBac* transposon system, with subsequent excision of the transposon cassette by the *piggyBac* transposase [158].

1.5.3. Objective

The overall aim of this project was to develop scaffold materials for bone tissue engineering on a SF material basis. This comprises two approaches: The first one was to make a porous composite material of SF and cellulose, thereby taking advantage of the mechanical strength of cellulose and the cell growth ability of SF. The second approach consisted of making recombinant SF, by making and rearing transgenic silkworms. The recombinant SF was designed to contain a basic fibroblast growth factor (bFGF) specific binding sequence that allows the loading of the SF material with bFGF for a timed release.

The third approach was to develop another solvent system to fabricate SF/cellulose composites in order to achieve a safer and simpler process. A $ZnCl_2$ based solvent was investigated for dissolving SF and cellulose. However, this method was found not to be adequate for making composites because of a lack of a suitable coprecipitation mechanism. But very fine and small fibers appeared during the precipitation of cellulose, so the objective of the third approach was changed to the development of a cellulose nanofiber fabrication technology, thereby contributing to the BTE applicability of cellulose nanofibrils as explained in chapter 1.3.4. In this project the treatment of cellulose pulp with $ZnCl_2$ for energy-saving production of cellulose nanofibers was investigated. The scope of the project was expanded by elaborating on the catalytic and flame retardant functionalization introducible by $ZnCl_2$ application. When used to supplement SF scaffolds for BTE, the cellulose nanofibers obtained by our new process will be useful for improving the mechanical properties.

1.6. References

1. Rupp, M.; Biehl, C.; Budak, M.; Thormann, U.; Heiss, C.; Alt, V. Diaphyseal long bone nonunions - types, aetiology, economics, and treatment recommendations. Int. Orthop. 2018, 42, 247–258, doi:10.1007/s00264-017-3734-5.

2. Frölke, J.P.M.; Patka, P. Definition and classification of fracture non-unions. Injury 2007, 38, S19-S22, doi:10.1016/s0020-1383(07)80005-2.

3. Mills, L.A.; Aitken, S.A.; Simpson, A.H.R.W. The risk of non-union per fracture: current myths and revised figures from a population of over 4 million adults. Acta Orthop. 2017, 88, 434–439, doi:10.1080/17453674.2017.1321351.

4. Mills, L.A.; Simpson, A.H.R.W. The relative incidence of fracture non-union in the Scottish population (5.17 million): a 5-year epidemiological study. BMJ Open 2013, 3, doi:10.1136/bmjopen-2012-002276.

5. Claes, L.; Grass, R.; Schmickal, T.; Kisse, B.; Eggers, C.; Gerngross, H.; Mutschler, W.; Arand, M.; Wintermeyer, T.; Wentzensen, A. Monitoring and healing analysis of 100 tibial shaft fractures. Langenbecks. Arch. Surg. 2002, 387, 146–152, doi:10.1007/s00423-002-0306-x.

6. Drosos, G.I.; Bishay, M.; Karnezis, I.A.; Alegakis, A.K. Factors affecting fracture healing after intramedullary nailing of the tibial diaphysis for closed and grade I open fractures. J. Bone Joint Surg. Br. 2006, 88, 227–231, doi:10.1302/0301-620X.88B2.16456.

7. Gaebler, C.; Berger, U.; Schandelmaier, P.; Greitbauer, M.; Schauwecker, H.H.; Applegate, B.; Zych, G.; Vécsei, V. Rates and odds ratios for complications in closed and open tibial fractures treated with unreamed, small diameter tibial nails: a multicenter analysis of 467 cases. J. Orthop. Trauma 2001, 15, 415–423, doi:10.1097/00005131-200108000-00006.

8. Zura, R.; Xiong, Z.; Einhorn, T.; Watson, J.T.; Ostrum, R.F.; Prayson, M.J.; Della Rocca, G.J.; Mehta, S.; McKinley, T.; Wang, Z.; et al. Epidemiology of Fracture Nonunion in 18 Human Bones. JAMA Surg. 2016, 151, e162775, doi:10.1001/jamasurg.2016.2775.

9. Giannoudis, P.V.; Einhorn, T.A.; Marsh, D. Fracture healing: The diamond concept. Injury 2007, 38, S3-S6, doi:10.1016/s0020-1383(08)70003-2.

10. Rudloff, M.I.; Smith, W.R. Intramedullary nailing of the femur: current concepts concerning reaming. J. Orthop. Trauma 2009, 23, S12-7, doi:10.1097/BOT.0b013e31819f258a.

11. Claes, L. Dynamisierung der Osteosynthese : Zeitpunkt und Methoden. Unfallchirurg 2018, 121, 3–9, doi:10.1007/s00113-017-0455-6.

12. Brinker, M.R.; O'Connor, D.P. Exchange nailing of ununited fractures. J. Bone Joint Surg. Am. 2007, 89, 177–188, doi:10.2106/JBJS.F.00742.

13. Wenisch, S.; Trinkaus, K.; Hild, A.; Hose, D.; Herde, K.; Heiss, C.; Kilian, O.; Alt, V.; Schnettler, R. Human reaming debris: a source of multipotent stem cells. Bone 2005, 36, 74–83, doi:10.1016/j.bone.2004.09.019.

14. Harshwal, R.K.; Sankhala, S.S.; Jalan, D. Management of nonunion of lower-extremity long bones using mono-lateral external fixator--report of 37 cases. Injury 2014, 45, 560–567, doi:10.1016/j.injury.2013.11.019.

15. Park, J.; Yang, K.H. Indications and outcomes of augmentation plating with decortication and autogenous bone grafting for femoral shaft nonunions. Injury 2013, 44, 1820–1825, doi:10.1016/j.injury.2013.02.021.

16. Sen, M.K.; Miclau, T. Autologous iliac crest bone graft: should it still be the gold standard for treating nonunions? Injury 2007, 38 Suppl 1, S75-80, doi:10.1016/j.injury.2007.02.012.

17. DiGiovanni, C.W.; Petricek, J.M. The evolution of rhPDGF-BB in musculoskeletal repair and its role in foot and ankle fusion surgery. Foot Ankle Clin. 2010, 15, 621–640, doi:10.1016/j.fcl.2010.07.001.

18. Emara, K.M.; Diab, R.A.; Emara, A.K. Recent biological trends in management of fracture non-union. World J. Orthop. 2015, 6, 623–628, doi:10.5312/wjo.v6.i8.623.

19. Tomford, W.W. Bone allografts: past, present and future. Cell Tissue Bank. 2000, 1, 105–109, doi:10.1023/A:1010158731885.

20. Sutherland, A.G.; Raafat, A.; Yates, P.; Hutchison, J.D. Infection associated with the use of allograft bone from the North East Scotland Bone Bank. Journal of Hospital Infection 1997, 35, 215–222, doi:10.1016/S0195-6701(97)90209-7.

21. Liu, J.W.; Chao, L.H.; Su, L.H.; Wang, J.W.; Wang, C.J. Experience with a bone bank operation and allograft bone infection in recipients at a medical centre in southern Taiwan. J. Hosp. Infect. 2002, 50, 293–297, doi:10.1053/jhin.2002.1192.

22. Singh, R.; Bleibleh, S.; Kanakaris, N.K.; Giannoudis, P.V. Upper limb non-unions treated with BMP-7: efficacy and clinical results. Injury 2016, 47, S33-S39, doi:10.1016/S0020-1383(16)30837-3.

23. Pneumaticos, S.G.; Panteli, M.; Triantafyllopoulos, G.K.; Papakostidis, C.; Giannoudis, P.V. Management and outcome of diaphyseal aseptic non-unions of the lower limb: a systematic review. Surgeon 2014, 12, 166–175, doi:10.1016/j.surge.2013.10.007.

24. Alt, V.; Meyer, C.; Litzlbauer, H.D.; Schnettler, R. Treatment of a double nonunion of the femur by rhBMP-2. J. Orthop. Trauma 2007, 21, 734–737, doi:10.1097/BOT.0b013e3181589700.

25. Garrison, K.R.; Shemilt, I.; Donell, S.; Ryder, J.J.; Mugford, M.; Harvey, I.; Song, F.; Alt, V. Bone morphogenetic protein (BMP) for fracture healing in adults. Cochrane Database Syst. Rev. 2010, CD006950, doi:10.1002/14651858.CD006950.pub2.

26. Miska, M.; Findeisen, S.; Tanner, M.; Biglari, B.; Studier-Fischer, S.; Grützner, P.A.; Schmidmaier, G.; Moghaddam, A. Treatment of nonunions in fractures of the humeral shaft according to the Diamond Concept. Bone Joint J. 2016, 98-B, 81–87, doi:10.1302/0301-620X.98B1.35682.

27. Roberts, T.T.; Rosenbaum, A.J. Bone grafts, bone substitutes and orthobiologics: the bridge between basic science and clinical advancements in fracture healing. Organogenesis 2012, 8, 114–124, doi:10.4161/org.23306.

28. Schell, H.; Duda, G.N.; Peters, A.; Tsitsilonis, S.; Johnson, K.A.; Schmidt-Bleek, K. The haematoma and its role in bone healing. J. Exp. Orthop. 2017, 4, 5, doi:10.1186/s40634-017-0079-3.

29. Bruder, S.P.; Kurth, A.A.; Shea, M.; Hayes, W.C.; Jaiswal, N.; Kadiyala, S. Bone regeneration by implantation of purified, culture-expanded human mesenchymal stem cells. J. Orthop. Res. 1998, 16, 155–162, doi:10.1002/jor.1100160202.

30. CONNOLLY, J.F.; GUSE, R.O.; TIEDEMAN, J.; DEHNE, R. Autologous Marrow Injection as a Substitute for Operative Grafting of Tibial Nonunions. Clinical Orthopaedics and Related Research 1991, &NA;, 259???270, doi:10.1097/00003086-199105000-00038.

31. Hernigou, P.; Poignard, A.; Beaujean, F.; Rouard, H. Percutaneous autologous bone-marrow grafting for nonunions. Influence of the number and concentration of progenitor cells. J. Bone Joint Surg. Am. 2005, 87, 1430–1437, doi:10.2106/JBJS.D.02215.

32. Quarto, R.; Mastrogiacomo, M.; Cancedda, R.; Kutepov, S.M.; Mukhachev, V.; Lavroukov, A.; Kon, E.; Marcacci, M. Repair of large bone defects with the use of autologous bone marrow stromal cells. N. Engl. J. Med. 2001, 344, 385–386, doi:10.1056/NEJM200102013440516.

33. Wu, S.; Liu, X.; Yeung, K.W.; Liu, C.; Yang, X. Biomimetic porous scaffolds for bone tissue engineering. Materials Science and Engineering: R: Reports 2014, 80, 1–36, doi:10.1016/j.mser.2014.04.001.

34. Altman, G.H.; Diaz, F.; Jakuba, C.; Calabro, T.; Horan, R.L.; Chen, J.; Lu, H.; Richmond, J.; Kaplan, D.L. Silk-based biomaterials. Biomaterials 2003, 24, 401–416, doi:10.1016/S0142-9612(02)00353-8.

35. Jung, S.-R.; Song, N.-J.; Yang, D.K.; Cho, Y.-J.; Kim, B.-J.; Hong, J.-W.; Yun, U.J.; Jo, D.-G.; Lee, Y.M.; Choi, S.Y.; et al. Silk proteins stimulate osteoblast differentiation by suppressing the Notch signaling pathway in mesenchymal stem cells. Nutr. Res. 2013, 33, 162–170, doi:10.1016/j.nutres.2012.11.006.

36. Curran, J.M.; Chen, R.; Hunt, J.A. Controlling the phenotype and function of mesenchymal stem cells in vitro by adhesion to silane-modified clean glass surfaces. Biomaterials 2005, 26, 7057–7067, doi:10.1016/j.biomaterials.2005.05.008.

37. Das, S.; Pati, F.; Choi, Y.-J.; Rijal, G.; Shim, J.-H.; Kim, S.W.; Ray, A.R.; Cho, D.-W.; Ghosh, S. Bioprintable, cell-laden silk fibroin-gelatin hydrogel supporting multilineage differentiation of stem cells for fabrication of three-dimensional tissue constructs. Acta Biomater. 2015, 11, 233–246, doi:10.1016/j.actbio.2014.09.023.

38. You, R.; Xu, Y.; Liu, G.; Liu, Y.; Li, X.; Li, M. Regulating the degradation rate of silk fibroin films through changing the genipin crosslinking degree. Polymer Degradation and Stability 2014, 109, 226–232, doi:10.1016/j.polymdegradstab.2014.07.029.

39. Wang, Y.; Rudym, D.D.; Walsh, A.; Abrahamsen, L.; Kim, H.-J.; Kim, H.S.; Kirker-Head, C.; Kaplan, D.L. In vivo degradation of three-dimensional silk fibroin scaffolds. Biomaterials 2008, 29, 3415–3428, doi:10.1016/j.biomaterials.2008.05.002.

40. Jin, H.-J.; Park, J.; Karageorgiou, V.; Kim, U.-J.; Valluzzi, R.; Cebe, P.; Kaplan, D.L. Water-Stable Silk Films with Reduced β-Sheet Content. Adv. Funct. Mater. 2005, 15, 1241–1247, doi:10.1002/adfm.200400405.

41. Courtenay, J.C.; Sharma, R.I.; Scott, J.L. Recent Advances in Modified Cellulose for Tissue Culture Applications. Molecules 2018, 23, doi:10.3390/molecules23030654.

42. Zhou, L.; Wang, Q.; Wen, J.; Chen, X.; Shao, Z. Preparation and characterization of transparent silk fibroin/cellulose blend films. Polymer 2013, 54, 5035–5042, doi:10.1016/j.polymer.2013.07.002.

43. Singh, N.; Rahatekar, S.S.; Koziol, K.K.K.; Ng, T.S.; Patil, A.J.; Mann, S.; Hollander, A.P.; Kafienah, W. Directing chondrogenesis of stem cells with specific blends of cellulose and silk. Biomacromolecules 2013, 14, 1287–1298, doi:10.1021/bm301762p.

44. Freddi, G.; Romanò, M.; Massafra, M.R.; Tsukada, M. Silk fibroin/cellulose blend films: Preparation, structure, and physical properties. J. Appl. Polym. Sci. 1995, 56, 1537–1545, doi:10.1002/app.1995.070561203.

45. Oliveira Barud, H.G.; Da Barud, H.S.; Cavicchioli, M.; do Amaral, T.S.; Oliveira Junior, O.B. de; Santos, D.M.; Petersen, A.L.d.O.A.; Celes, F.; Borges, V.M.; Oliveira, C.I. de; et al. Preparation and characterization of a bacterial cellulose/silk fibroin sponge scaffold for tissue regeneration. Carbohydr. Polym. 2015, 128, 41–51, doi:10.1016/j.carbpol.2015.04.007.

46. Sutherland, T.D.; Young, J.H.; Weisman, S.; Hayashi, C.Y.; Merritt, D.J. Insect silk: one name, many materials. Annu. Rev. Entomol. 2010, 55, 171–188, doi:10.1146/annurev-ento-112408-085401.

47. Inoue, S.; Tanaka, K.; Arisaka, F.; Kimura, S.; Ohtomo, K.; Mizuno, S. Silk fibroin of Bombyx mori is secreted, assembling a high molecular mass elementary unit consisting of H-chain, L-chain, and P25, with a 6:6:1 molar ratio. J. Biol. Chem. 2000, 275, 40517–40528, doi:10.1074/jbc.M006897200.

48. Tanaka, K.; Inoue, S.; Mizuno, S. Hydrophobic interaction of P25, containing Asn-linked oligosaccharide chains, with the H-L complex of silk fibroin produced by Bombyx mori. Insect Biochemistry and Molecular Biology 1999, 29, 269–276, doi:10.1016/S0965-1748(98)00135-0.

49. Aramwit, P.; Kanokpanont, S.; De-Eknamkul, W.; Srichana, T. Monitoring of inflammatory mediators induced by silk sericin. J. Biosci. Bioeng. 2009, 107, 556–561, doi:10.1016/j.jbiosc.2008.12.012.

50. Marsano, E.; Canetti, M.; Conio, G.; Corsini, P.; Freddi, G. Fibers based on cellulose–silk fibroin blend. J. Appl. Polym. Sci. 2007, 104, 2187–2196, doi:10.1002/app.24856.

51. Gil, E.S.; Kluge, J.A.; Rockwood, D.N.; Rajkhowa, R.; Wang, L.; Wang, X.; Kaplan, D.L. Mechanical improvements to reinforced porous silk scaffolds. J. Biomed. Mater. Res. A 2011, 99, 16–28, doi:10.1002/jbm.a.33158.

52. Ak, F.; Oztoprak, Z.; Karakutuk, I.; Okay, O. Macroporous silk fibroin cryogels. Biomacromolecules 2013, 14, 719–727, doi:10.1021/bm3018033.

53. Anh Tuan, H.; Hirai, S.; Inoue, S.; A H Mohammed, A.; Akioka, S.; Ngo Trinh, T. Fabrication of Silk Resin with High Bending Properties by Hot-Pressing and Subsequent Hot-Rolling. Materials (Basel) 2020, 13, doi:10.3390/ma13122716.

54. Hu, X.; Shmelev, K.; Sun, L.; Gil, E.-S.; Park, S.-H.; Cebe, P.; Kaplan, D.L. Regulation of silk material structure by temperature-controlled water vapor annealing. Biomacromolecules 2011, 12, 1686–1696, doi:10.1021/bm200062a.

55. Tamada, Y. New process to form a silk fibroin porous 3-D structure. Biomacromolecules 2005, 6, 3100–3106, doi:10.1021/bm050431f.

56. Rnjak-Kovacina, J.; Wray, L.S.; Burke, K.A.; Torregrosa, T.; Golinski, J.M.; Huang, W.; Kaplan, D.L. Lyophilized Silk Sponges: A Versatile Biomaterial Platform for Soft Tissue Engineering. ACS Biomater. Sci. Eng. 2015, 1, 260–270, doi:10.1021/ab500149p.

57. Wray, L.S.; Rnjak-Kovacina, J.; Mandal, B.B.; Schmidt, D.F.; Gil, E.S.; Kaplan, D.L. A silk-based scaffold platform with tunable architecture for engineering critically-sized tissue constructs. Biomaterials 2012, 33, 9214–9224, doi:10.1016/j.biomaterials.2012.09.017.

58. Kim, U.-J.; Park, J.; Kim, H.J.; Wada, M.; Kaplan, D.L. Three-dimensional aqueous-derived biomaterial scaffolds from silk fibroin. Biomaterials 2005, 26, 2775–2785, doi:10.1016/j.biomaterials.2004.07.044.

59. Wharram, S.E.; Zhang, X.; Kaplan, D.L.; McCarthy, S.P. Electrospun silk material systems for wound healing. Macromol. Biosci. 2010, 10, 246–257, doi:10.1002/mabi.200900274.

60. Y.Tamada. シルクの新しい展開 [繊維トレンド], 2016, 121 (11&12 月).

61. Cao, Y.; Wang, B. Biodegradation of silk biomaterials. Int. J. Mol. Sci. 2009, 10, 1514–1524, doi:10.3390/ijms10041514.

62. Koh, L.-D.; Cheng, Y.; Teng, C.-P.; Khin, Y.-W.; Loh, X.-J.; Tee, S.-Y.; Low, M.; Ye, E.; Yu, H.-D.; Zhang, Y.-W.; et al. Structures, mechanical properties and

applications of silk fibroin materials. Progress in Polymer Science 2015, 46, 86–110, doi:10.1016/j.progpolymsci.2015.02.001.

63. Thurber, A.E.; Omenetto, F.G.; Kaplan, D.L. In vivo bioresponses to silk proteins. Biomaterials 2015, 71, 145–157, doi:10.1016/j.biomaterials.2015.08.039.

64. Langer, R.; Vacanti, J.P. Tissue engineering. Science 1993, 260, 920–926, doi:10.1126/science.8493529.

65. Koch, G. Raw Material for Pulp. In Handbook of Pulp; Sixta, H., Ed.; Wiley-VCH Verlag GmbH: Weinheim, Germany, 2006; pp 21–68, ISBN 9783527619887.

66. Chemical Pulping Processe: Sections 4.2.8–4.3.6.5. In Handbook of Pulp; Sixta, H., Ed.; Wiley-VCH Verlag GmbH: Weinheim, Germany, 2006; pp 366–509, ISBN 9783527619887.

67. Sixta, H.; Potthast, A.; Krotschek, A.W. Chemical Pulping Processe: Sections 4.1–4.2.5. In Handbook of Pulp; Sixta, H., Ed.; Wiley-VCH Verlag GmbH: Weinheim, Germany, 2006; pp 109–229, ISBN 9783527619887.

68. Sixta, H. Introduction. In Handbook of Pulp; Sixta, H., Ed.; Wiley-VCH Verlag GmbH: Weinheim, Germany, 2006; pp 2–19, ISBN 9783527619887.

69. Chemical Pulping Processe: Sections 4.2.6–4.2.7. In Handbook of Pulp; Sixta, H., Ed.; Wiley-VCH Verlag GmbH: Weinheim, Germany, 2006; pp 229–365, ISBN 9783527619887.

70. Sixta, H.; Sss, H.-U.; Potthast, A.; Schwanninger, M.; Krotscheck, A.W. Pulp Bleaching: Sections 7.1–7.3.5. In Handbook of Pulp; Sixta, H., Ed.; Wiley-VCH Verlag GmbH: Weinheim, Germany, 2006; pp 609–708, ISBN 9783527619887.

71. Ozipek, B.; Karakas, H. Wet spinning of synthetic polymer fibers. Advances in Filament Yarn Spinning of Textiles and Polymers; Elsevier, 2014; pp 174–186, ISBN 9780857094995.

72. Johns, M.A.; Bae, Y.; Guimarães, F.E.G.; Lanzoni, E.M.; Costa, C.A.R.; Murray, P.M.; Deneke, C.; Galembeck, F.; Scott, J.L.; Sharma, R.I. Predicting

Ligand-Free Cell Attachment on Next-Generation Cellulose-Chitosan Hydrogels. ACS Omega 2018, 3, 937–945, doi:10.1021/acsomega.7b01583.

73. Chang, C.; Zhang, L. Cellulose-based hydrogels: Present status and application prospects. Carbohydr. Polym. 2011, 84, 40–53, doi:10.1016/j.carbpol.2010.12.023.

74. MA, Z.; RAMAKRISHNA, S. Electrospun regenerated cellulose nanofiber affinity membrane functionalized with protein A/G for IgG purification. Journal of Membrane Science 2008, 319, 23–28, doi:10.1016/j.memsci.2008.03.045.

75. Kim, N.-H.; Imai, T.; Wada, M.; Sugiyama, J. Molecular directionality in cellulose polymorphs. Biomacromolecules 2006, 7, 274–280, doi:10.1021/bm0506391.

76. Chavan RB. Development and processing of lyocell. Indian J Fibre Text Res 2004, 483–492.

77. Yue, Y.; Zhou, C.; French, A.D.; Xia, G.; Han, G.; Wang, Q.; Wu, Q. Comparative properties of cellulose nano-crystals from native and mercerized cotton fibers. Cellulose 2012, 19, 1173–1187, doi:10.1007/s10570-012-9714-4.

78. French, A.D.; Pérez, S.; Bulone, V.; Rosenau, T.; Gray, D. Encyclopedia of Polymer Science. Cellulose, 2018.

79. Song, N.; Hou, X.; Li Chen; Cui, S.; Shi, L.; Ding, P. A Green Plastic Constructed from Cellulose and Functionalized Graphene with High Thermal Conductivity. ACS Appl. Mater. Interfaces 2017, 9, 17914–17922, doi:10.1021/acsami.7b02675.

80. Valo, H.; Arola, S.; Laaksonen, P.; Torkkeli, M.; Peltonen, L.; Linder, M.B.; Serimaa, R.; Kuga, S.; Hirvonen, J.; Laaksonen, T. Drug release from nanoparticles embedded in four different nanofibrillar cellulose aerogels. Eur. J. Pharm. Sci. 2013, 50, 69–77, doi:10.1016/j.ejps.2013.02.023.

81. Hickey, R.J.; Pelling, A.E. Cellulose Biomaterials for Tissue Engineering. Front. Bioeng. Biotechnol. 2019, 7, 45, doi:10.3389/fbioe.2019.00045.

82. Sulaeva, I.; Hettegger, H.; Bergen, A.; Rohrer, C.; Kostic, M.; Konnerth, J.; Rosenau, T.; Potthast, A. Fabrication of bacterial cellulose-based wound dressings with improved performance by impregnation with alginate. Mater. Sci. Eng. C Mater. Biol. Appl. 2020, 110, 110619, doi:10.1016/j.msec.2019.110619.

83. Sulaeva, I.; Henniges, U.; Rosenau, T.; Potthast, A. Bacterial cellulose as a material for wound treatment: Properties and modifications. A review. Biotechnol. Adv. 2015, 33, 1547–1571, doi:10.1016/j.biotechadv.2015.07.009.

84. Märtson, M.; Viljanto, J.; Hurme, T.; Laippala, P.; Saukko, P. Is cellulose sponge degradable or stable as implantation material? An in vivo subcutaneous study in the rat. Biomaterials 1999, 20, 1989–1995, doi:10.1016/S0142-9612(99)00094-0.

85. Abdul Khalil, H.P.S.; Davoudpour, Y.; Islam, M.N.; Mustapha, A.; Sudesh, K.; Dungani, R.; Jawaid, M. Production and modification of nanofibrillated cellulose using various mechanical processes: a review. Carbohydr. Polym. 2014, 99, 649–665, doi:10.1016/j.carbpol.2013.08.069.

86. Nagasawa T. The Promise of Cellulose Nanofibers. http://www.nippon.com/en/genre/economy/l00151/ (accessed on 16 December 2020).

87. Nagata K. Japan pins tech hopes on game-changing nanofiber. http://www.japantimes.co.jp/news/2016/04/11/business/tech/japan-pins-tech-hopes-game-changing-nanofiber/ (accessed on 16 December 2020).

88. Chinte-Sanchez, P. Philippine fermented foods. Principles and technology; University of the Philippines Press: Quezon City, op. 2008, ISBN 9789715425544.

89. Eichhorn, S.J.; Dufresne, A.; Aranguren, M.; Marcovich, N.E.; Capadona, J.R.; Rowan, S.J.; Weder, C.; Thielemans, W.; Roman, M.; Renneckar, S.; et al. Review: current international research into cellulose nanofibres and nanocomposites. J Mater Sci 2010, 45, 1–33, doi:10.1007/s10853-009-3874-0.

90. an Nakagaito; Kondo, H.; Takagi, H. Cellulose nanofiber aerogel production and applications. Journal of Reinforced Plastics and Composites 2013, 32, 1547–1552, doi:10.1177/0731684413494110.

91. Habibi, Y.; Lucia, L.A.; Rojas, O.J. Cellulose nanocrystals: chemistry, self-assembly, and applications. Chem. Rev. 2010, 110, 3479–3500, doi:10.1021/cr900339w.

92. Ferreira, F.V.; Souza, L.P.; Martins, T.M.M.; Lopes, J.H.; Mattos, B.D.; Mariano, M.; Pinheiro, I.F.; Valverde, T.M.; Livi, S.; Camilli, J.A.; et al. Nanocellulose/bioactive glass cryogels as scaffolds for bone regeneration. Nanoscale 2019, 11, 19842–19849, doi:10.1039/C9NR05383B.

93. Osorio, D.A.; Lee, B.E.J.; Kwiecien, J.M.; Wang, X.; Shahid, I.; Hurley, A.L.; Cranston, E.D.; Grandfield, K. Cross-linked cellulose nanocrystal aerogels as viable bone tissue scaffolds. Acta Biomater. 2019, 87, 152–165, doi:10.1016/j.actbio.2019.01.049.

94. Ferreira, F.V.; Otoni, C.G.; France, K.J. de; Barud, H.S.; Lona, L.M.; Cranston, E.D.; Rojas, O.J. Porous nanocellulose gels and foams: Breakthrough status in the development of scaffolds for tissue engineering. Materials Today 2020, 37, 126–141, doi:10.1016/j.mattod.2020.03.003.

95. Hickey, R.J.; Modulevsky, D.J.; Cuerrier, C.M.; Pelling, A.E. Customizing the Shape and Microenvironment Biochemistry of Biocompatible Macroscopic Plant-Derived Cellulose Scaffolds. ACS Biomater. Sci. Eng. 2018, 4, 3726–3736, doi:10.1021/acsbiomaterials.8b00178.

96. Melke, J.; Midha, S.; Ghosh, S.; Ito, K.; Hofmann, S. Silk fibroin as biomaterial for bone tissue engineering. Acta Biomater. 2016, 31, 1–16, doi:10.1016/j.actbio.2015.09.005.

97. Buckwalter, J.A.; Glimcher, M.J.; Cooper, R.R.; Recker, R. Bone biology. I: Structure, blood supply, cells, matrix, and mineralization. Instr. Course Lect. 1996, 45, 371–386.

98. Fratzl, P.; Gupta, H.S.; Paschalis, E.P.; Roschger, P. Structure and mechanical quality of the collagen–mineral nano-composite in bone. J. Mater. Chem. 2004, 14, 2115–2123, doi:10.1039/B402005G.

99. Robling, A.G.; Castillo, A.B.; Turner, C.H. Biomechanical and molecular regulation of bone remodeling. Annu. Rev. Biomed. Eng. 2006, 8, 455–498, doi:10.1146/annurev.bioeng.8.061505.095721.

100. Wang, X.; Wang, Y.; Gou, W.; Lu, Q.; Peng, J.; Lu, S. Role of mesenchymal stem cells in bone regeneration and fracture repair: a review. Int. Orthop. 2013, 37, 2491–2498, doi:10.1007/s00264-013-2059-2.

101. Franz-Odendaal, T.A.; Hall, B.K.; Witten, P.E. Buried alive: how osteoblasts become osteocytes. Dev. Dyn. 2006, 235, 176–190, doi:10.1002/dvdy.20603.

102. Dallas, S.L.; Bonewald, L.F. Dynamics of the transition from osteoblast to osteocyte. Ann. N. Y. Acad. Sci. 2010, 1192, 437–443, doi:10.1111/j.1749-6632.2009.05246.x.

103. Klein-Nulend, J.; Bacabac, R.G.; Bakker, A.D. Mechanical loading and how it affects bone cells: the role of the osteocyte cytoskeleton in maintaining our skeleton. Eur. Cell. Mater. 2012, 24, 278–291, doi:10.22203/ecm.v024a20.

104. Leong, K.F.; Cheah, C.M.; Chua, C.K. Solid freeform fabrication of three-dimensional scaffolds for engineering replacement tissues and organs. Biomaterials 2003, 24, 2363–2378, doi:10.1016/S0142-9612(03)00030-9.

105. Amin Yavari, S.; van der Stok, J.; Chai, Y.C.; Wauthle, R.; Tahmasebi Birgani, Z.; Habibovic, P.; Mulier, M.; Schrooten, J.; Weinans, H.; Zadpoor, A.A. Bone regeneration performance of surface-treated porous titanium. Biomaterials 2014, 35, 6172–6181, doi:10.1016/j.biomaterials.2014.04.054.

106. Dalby, M.J.; Gadegaard, N.; Tare, R.; Andar, A.; Riehle, M.O.; Herzyk, P.; Wilkinson, C.D.W.; Oreffo, R.O.C. The control of human mesenchymal cell differentiation using nanoscale symmetry and disorder. Nat. Mater. 2007, 6, 997–1003, doi:10.1038/nmat2013.

107. Engler, A.J.; Sen, S.; Sweeney, H.L.; Discher, D.E. Matrix elasticity directs stem cell lineage specification. Cell 2006, 126, 677–689, doi:10.1016/j.cell.2006.06.044.

108. Ghibaudo, M.; Saez, A.; Trichet, L.; Xayaphoummine, A.; Browaeys, J.; Silberzan, P.; Buguin, A.; Ladoux, B. Traction forces and rigidity sensing regulate cell functions. Soft Matter 2008, 4, 1836, doi:10.1039/b804103b.

109. Liu, L.; Ratner, B.D.; Sage, E.H.; Jiang, S. Endothelial cell migration on surface-density gradients of fibronectin, VEGF, or both proteins. Langmuir 2007, 23, 11168–11173, doi:10.1021/la701435x.

110. McMurray, R.J.; Wann, A.K.T.; Thompson, C.L.; Connelly, J.T.; Knight, M.M. Surface topography regulates wnt signaling through control of primary cilia structure in mesenchymal stem cells. Sci. Rep. 2013, 3, 3545, doi:10.1038/srep03545.

111. Unadkat, H.V.; Hulsman, M.; Cornelissen, K.; Papenburg, B.J.; Truckenmüller, R.K.; Carpenter, A.E.; Wessling, M.; Post, G.F.; Uetz, M.; Reinders, M.J.T.; et al. An algorithm-based topographical biomaterials library to instruct cell fate. Proc. Natl. Acad. Sci. U. S. A. 2011, 108, 16565–16570, doi:10.1073/pnas.1109861108.

112. Won, Y.-W.; Patel, A.N.; Bull, D.A. Cell surface engineering to enhance mesenchymal stem cell migration toward an SDF-1 gradient. Biomaterials 2014, 35, 5627–5635, doi:10.1016/j.biomaterials.2014.03.070.

113. Watt, F.M.; Hogan, B.L. Out of Eden: stem cells and their niches. Science 2000, 287, 1427–1430, doi:10.1126/science.287.5457.1427.

114. Watt, F.M.; Huck, W.T.S. Role of the extracellular matrix in regulating stem cell fate. Nat. Rev. Mol. Cell Biol. 2013, 14, 467–473, doi:10.1038/nrm3620.

115. Kim, S.; Bedigrew, K.; Guda, T.; Maloney, W.J.; Park, S.; Wenke, J.C.; Yang, Y.P. Novel osteoinductive photo-cross-linkable chitosan-lactide-fibrinogen hydrogels enhance bone regeneration in critical size segmental bone defects. Acta Biomater. 2014, 10, 5021–5033, doi:10.1016/j.actbio.2014.08.028.

116. Bose, S.; Roy, M.; Bandyopadhyay, A. Recent advances in bone tissue engineering scaffolds. Trends Biotechnol. 2012, 30, 546–554, doi:10.1016/j.tibtech.2012.07.005.

117. Nazarov, R.; Jin, H.-J.; Kaplan, D.L. Porous 3-D scaffolds from regenerated silk fibroin. Biomacromolecules 2004, 5, 718–726, doi:10.1021/bm034327e.

118. Murphy, C.M.; Haugh, M.G.; O'Brien, F.J. The effect of mean pore size on cell attachment, proliferation and migration in collagen-glycosaminoglycan scaffolds for bone tissue engineering. Biomaterials 2010, 31, 461–466, doi:10.1016/j.biomaterials.2009.09.063.

119. O'Brien, F.J.; Harley, B.A.; Yannas, I.V.; Gibson, L.J. The effect of pore size on cell adhesion in collagen-GAG scaffolds. Biomaterials 2005, 26, 433–441, doi:10.1016/j.biomaterials.2004.02.052.

120. O'Brien, F.J.; Harley, B.A.; Waller, M.A.; Yannas, I.V.; Gibson, L.J.; Prendergast, P.J. The effect of pore size on permeability and cell attachment in collagen scaffolds for tissue engineering. THC 2006, 15, 3–17, doi:10.3233/THC-2007-15102.

121. Tsuruga, E.; Takita, H.; Itoh, H.; Wakisaka, Y.; Kuboki, Y. Pore size of porous hydroxyapatite as the cell-substratum controls BMP-induced osteogenesis. J. Biochem. 1997, 121, 317–324, doi:10.1093/oxfordjournals.jbchem.a021589.

122. Kuboki, Y.; Jin, Q.; Takita, H. Geometry of carriers controlling phenotypic expression in BMP-induced osteogenesis and chondrogenesis. J. Bone Joint Surg. Am. 2001, 83-A Suppl 1, S105-15.

123. Karageorgiou, V.; Kaplan, D. Porosity of 3D biomaterial scaffolds and osteogenesis. Biomaterials 2005, 26, 5474–5491, doi:10.1016/j.biomaterials.2005.02.002.

124. Pelham, R.J.; Wang, Y.l. Cell locomotion and focal adhesions are regulated by substrate flexibility. Proc. Natl. Acad. Sci. U. S. A. 1997, 94, 13661–13665, doi:10.1073/pnas.94.25.13661.

125. Dabrowski, B.; Swieszkowski, W.; Godlinski, D.; Kurzydlowski, K.J. Highly porous titanium scaffolds for orthopaedic applications. J. Biomed. Mater. Res. B Appl. Biomater. 2010, 95, 53–61, doi:10.1002/jbm.b.31682.

126. Balla, V.K.; Bodhak, S.; Bose, S.; Bandyopadhyay, A. Porous tantalum structures for bone implants: fabrication, mechanical and in vitro biological properties. Acta Biomater. 2010, 6, 3349–3359, doi:10.1016/j.actbio.2010.01.046.

127. Jones, J.R.; Ehrenfried, L.M.; Hench, L.L. Optimising bioactive glass scaffolds for bone tissue engineering. Biomaterials 2006, 27, 964–973, doi:10.1016/j.biomaterials.2005.07.017.

128. Rezwan, K.; Chen, Q.Z.; Blaker, J.J.; Boccaccini, A.R. Biodegradable and bioactive porous polymer/inorganic composite scaffolds for bone tissue engineering. Biomaterials 2006, 27, 3413–3431, doi:10.1016/j.biomaterials.2006.01.039.

129. Lee, S.-H.; Shin, H. Matrices and scaffolds for delivery of bioactive molecules in bone and cartilage tissue engineering. Adv. Drug Deliv. Rev. 2007, 59, 339–359, doi:10.1016/j.addr.2007.03.016.

130. Singh, B.N.; Panda, N.N.; Mund, R.; Pramanik, K. Carboxymethyl cellulose enables silk fibroin nanofibrous scaffold with enhanced biomimetic potential for bone tissue engineering application. Carbohydr. Polym. 2016, 151, 335–347, doi:10.1016/j.carbpol.2016.05.088.

131. Fragal, E.H.; Cellet, T.S.P.; Fragal, V.H.; Companhoni, M.V.P.; Ueda-Nakamura, T.; Muniz, E.C.; Silva, R.; Rubira, A.F. Hybrid materials for bone tissue engineering from biomimetic growth of hydroxiapatite on cellulose nanowhiskers. Carbohydr. Polym. 2016, 152, 734–746, doi:10.1016/j.carbpol.2016.07.063.

132. Wu, C.; Zhang, Y.; Zhou, Y.; Fan, W.; Xiao, Y. A comparative study of mesoporous glass/silk and non-mesoporous glass/silk scaffolds: physiochemistry and in vivo osteogenesis. Acta Biomater. 2011, 7, 2229–2236, doi:10.1016/j.actbio.2010.12.019.

133. Zhao, J.; Zhang, Z.; Wang, S.; Sun, X.; Zhang, X.; Chen, J.; Kaplan, D.L.; Jiang, X. Apatite-coated silk fibroin scaffolds to healing mandibular border defects in canines. Bone 2009, 45, 517–527, doi:10.1016/j.bone.2009.05.026.

134. Hutmacher, D.W. Scaffolds in tissue engineering bone and cartilage. Biomaterials 2000, 21, 2529–2543, doi:10.1016/s0142-9612(00)00121-6.

135. Stevens, M.M. Biomaterials for bone tissue engineering. Materials Today 2008, 11, 18–25, doi:10.1016/S1369-7021(08)70086-5.

136. Whitelaw, C.B.A.; Sheets, T.P.; Lillico, S.G.; Telugu, B.P. Engineering large animal models of human disease. J. Pathol. 2016, 238, 247–256, doi:10.1002/path.4648.

137. Silva, J.A.; Araujo, R.C.; Baltatu, O.; Oliveira, S.M.; Tschöpe, C.; Fink, E.; Hoffmann, S.; Plehm, R.; Chai, K.X.; Chao, L.; et al. Reduced cardiac hypertrophy and altered blood pressure control in transgenic rats with the human tissue kallikrein gene. FASEB J. 2000, 14, 1858–1860, doi:10.1096/fj.99-1010fje.

138. Wall, R.J.; Powell, A.M.; Paape, M.J.; Kerr, D.E.; Bannerman, D.D.; Pursel, V.G.; Wells, K.D.; Talbot, N.; Hawk, H.W. Genetically enhanced cows resist intramammary Staphylococcus aureus infection. Nat. Biotechnol. 2005, 23, 445–451, doi:10.1038/NBT1078.

139. Damak, S.; Jay, N.P.; Barrell, G.K.; Bullock, D.W. Targeting gene expression to the wool follicle in transgenic sheep. Biotechnology. (N Y) 1996, 14, 181–184, doi:10.1038/NBT0296-181.

140. Damak, S.; Su, H.; Jay, N.P.; Bullock, D.W. Improved wool production in transgenic sheep expressing insulin-like growth factor 1. Biotechnology. (N Y) 1996, 14, 185–188, doi:10.1038/NBT0296-185.

141. Lonberg, N. Human antibodies from transgenic animals. Nat. Biotechnol. 2005, 23, 1117–1125, doi:10.1038/nbt1135.

142. Niemann, H.; Kues, W.A. Transgenic farm animals: an update. Reprod. Fertil. Dev. 2007, 19, 762–770, doi:10.1071/RD07040.

143. Oliveira, S.M. de; Baptista, H.A.; Pesquero, J.B. Transgenic Animals: Principles, Methods and Applications. In Rodent Model as Tools in Ethical Biomedical Research; Andersen, M.L., Tufik, S., Eds.; Springer International Publishing: Cham, 2016; pp 169‑185, ISBN 978-3-319-11577-1.

144. Fukamizu, A. Transgenic animals in endocrinological investigation. J. Endocrinol. Invest. 1993, 16, 461–473, doi:10.1007/BF03348883.

145. Gordon, J.W.; Scangos, G.A.; Plotkin, D.J.; Barbosa, J.A.; Ruddle, F.H. Genetic transformation of mouse embryos by microinjection of purified DNA. Proc. Natl. Acad. Sci. U. S. A. 1980, 77, 7380–7384, doi:10.1073/pnas.77.12.7380.

146. Nagano, M.; Brinster, C.J.; Orwig, K.E.; Ryu, B.Y.; Avarbock, M.R.; Brinster, R.L. Transgenic mice produced by retroviral transduction of male germ-line stem cells. Proc. Natl. Acad. Sci. U. S. A. 2001, 98, 13090–13095, doi:10.1073/pnas.231473498.

147. Richa, J.; Lo, C.W. Introduction of human DNA into mouse eggs by injection of dissected chromosome fragments. Science 1989, 245, 175–177, doi:10.1126/science.2749254.

148. Lavitrano, M.; Camaioni, A.; Fazio, V.M.; Dolci, S.; Farace, M.G.; Spadafora, C. Sperm cells as vectors for introducing foreign DNA into eggs: Genetic transformation of mice. Cell 1989, 57, 717–723, doi:10.1016/0092-8674(89)90787-3.

149. Wood, S.A.; Pascoe, W.S.; Schmidt, C.; Kemler, R.; Evans, M.J.; Allen, N.D. Simple and efficient production of embryonic stem cell-embryo chimeras by coculture. Proc. Natl. Acad. Sci. U. S. A. 1993, 90, 4582–4585, doi:10.1073/pnas.90.10.4582.

150. Gossler, A.; Doetschman, T.; Korn, R.; Serfling, E.; Kemler, R. Transgenesis by means of blastocyst-derived embryonic stem cell lines. Proc. Natl. Acad. Sci. U. S. A. 1986, 83, 9065–9069, doi:10.1073/pnas.83.23.9065.

151. Kojima, K.; Kuwana, Y.; Sezutsu, H.; Kobayashi, I.; Uchino, K.; Tamura, T.; Tamada, Y. A new method for the modification of fibroin heavy chain protein in the transgenic silkworm. Biosci. Biotechnol. Biochem. 2007, 71, 2943–2951, doi:10.1271/bbb.70353.

152. Fraser, M.J.; Ciszczon, T.; Elick, T.; Bauser, C. Precise excision of TTAA-specific lepidopteran transposons piggyBac (IFP2) and tagalong (TFP3) from the

baculovirus genome in cell lines from two species of Lepidoptera. Insect Mol. Biol. 1996, 5, 141–151, doi:10.1111/j.1365-2583.1996.tb00048.x.

153. Elick, T.A.; Lobo, N.; Fraser, M.J. Analysis of the cis-acting DNA elements required for piggyBac transposable element excision. Mol. Gen. Genet. 1997, 255, 605–610, doi:10.1007/s004380050534.

154. Li, X.; Harrell, R.A.; Handler, A.M.; Beam, T.; Hennessy, K.; Fraser, M.J. piggyBac internal sequences are necessary for efficient transformation of target genomes. Insect Mol. Biol. 2005, 14, 17–30, doi:10.1111/j.1365-2583.2004.00525.x.

155. Li, X.; Lobo, N.; Bauser, C.A.; Fraser, M.J. The minimum internal and external sequence requirements for transposition of the eukaryotic transformation vector piggyBac. Mol. Genet. Genomics 2001, 266, 190–198, doi:10.1007/s004380100525.

156. Kahlig, K.M.; Saridey, S.K.; Kaja, A.; Daniels, M.A.; George, A.L.; Wilson, M.H. Multiplexed transposon-mediated stable gene transfer in human cells. Proc. Natl. Acad. Sci. U. S. A. 2010, 107, 1343–1348, doi:10.1073/pnas.0910383107.

157. Nakanishi, H.; Higuchi, Y.; Kawakami, S.; Yamashita, F.; Hashida, M. piggyBac transposon-mediated long-term gene expression in mice. Mol. Ther. 2010, 18, 707–714, doi:10.1038/mt.2009.302.

158. Yusa, K.; Rad, R.; Takeda, J.; Bradley, A. Generation of transgene-free induced pluripotent mouse stem cells by the piggyBac transposon. Nat. Methods 2009, 6, 363–369, doi:10.1038/NMETH.1323.

2. Chapter
Porous
Silk Fibroin/Cellulose
Hydrogel for Bone
Tissue Engineering

2. Chapter – Porous Silk Fibroin/Cellulose Hydrogel for Bone Tissue Engineering

2.1. Introduction

The aim of Bone Tissue Engineering (BTE) is to investigate methods for regeneration of bone for tissue models and clinical use. Artificially made BTE grafts are transplanted for healing of critical bone defects and provide an additional option for current clinical treatments [1]. Bone tissue is consistently remodeled and renewed by formation and resorption, which is performed by osteoblasts (bone forming) and osteoclasts (bone resorbing) [1,2]. For tissue matrix mineralization osteoblasts express an important enzyme called alkaline phosphatase (ALP), and as they become encapsulated within their own matrix they are referred to as osteocytes [2–4]. Generally sponge-like materials are prefered for BTE, since pores were shown to support nutrient/waste flow, cell proliferation, adhesion and migration [5]. Apart from porosity, stiffness is a distinct factor that contributes to not only mechanical stability. Mesenchymal stem cells (MSCs) exhibited a varying extent of cell adhesion and different differentiation lineages depending on culture substrate elasticity, whereas stiff matrices were shown to be osteogenic [6,7].

Various beneficial properties of SF for tissue engineering have been determined, which lead to investigation of SF as scaffold base material [8–10]. SF possesses characteristics particularly suitable for BTE such as suppression of an osteoblastogenesis down regulating pathway [11], osteogenic surface amide groups [12] and high β-sheet content in SF was shown to promote osteogenic differentiation of MSCs [13]. The β-sheet content is dependent on the processing method of SF [9,14] and influences the degradation time *in vivo*, whereas a higher content results in a longer degradation time [15]. In order to enhance the SF performance for BTE, several composite materials have been proposed and studied, among which, calcium phosphate-based inorganic compounds and collagen are components, due to their presence *in vivo*, and also other materials such as cellulose have been employed to reinforce the scaffold [16–18]. Composition of cellulose and SF results in an increase of mechanical strength of the scaffold material with increasing cellulose content [19–21], whereas cell

adhesion and viability increased when using cellulose and SF together rather than cellulose alone [22]. SF/cellulose composites have been prepared in various manners based on organic and aqueous solvents as well as ionic liquids, with some of them having been investigated for their cell culture performance with promising results and success in *in vivo* application. However, these composites have some disadvantages as many were only developed for fiber or film application, had insufficient pore size, required regenerated SF as substrate, or needed high temperature treatment for dissolving SF [18–20,23–26].

The aim of this work is to develop a novel process to fabricate a composite of SF and cellulose with a porous structure suitable for BTE with improved mechanical properties through the use of cellulose. The composite preparation method used in this work is based on the *N*,*N*-dimethylacetamide/LiCl (DMAc/LiCl) solvent, NaCl as water-leachable porogen, and a novel sequential regeneration process by a combined water vapor and MeOH treatment.

2.2. Materials and Methods

Dried bleached beech sulfite dissolving pulp (Mw = 303.7 kg/mol) was provided by Lenzing AG (Lenzing, Austria). Silk cocoons (*Bombyx mori*) were obtained from an experimental farm in Faculty of Textile Science and Technology, Shinshu University, Ueda, Japan. The used chemicals were obtained from Wako, Japan unless otherwise stated.

2.2.1. SF/Cellulose Hydrogel Preparation

2.2.1.1. Dissolution

Silk (*Bombyx mori*) cocoons were cut into small pieces and degummed in 0.25 g/L Na_2CO_3 solution at 98 °C for 30 min. After washing with reverse osmosis water (ROW) the silk fibroin fibers were dried at 50 °C for storage. The fibers were washed consecutively with reverse osmosis water (ROW), ethanol, dimethylsulfoxide (DMSO), and *N*,*N*-dimethylacetamide (DMAc) and then stored in DMAc for more than 12 h. The DMAc was removed by filtration under reduced pressure and the fibers were added to DMAc/LiCl (9 wt%). The suspension was kept stirring for 24 h at room temperature to yield a solution with a silk fibroin concentration of 5 wt%. In order to remove undissolved impurities, the solution was centrifuged for 5 min at 30,000 × g rcf and the supernatant was further used.

Dried cellulose pulp was swelled in water and blended by a mixer (Iwatani, IFM-800DG, 20,000× g) at room temperature. The cellulose fibers were washed with ROW, ethanol, and DMAc and kept in DMAc for more than 12 h. After vacuum-filtration, the cellulose fibers were added to the 5 wt% silk fibroin solution in DMAc/LiCl, to yield cellulose concentrations of 0.3 wt%, 0.5 wt% and 1 wt% (w/v). Samples made with these solutions were named S5C0.3, S5C0.5, and S5C1.0, respectively. The solution was kept stirring for 24 h at room temperature.

2.2.1.2. Hydrogel preparation

Molds were prepared by cutting off the outer stamp and head of 10 ml disposal syringes (TERUMO Co. Ltd., Tokyo, Japan). The syringe body was filled with 3.6 g of NaCl powder (mean grain size: 440 µm, Wako Co. Ltd., Tokyo, Japan). Approximately 1 ml of the SF/cellulose solution was added to cover the NaCl in the syringe and the syringe was centrifuged at 30,000× g rcf for 5 min to settle the NaCl powder. The syringes were placed into an airtight vessel containing 100 ml of saturated $MgCl_2$ solution to maintain a relative humidity of 33 % [27]. The syringes were kept at room temperature for 7 days. The formed bodies were pushed out from the syringes and immersed in methanol for 24 h with shaking. The resulting composite bodies were soaked in ROW for at least 8 h and solvent exchange was repeated 10 times to completely remove remaining solvents (methanol and DMAc). During this process, the NaCl in the hydrogels was also dissolved and leached out. The hydrogels were kept in ROW and autoclaved for storage to prevent microbial growth. As control, a solution of 5 wt% SF in DMAc/9% LiCl without cellulose was prepared and processed as above except for solidification in gaseous methanol and not by aqueous humidity. The control sample was named S5C0.

2.2.2. Cell Proliferation and Adhesion

For the evaluation of cell adhesion and proliferation behavior on the hydrogels, MC3T3-E1 cells (RIKEN BRC, Tsukuba, Japan) which can differentiate to osteoblast-like cells, were cultured on the hydrogels. The cylindrical hydrogels were cut into disks with a thickness of 1–2 mm and disks with a diameter of 10 mm were punched out. These disks were autoclaved and placed into the wells of a 48 well cell culture plate. The suspended MC3T3 cells (5×10^4 cells/100 µL in culture medium, Eagle MEM with 10% Fetal Bovine Serum) were seeded per

well and incubated at 37 °C, 5 % CO_2. After 1 day of culturing, 900 µL of medium were added to each well. The hydrogels were taken on the 1st, 3rd, 5th, and 7th day after seeding, washed by PBS (-) buffer and immersed in 500 µL of 0.5% Triton X-100/PBS to make a cell lysate for cell counting by LDH activity assay. The LDH activity assay was performed according to a previous report [28].

2.2.3. ALP Expression Assay

For the evaluation of ALP expression of cells on the hydrogels, MC3T3-E1 cells were cultured on the disk hydrogels in the same manner as above described for the cell proliferation test. The culture was continued for 3 weeks and the hydrogels were taken on the 1st, 7th, 14th, and 21st day after seeding. As the samples were analyzed, cell number and ALP activity on the hydrogels were measured on the same day. TRACP & ALP assay kit (MK301, TakaraBio co ltd., Tokyo, Japan) was used for determination of the ALP activity and the assay was performed according to the manufacture's manual. Calf ALP (Lot No. 3628209, Toyobo co. ltd., Osaka, Japan) was used as a standard of ALP activity.

2.2.4. Pore Structure and Porosity

The hydrogels were lyophilized after solvent exchange with ethanol, followed by transfer to *tert*-BuOH. Dried samples were coated with platinum by vacuum evaporation (MSP-20UM, Vacuum Device, Mito-shi, Ibaraki, Japan)) and observed by Scanning Electron Micrography (SEM) (Keyence VE-9800 SEM, Keyence, Osaka, Japan) at 10 kV. The average pore size was estimated by SEM photographs using ImageJ (v1.53a NIH, Bethesda, MD, USA).

The porosity of the hydrogels was estimated by µCT measurement. The measurement was performed by an X-ray Micro-tomograph apparatus (Skyscan-1272, Bruker, Billerica, MA, USA) at 5 µm/pixel resolution. Data sets were reconstructed (NRecon v1.7.4.6, Bruker, USA) and representative segments were transformed into binary images with dynamic thresholds and applied for morphometric analysis (CT Analyzer v1.18.8.0+, Bruker) and for making 3-dimensional models (CTvox v3.3.0, Bruker). The porosity was calculated during the morphometric analysis process by CT Analyzer.

2.2.5. Compression Test

The compression test was performed on a Tensile Test device (EZ-SX, EZ Test, Shimadzu co. Ltd., Tokyo, Japan). The cylindrical hydrogels (diameter 13 mm) were cut to a height of around 9 mm and kept wet during the compression test. The round compression area was 133 mm^2 and the speed of compression was 5 mm/min. The compressive modulus was calculated from the initial slope of the stress-strain curve at 5% to 10% strain by Origin software (v9.65, OriginLab, Northampton, MA, USA). The compressive strength was determined from the stress at 30% strain, according to the literature [29,30].

2.2.6. FTIR

FTIR measurements were performed within the attenuated total reflectance (ATR) mode and transmission mode with KBr pellets (IRPrestige-21, Shimadzu co. Ltd., Tokyo, Japan). The hydrogels were lyophilized with water in order to prepare them for measurement. The measurement ranges were 4000–600 cm^{-1}, with an accumulation of 30 scans and resolution of 2 cm^{-1} for both modes.

The interpretation of the SF secondary structure was based on the analysis of the amide I region [31]. Briefly, a baseline was drawn between 1720 cm^{-1} and 1580 cm^{-1}. By calculating the second derivative of the spectral data, information on bands attributable to specific secondary protein confirmations was obtained; Gauss-shaped curves were assumed for band integration. Band area ratios acquired through band deconvolution were used to calculate the relative structural content of secondary protein conformations. The peak analysis was performed by Origin software.

2.3. Results and Discussion

2.3.1. Hydrogel Fabrication

SF/cellulose hydrogels with porous structure were fabricated by employing a two-step, sequential gelation process. As shown schematically in Figure 2.1, SF was dissolved in DMAc/LiCl first and subsequently cellulose was dissolved in the SF solution (“Dissolution” in Figure 2.1). After adding NaCl powder as porogen (“Templating” in Figure 2.1), the solution was allowed to absorb minor amounts of water from the atmosphere of a defined humidity at room temperature. Acting as

the antisolvent, the water caused gelation/regeneration of the cellulose, while SF was held in solution ("Regeneration Step 1" in Figure 2.1). At this stage, the binary solution turned to a gel structure around the porogen. This gel-like structure was immersed in methanol, which caused the insolubilization of SF through the crystallization of SF molecules ("Regeneration Step 2" in Figure 2.1), the solidification of the cellulose gel, and reprecipitation of residual dissolved cellulose. The final structure of the hydrogels was assumed as crystallized SF material embedded in the cellulose scaffold, both arranged around the NaCl porogen. These NaCl templates were removed through leaching in ROW (reverse osmosis water) at the final step ("Washing" in Figure 2.1). The samples were named S5C0.3, S5C0.5, and S5C1.0 according to the wt% contents of silk fibroin (S) and cellulose (C) in the "Dissolution" step. The control without cellulose was named S5C0.

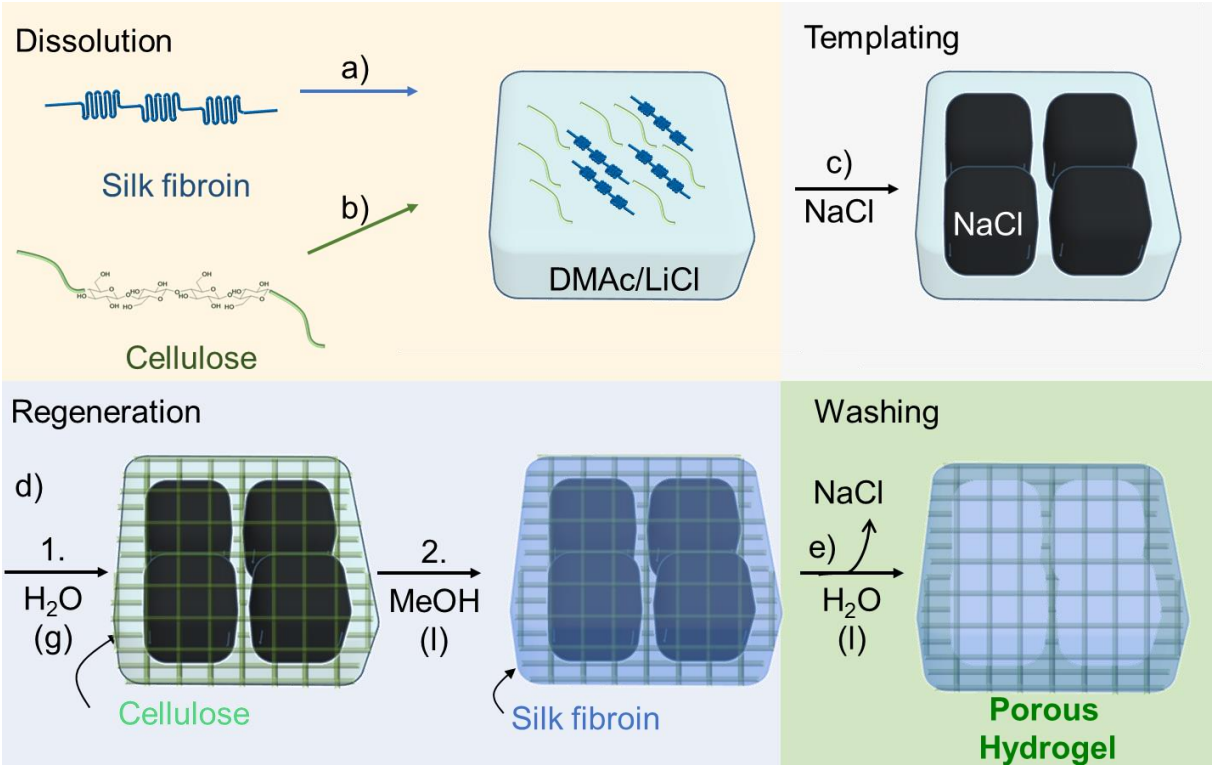

Figure 2.1: Hydrogel preparation. Dissolution: a) Dissolving silk fibroin (SF) in DMAc/LiCl. b) Dissolving cellulose in the SF solution. c) Templating: Addition of NaCl powder. d) Regeneration: 1. Cellulose is regenerated by water entering from air, gelation occurs; 2. soaking in methanol, SF is insolubilized. e) Washing: Removal of porogen and solvent, a porous hydrogel is formed.

2.3.2. Structural analysis by FTIR

Figure 2.2A and 2.2B show FTIR spectra of SF/cellulose hydrogels measured in transmission mode with KBr pellets and attenuated total reflectance (ATR) mode, respectively. The amide I band at 1630 cm^{-1} and amide II band at 1530 cm^{-1}, which are attributed to SF [20], were clearly observed in the spectra of SF/cellulose hydrogels and bands at 1019 cm^{-1} (C-O stretching band) and 1162 cm^{-1} (C-O-C stretching, glycosidic linkage) assigned to cellulose [32] also appeared in the spectra. The composition of both SF and cellulose was confirmed by this result. As all spectra were normalized to the cellulose-specific band area in the range of 1100 cm^{-1} to 960 cm^{-1}, a decrease in the amide band area corresponding to an increase in cellulose content was observed.

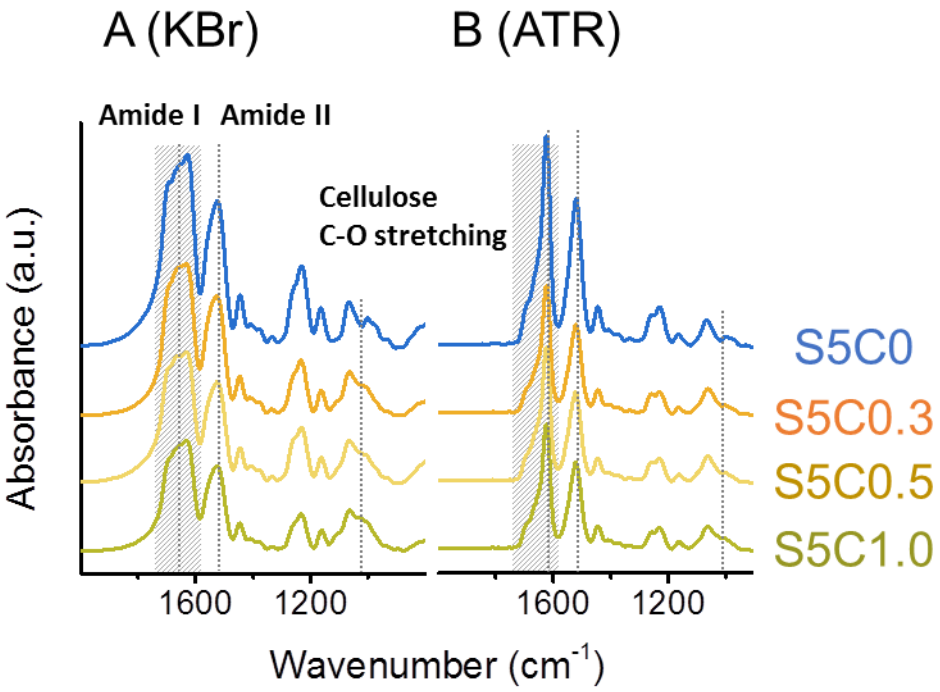

Figure 2.2: FTIR spectra of hydrogels. (A) Transmission (KBr) set up, (B) attenuated total reflectance (ATR) set up. Significant bands (amide I 1630 cm^{-1}, amide II 1530 cm^{-1}, cellulose C-O stretching 1019 cm^{-1}) are marked by dotted lines. Amide I peak area for deconvolution is marked in hatching.

Upon comparison of spectra taken in transmission mode (Figure 2.2A) and ATR mode (Figure 2.2B) a distinct difference in the peak shape of the amide I band can be noted. The amide I band reflects the secondary structure of proteins, such as SF. The amide I band of the spectra was deconvoluted to several peaks which

are assigned to the secondary structures of SF. β-sheet, α-helix/random coil, and turn/bend structures were assigned to peaks at 1622 cm^{-1} and 1639 cm^{-1}, 1658 cm^{-1}, and 1660~1700 cm^{-1}, respectively [31]. The ratio of the secondary structures was estimated from the peak areas. Deconvolution of amide I bands is shown in more detail in Figure S2.2. Table 2.1 summarizes the results of both transmission mode and ATR mode measurements.

Table 2.1: Secondary structure ratio of SF in the SF/cellulose hydrogel hydrogels by analysis of FTIR.

Content	Mode	S5C1	S5C0.5	S5C0. 3	S5C0
β sheet, %	ATR	64 ± 3	65 ± 2	65 ± 2	65 ± 1
	Transmission	36 ± 1	36 ± 1	32 ± 7	37 ± 6
α-helix and random coil, %	ATR	18 ± 4	17 ± 2	19 ± 4	18 ± 2
	Transmission	35 ± 2	24 ± 4	29 ± 10	27 ± 12
Turns and Bends, %	ATR	17 ± 2	18 ± 2	17 ± 2	17 ± 1
	Transmission	29 ± 2	40 ± 5	39 ± 8	36 ± 7

By transmission mode measurement, the β-sheet content for hydrogels was 32% to 37%. On the other hand, by ATR mode measurement, the cellulose-independent β-sheet content for hydrogels was estimated to be at around 64%. The ATR-reportable parts of the SF/cellulose hydrogels thus had a highly ordered crystalline structure. The difference of β-sheet contents measured originates from the different penetration depths of IR transmission and ATR modes, which is why they react differently to the internal structure of the composites. The samples measured in both modes were powders prepared by crushing the freeze-dried hydrogels. While in transmission mode the IR light detects the structural information from the bulk composite, ATR mode provides the molecular structural information only from the surface-near region, because the IR light penetration depth is limited to several μm from the surface. The penetration depth can be estimated by Eq. 1. [33]:

$$Penetration\ depth = \frac{\lambda}{2\pi\sqrt{sin^2\theta - (\frac{n_2}{n_1})^2}} \qquad \text{(Eq. 1)}$$

6.25 µm for λ at the amide I region wavelength (1600 cm^{-1}) were used. n_1 and n_2 are the refractive indices of diamond (2.376 at 6.25 µm) [34] and SF (1.530 at 1.5 µm) [35] used for calculation, respectively. θ is the incident angle of IR light to the prism, set at 45°. The resulting calculated penetration depth was 1.79 µm. Since the apparent powder size for ATR FTIR measurement was at several hundred µm, the ATR spectra were accumulated only from the near-surface region of the powder material. The difference in β-sheet content obtained by ATR and transmission FTIR measurements can likely be attributed to the solvent penetration dynamics of methanol in the composite, which seem to favor surface-near regions. These results indicate that the SF/cellulose hydrogels fabricated by our process have a characteristic structure of non-uniform crystallinity.

Due to the sequential regeneration step, we assume further the presence of a cellulose framework structure embedded into a silk fibroin matrix. The regeneration with water vapor causes the formation of a mechanically robust cellulose scaffold, which is a typical observation for cellulose gels prepared by comparable processes [36,37]. We further confirmed this structure, by washing the hydrogel after this treatment directly with water without the additional MeOH step (thereby dissolved silk was removed), and the IR spectrum of this cellulose-rich sample is shown in Figure S2.3. In the process with the MeOH regeneration step, SF is immobilized, surrounding the cellulose-rich network. Due to this special bicontinuous SF/cellulose composite structure, we also expected differences in the cellulose/silk ratio determined from IR measurements at the sample surface (ATR mode) and the whole bulk sample (transmission mode), which are clearly shown in Figure S2.4.

2.3.3. Structural characterization and mechanical properties of the cellulose-SF hydrogels

The hydrogels have a uniform porous structure with homogenous surface and pore distribution independent of cellulose composition (Figure 2.3). The determined average pore size and porosity are summarized in Table 2.2. The pore size and the porosity of the SF/cellulose hydrogels were 340 to 370 µm and 73% to 74%, respectively. There is no significant difference of pore structure, size, and porosity among samples. These results indicate that the amount of cellulose in the hydrogel did not affect the pore structure, size, and distribution, which were

solely determined by the NaCl porogen. Previous reports emphasized the importance of a minimum pore size of 300 µm to enable adequate tissue in-growth in 3D scaffolds [38–40]. The pore sizes in our hydrogels fulfill this requirement.

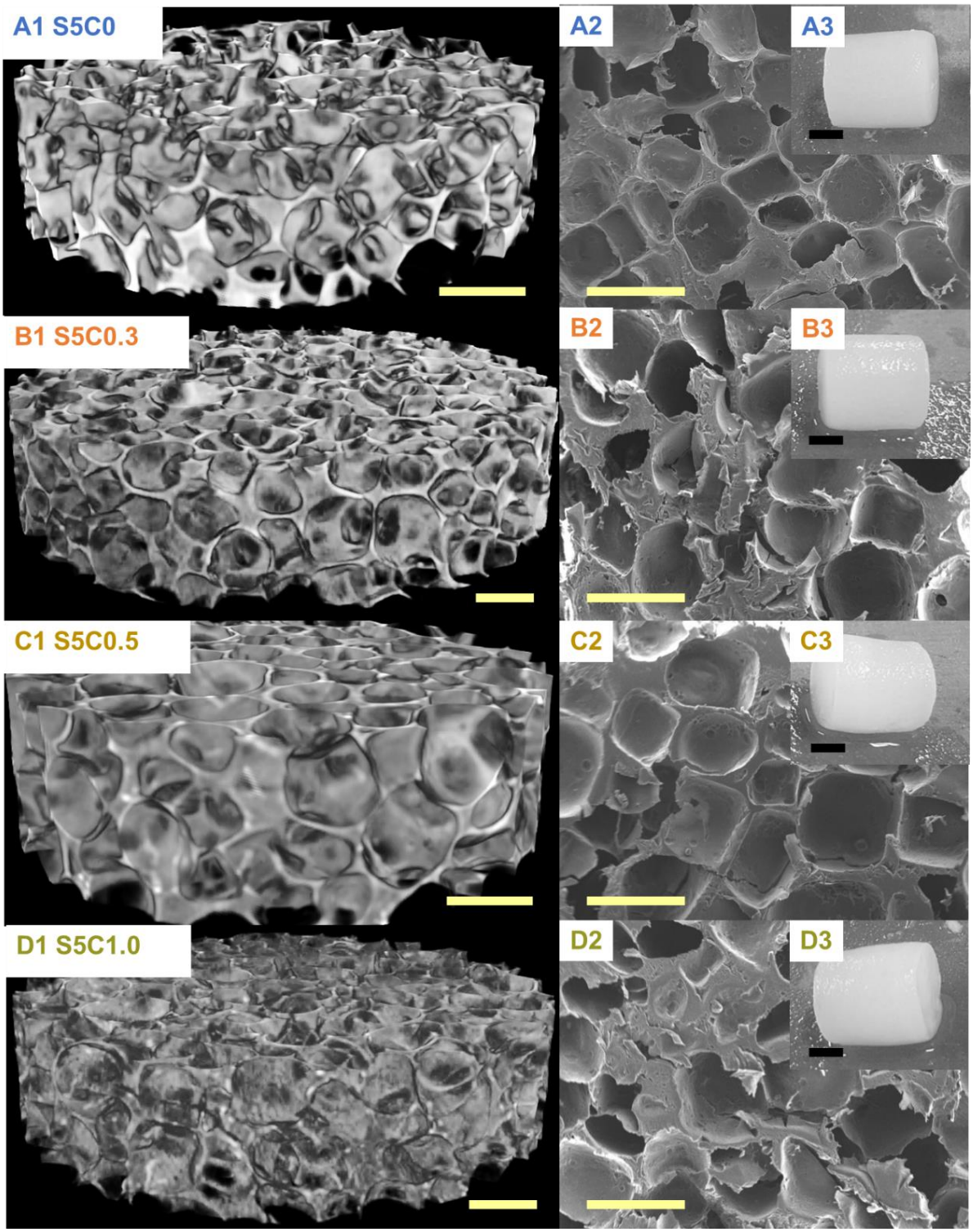

Figure 2.3: µCT images (A1–D1) and SEM photographs (A2–D2); yellow scale bar, 500 µm. Appearances of SF/cellulose hydrogels and control (A3–D3); black scale bar, 5 mm. A: S5C0, B: S5C0.3, C: S5C0.5, D: S5C1.0

Table 2.2: Porosity, pore size and compression properties of hydrogels

Property	S5C1.0	S5C0.5	S5C0.3	S5C0
Cellulose content[a], wt%	17	10	5	0
Porosity, %	74	71	73	74
Pore Size, μm	346 ± 106	339 ± 124	367 ± 104	345 ± 103
Modulus*, kPa	70.5 ± 17.2	68.4 ± 11.8	72.4 ± 13.9	53.3 ± 3.8
Compressive Strength*, kPa	17.0 ± 0.5	15.2 ± 2.0	12.9 ± 1.1	11.7 ± 1.0

[a] Estimated cellulose amount calculated from the respective cellulose and silk content in the precursor solutions.

* Samples were measured in wet hydrogel state

The compression properties of the hydrogels are summarized in Table 2.2, while Figure 2.4 shows the change of compression modulus and strength according to the amount of cellulose in the SF/cellulose hydrogels. The compressive modulus significantly increased by the first addition of cellulose to SF, but did not significantly increase further with higher cellulose contents. On the other hand, the compressive strength increased according to the amount of cellulose. The 17 wt% cellulose content showed an improvement of the compressive strength by a factor of 1.4. These results indicate that the presence of cellulose increases the mechanical strength and the stiffness of the SF material. Representative stress-strain curves measured for all samples are shown in Figure S2.1. The elastic modulus of cell substrates has been reported to be a directing factor to determine stem cell fate. As the material stiffness contributes to the osteogenic ability of BTE scaffolds [6,7], cellulose addition causes an important improvement of the osteogenic performance of the SF material.

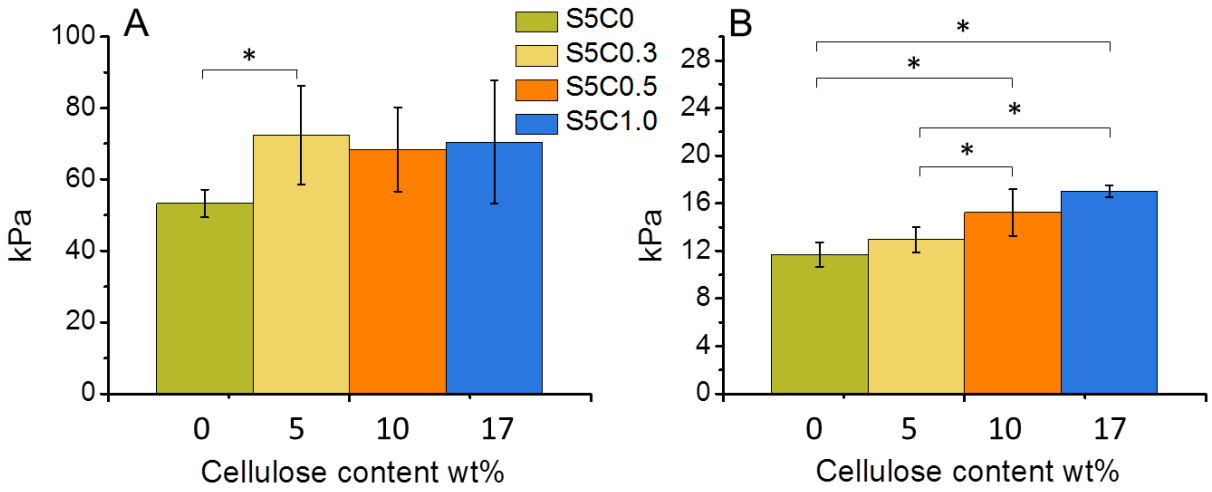

Figure 2.4: Change of compressive modulus (A) and compressive strength at 30 % strain (B) of wet SF/cellulose hydrogels depending on the amount of cellulose. Significant difference ($p < 0.05$) is indicated by an asterisk symbol (*).

2.3.4. Biological properties of the cellulose/SF Hydrogels

Initial cell adhesion and cell proliferation experiments were performed on the hydrogels and the SF control (S5C0) samples. As shown in Figure 2.5A, no significant differences among the samples with regard to initial cell adhesion were observed on day 1. SF has been reported to be a good substrate for supporting cell adhesion. The good cell adhesion of the SF control sample was maintained in the case of the hydrogels with cellulose, which had similarly good cell adhesion abilities.

Figure 2.5A also shows the proliferation curve of MC3T3-E1 cells cultured on the hydrogels and the SF control samples. The cell proliferation profiles on all samples were similar. Good cell growth on the hydrogels was observed, the same as for the SF sample. The doubling time for cell growth calculated at logarithmic growth was estimated to be around 2 days. This is in agreement with the reported typical time of around 1 to 2 days [41]. Thus, the hydrogels showed the same biocompatibility as SF.

The function of ALP in bone tissue is to catalyze the hydrolysis of extracellular pyrophosphates and to increase the local concentration of inorganic phosphates, which elicits biomineralization [42]. ALP expression is upregulated for osteoprogenitor cells and osteoblasts, and decreases with ongoing differentiation

to osteocytes, and no ALP expression occurs in mature osteocytes where the matrix has already mineralized [42,43].

Figure 2.5B shows the ALP activity for a calculated amount of 1×10^6 cells for all samples and the SF control (S5C0) over a time span of 3 weeks. Samples were taken on the 1st, 7th, 14th, and 21st day after seeding, while the ALP activity was measured and the cell number counted. There was no relevant difference between ALP activity between the samples. This result indicates that the presence of cellulose in the hydrogels did not impair the advantage of SF on MC3T3 cell differentiation to osteocytes. Figure 2.5B shows a maximum ALP activity around 7 days after seeding. From this result, it can be concluded that osteoblast differentiation to osteocytes was well progressing until at least 7 days of culture on the hydrogels, while other studies reported that a decrease of ALP expression was observed after 14 days of culture on cross-linked SF gelatin scaffolds [13] and 21 days of culture on water based, methanol treated SF scaffolds [44]. Evidently, an acceleration of MC3T3-E1 differentiation to osteocytes occurred on our SF/cellulose hydrogels.

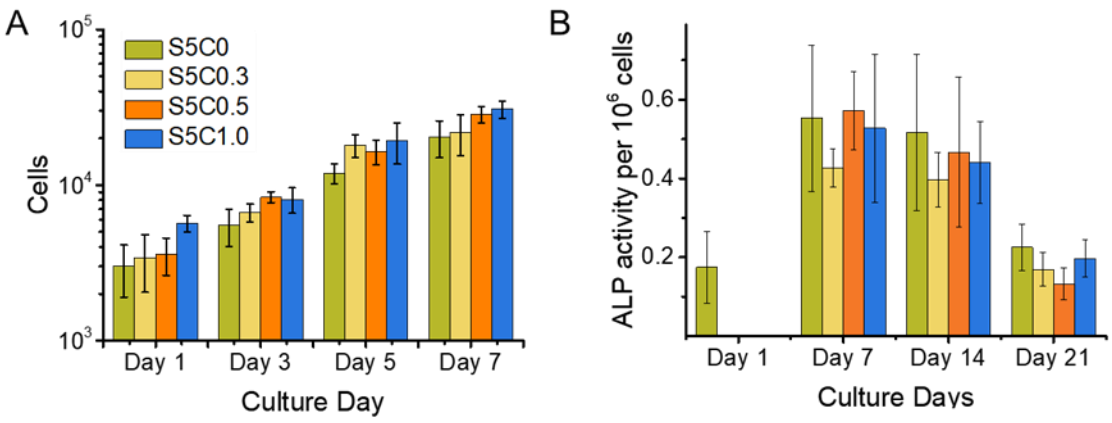

Figure 2.5: Cell Proliferation and alkaline phosphatase (ALP) Expression. (A) Cell proliferation of MC3T3 cells on hydrogel and control sample scaffolds during a time span of 7 days. Cell number is shown in logarithmic scale (B) ALP activity of MC3T3 cells cultured on hydrogel (S5C1, S5C0.5, S5C0.3) and control (S5C0) samples over a time span of 3 weeks. Cell proliferation was observed simultaneously with the same experimental set up in order to obtain cell numbers for normalization of measured ALP activity.

We propose that the mechanism of the earlier differentiation of MC3T3-E1 cells is due to the presence of low molecular-weight SF which is retained in the hydrogels, as no dialysis process to make SF solution is used. Low-molecular weight SF has been reported to be an inhibitor of the Notch pathway, which is involved in the down regulation of osteogenesis and thereby also an up regulator of ALP expression at an earlier time. The study suggested that the specific length of polypeptides, a combination of particular amino acids or a particular mixture of peptides of low molecular-weight SF is osteogenic, whereas isolated single repetitive motifs of the heavy chain (GAGVGY, GAGAGY, GAGAGS) did not show the same effect as the peptide mixture [11].

2.4. Conclusion

SF/cellulose hydrogels with a defined porous structure were successfully developed by a new approach that uses a binary solution of predissolved, native, degummed SF and cellulose in DMAc/LiCl and NaCl powder as a porogen. The pore size and the porosity of the SF/cellulose hydrogels were 340 to 370 µm and 73% to 74%, respectively. They did not change with the cellulose contents in the hydrogels. The presence of cellulose improved the mechanical stiffness and strength of the SF material. The sequential regeneration favors the formation of a reinforcing cellulose framework, regenerated first by atmospheric humidity, upon which, in a second step, SF is assembled by the action of methanol as the antisolvent. This causes the formation of a reinforcing cellulose framework structure embedded in a SF matrix. In surface-near layers, the secondary structure of SF in the hydrogels assumed abundant β-sheet conformation, whereas deeper layers of the scaffold show decreased β-sheet contents. As *in vivo* SF degradation inversely scales with β-sheet content, this offers great potential for resorption of the material upon sufficient bone regeneration by the body. The cellulose framework/SF matrix structure maximized material dependent improvement of hydrogel properties, as the cellulose framework mainly contributed to mechanical property enhancement, while the SF matrix supported cell growth. Osteocyte differentiation of MC3T3-E1 cells cultured on the hydrogels was observed. Even more, the good differentiation properties of SF materials were not impaired by the incorporation of cellulose, and the osteocyte

differentiation was accelerated compared to other SF substrates. These results show SF/cellulose hydrogels to be a suitable scaffold for BTE.

2.5. Supplementary Materials

2.5.1. Compression test data

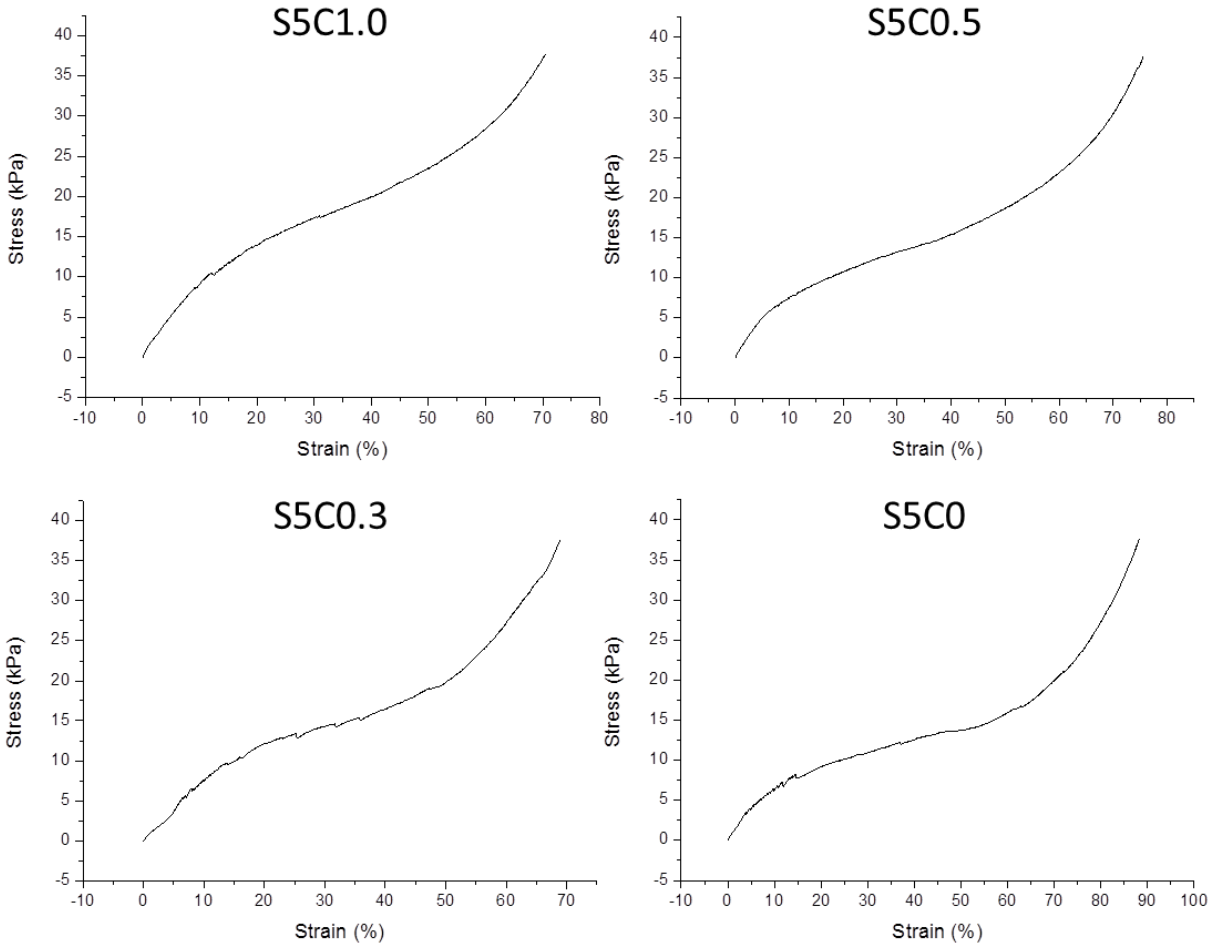

Figure S2.1: Stress-strain curves of all samples and control. Number of samples measured: S5C1.0 n=5; S5C0.5 n=5; S5C0.3 n=6; S5C0 n=4.

2.5.2. Deconvolution results

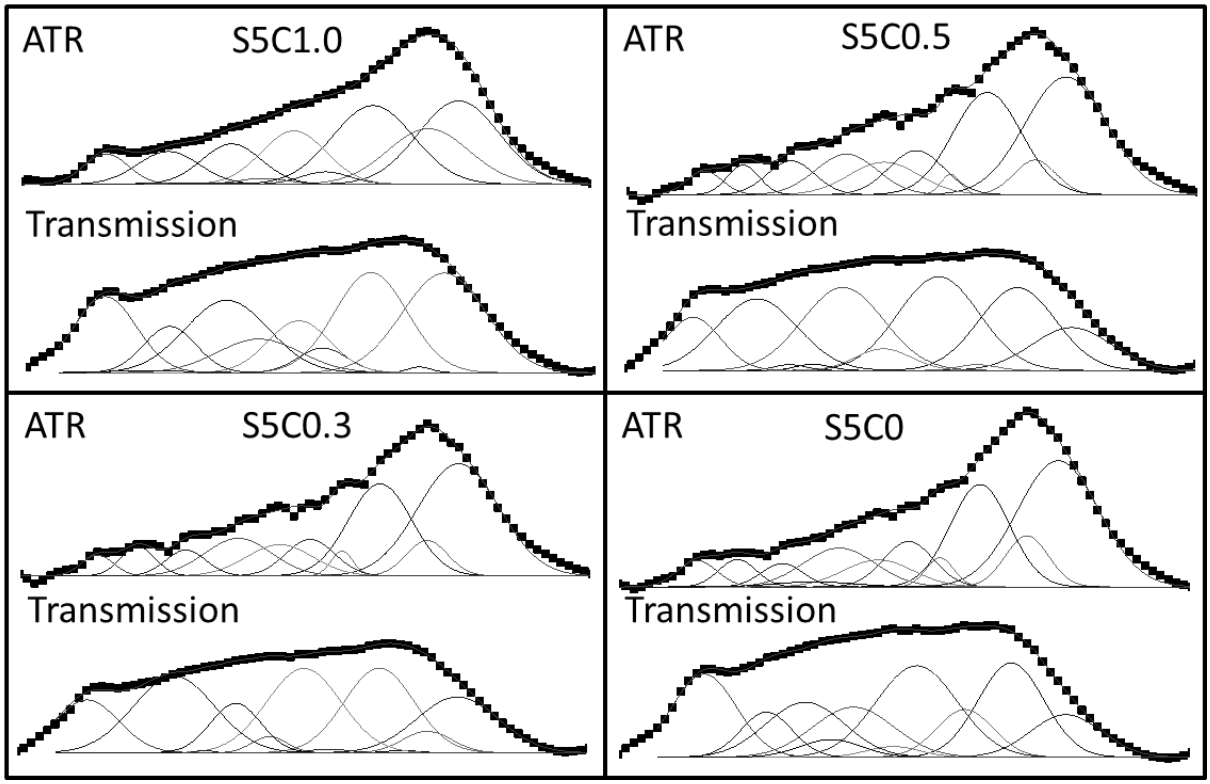

Figure S2.2: Diagrams of deconvoluted peaks in amide I band region. Bands for peak allocation to secondary structure are: β-sheet: 1611 cm^{-1}, 1619 cm^{-1}, 1626 cm^{-1}, 1699 cm^{-1}. α-helix/random coil: 1631 cm^{-1}, 1641 cm^{-1}, 1649 cm^{-1}. Turns and bends: 1659 cm^{-1}, 1668 cm^{-1}, 1674 cm^{-1}, 1682 cm^{-1}.

2.5.3. SF matrix /cellulose scaffold composite structure

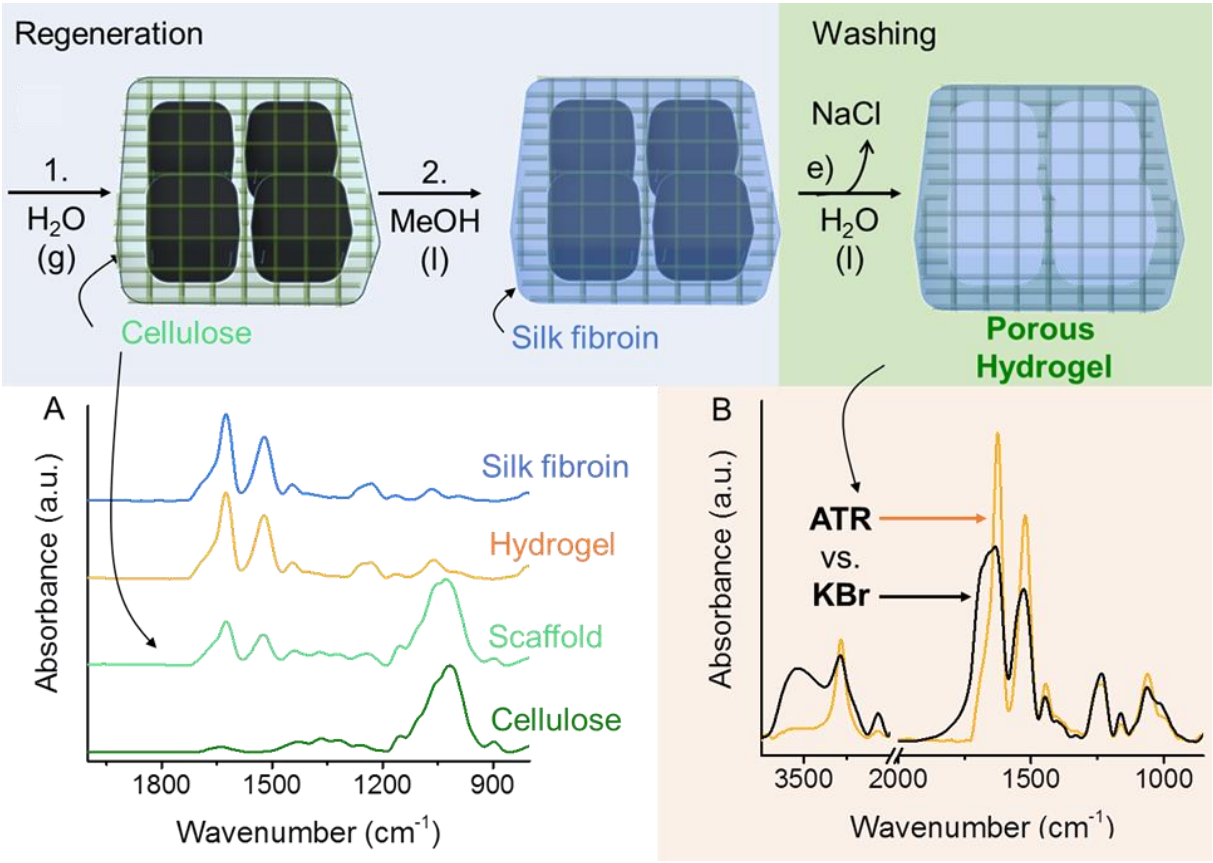

Figure S2.3: Cellulose framework structure embedded in a SF matrix. (A) Cellulose framework: By omitting methanol treatment of samples, a cellulose-rich, very stable hydrogel formed ("Scaffold" spectrum); that sample was compared with regenerated cellulose, degummed silk fibroin and lyophilized SF/cellulose hydrogel by ATR FTIR. (B) SF matrix: ATR and transmission spectra (KBr) normalized to the cellulose-specific band area 1100 cm^{-1} to 960 cm^{-1} of a lyophilized hydrogel. The larger amide band area in ATR mode indicates a relatively increased SF content in the surface-near region compared to the bulk.

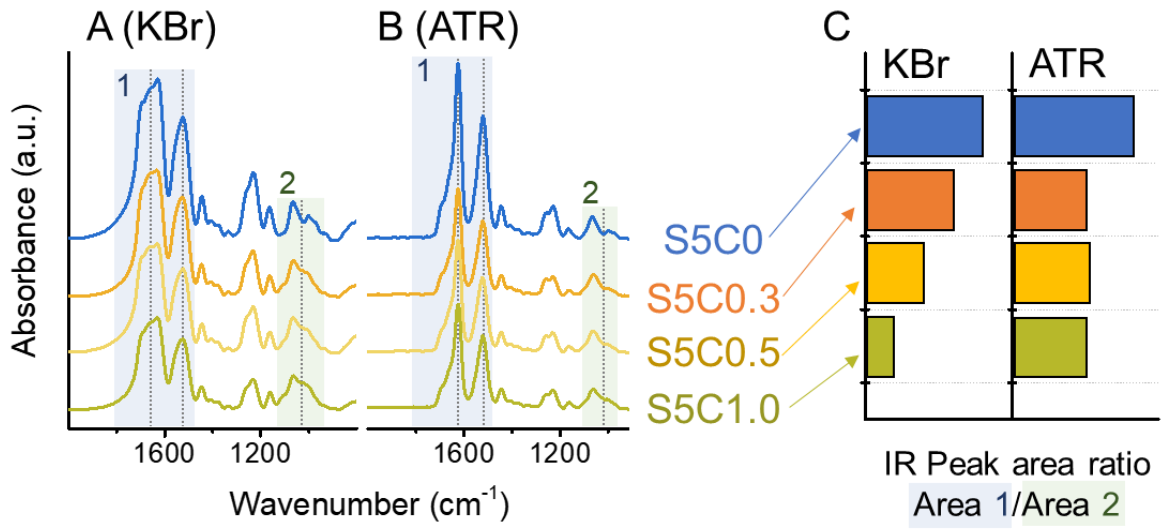

Figure S2.4: Different bulk and surface composition. Ratios of silk fibroin (SF) specific amide I and II band area and cellulose-specific band area at 1100 cm^{-1} to 960 cm^{-1} (respectively area 1 and 2 in A and B) of all samples decrease with increasing cellulose content in transmission mode (KBr) (C). In ATR mode ratios of samples do not differ, but show a lower ratio compared to the SF control. This indicates a richer SF structure in the surface regions of the hydrogel compared to bulk composition.

2.6. References

1. Melke, J.; Midha, S.; Ghosh, S.; Ito, K.; Hofmann, S. Silk fibroin as biomaterial for bone tissue engineering. Acta Biomater. 2016, 31, 1–16, doi:10.1016/j.actbio.2015.09.005.

2. Robling, A.G.; Castillo, A.B.; Turner, C.H. Biomechanical and molecular regulation of bone remodeling. Annu. Rev. Biomed. Eng. 2006, 8, 455–498, doi:10.1146/annurev.bioeng.8.061505.095721.

3. Franz-Odendaal, T.A.; Hall, B.K.; Witten, P.E. Buried alive: how osteoblasts become osteocytes. Dev. Dyn. 2006, 235, 176–190, doi:10.1002/dvdy.20603.

4. Dallas, S.L.; Bonewald, L.F. Dynamics of the transition from osteoblast to osteocyte. Ann. N. Y. Acad. Sci. 2010, 1192, 437–443, doi:10.1111/j.1749-6632.2009.05246.x.

5. Murphy, C.M.; Haugh, M.G.; O'Brien, F.J. The effect of mean pore size on cell attachment, proliferation and migration in collagen-glycosaminoglycan scaffolds for bone tissue engineering. Biomaterials 2010, 31, 461–466, doi:10.1016/j.biomaterials.2009.09.063.

6. Engler, A.J.; Sen, S.; Sweeney, H.L.; Discher, D.E. Matrix elasticity directs stem cell lineage specification. Cell 2006, 126, 677–689, doi:10.1016/j.cell.2006.06.044.

7. Pelham, R.J.; Wang, Y.l. Cell locomotion and focal adhesions are regulated by substrate flexibility. Proc. Natl. Acad. Sci. U. S. A. 1997, 94, 13661–13665, doi:10.1073/pnas.94.25.13661.

8. Altman, G.H.; Diaz, F.; Jakuba, C.; Calabro, T.; Horan, R.L.; Chen, J.; Lu, H.; Richmond, J.; Kaplan, D.L. Silk-based biomaterials. Biomaterials 2003, 24, 401–416, doi:10.1016/S0142-9612(02)00353-8.

9. You, R.; Xu, Y.; Liu, G.; Liu, Y.; Li, X.; Li, M. Regulating the degradation rate of silk fibroin films through changing the genipin crosslinking degree. Polymer Degradation and Stability 2014, 109, 226–232, doi:10.1016/j.polymdegradstab.2014.07.029.

10. Thurber, A.E.; Omenetto, F.G.; Kaplan, D.L. In vivo bioresponses to silk proteins. Biomaterials 2015, 71, 145–157, doi:10.1016/j.biomaterials.2015.08.039.

11. Jung, S.-R.; Song, N.-J.; Yang, D.K.; Cho, Y.-J.; Kim, B.-J.; Hong, J.-W.; Yun, U.J.; Jo, D.-G.; Lee, Y.M.; Choi, S.Y.; et al. Silk proteins stimulate osteoblast differentiation by suppressing the Notch signaling pathway in mesenchymal stem cells. Nutr. Res. 2013, 33, 162–170, doi:10.1016/j.nutres.2012.11.006.

12. Curran, J.M.; Chen, R.; Hunt, J.A. Controlling the phenotype and function of mesenchymal stem cells in vitro by adhesion to silane-modified clean glass surfaces. Biomaterials 2005, 26, 7057–7067, doi:10.1016/j.biomaterials.2005.05.008.

13. Das, S.; Pati, F.; Choi, Y.-J.; Rijal, G.; Shim, J.-H.; Kim, S.W.; Ray, A.R.; Cho, D.-W.; Ghosh, S. Bioprintable, cell-laden silk fibroin-gelatin hydrogel supporting multilineage differentiation of stem cells for fabrication of three-dimensional tissue constructs. Acta Biomater. 2015, 11, 233–246, doi:10.1016/j.actbio.2014.09.023.

14. Wang, Y.; Rudym, D.D.; Walsh, A.; Abrahamsen, L.; Kim, H.-J.; Kim, H.S.; Kirker-Head, C.; Kaplan, D.L. In vivo degradation of three-dimensional silk fibroin scaffolds. Biomaterials 2008, 29, 3415–3428, doi:10.1016/j.biomaterials.2008.05.002.

15. Jin, H.-J.; Park, J.; Karageorgiou, V.; Kim, U.-J.; Valluzzi, R.; Cebe, P.; Kaplan, D.L. Water-Stable Silk Films with Reduced β-Sheet Content. Adv. Funct. Mater. 2005, 15, 1241–1247, doi:10.1002/adfm.200400405.

16. He, P.; Sahoo, S.; Ng, K.S.; Chen, K.; Toh, S.L.; Goh, J.C.H. Enhanced osteoinductivity and osteoconductivity through hydroxyapatite coating of silk-based tissue-engineered ligament scaffold. J. Biomed. Mater. Res. A 2013, 101, 555–566, doi:10.1002/jbm.a.34333.

17. Zhang, Y.; Wu, C.; Friis, T.; Xiao, Y. The osteogenic properties of CaP/silk composite scaffolds. Biomaterials 2010, 31, 2848–2856, doi:10.1016/j.biomaterials.2009.12.049.

18. Chen, J.; Zhuang, A.; Shao, H.; Hu, X.; Zhang, Y. Robust silk fibroin/bacterial cellulose nanoribbon composite scaffolds with radial lamellae and intercalation structure for bone regeneration. J. Mater. Chem. B 2017, 5, 3640–3650, doi:10.1039/c7tb00485k.

19. Zhou, L.; Wang, Q.; Wen, J.; Chen, X.; Shao, Z. Preparation and characterization of transparent silk fibroin/cellulose blend films. Polymer 2013, 54, 5035–5042, doi:10.1016/j.polymer.2013.07.002.

20. Singh, N.; Rahatekar, S.S.; Koziol, K.K.K.; Ng, T.S.; Patil, A.J.; Mann, S.; Hollander, A.P.; Kafienah, W. Directing chondrogenesis of stem cells with specific blends of cellulose and silk. Biomacromolecules 2013, 14, 1287–1298, doi:10.1021/bm301762p.

21. Freddi, G.; Romanò, M.; Massafra, M.R.; Tsukada, M. Silk fibroin/cellulose blend films: Preparation, structure, and physical properties. J. Appl. Polym. Sci. 1995, 56, 1537–1545, doi:10.1002/app.1995.070561203.

22. Oliveira Barud, H.G.; Barud, H.d.S.; Cavicchioli, M.; do Amaral, T.S.; Oliveira Junior, O.B. de; Santos, D.M.; Petersen, A.L.d.O.A.; Celes, F.; Borges, V.M.; Oliveira, C.I. de; et al. Preparation and characterization of a bacterial cellulose/silk fibroin sponge scaffold for tissue regeneration. Carbohydr. Polym. 2015, 128, 41–51, doi:10.1016/j.carbpol.2015.04.007.

23. Marsano, E.; Corsini, P.; Canetti, M.; Freddi, G. Regenerated cellulose-silk fibroin blends fibers. Int. J. Biol. Macromol. 2008, 43, 106–114, doi:10.1016/j.ijbiomac.2008.03.009.

24. Lee, J.H.; Bae, C.H.; Park, B.-D.; Um, I.C. Preparation of Cellulose Nanofibril/Regenerated Silk Fibroin Composite Fibers. International Journal of Industrial Entomology 2013, 26, 81–88, doi:10.7852/ijie.2013.26.2.81.

25. Marsano, E.; Canetti, M.; Conio, G.; Corsini, P.; Freddi, G. Fibers based on cellulose–silk fibroin blend. J. Appl. Polym. Sci. 2007, 104, 2187–2196, doi:10.1002/app.24856.

26. Lee, J.M.; Kim, J.H.; Lee, O.J.; Park, C.H. The fixation effect of a silk fibroin-bacterial cellulose composite plate in segmental defects of the zygomatic

arch: an experimental study. JAMA Otolaryngol. Head Neck Surg. 2013, 139, 629–635, doi:10.1001/jamaoto.2013.3044.

27. Dubovikov, N.I.; Podmurnaya, O.A. Measuring the relative humidity over salt solutions. Measurement Techniques 2001, 44, 1260–1261, doi:10.1023/A:1014738608108.

28. Tamada, Y.; Ikada, Y. Fibroblast growth on polymer surfaces and biosynthesis of collagen. J. Biomed. Mater. Res. 1994, 28, 783–789, doi:10.1002/jbm.820280705.

29. Markstedt, K.; Mantas, A.; Tournier, I.; Martínez Ávila, H.; Hägg, D.; Gatenholm, P. 3D Bioprinting Human Chondrocytes with Nanocellulose-Alginate Bioink for Cartilage Tissue Engineering Applications. Biomacromolecules 2015, 16, 1489–1496, doi:10.1021/acs.biomac.5b00188.

30. Mohan, T.; Dobaj Štiglic, A.; Beaumont, M.; Konnerth, J.; Gürer, F.; Makuc, D.; Maver, U.; Gradišnik, L.; Plavec, J.; Kargl, R.; et al. Generic Method for Designing Self-Standing and Dual Porous 3D Bioscaffolds from Cellulosic Nanomaterials for Tissue Engineering Applications. ACS Appl. Bio Mater. 2020, 3, 1197–1209, doi:10.1021/acsabm.9b01099.

31. Tretinnikov, O.N.; Tamada, Y. Influence of Casting Temperature on the Near-Surface Structure and Wettability of Cast Silk Fibroin Films. Langmuir 2001, 17, 7406–7413, doi:10.1021/la010791y.

32. Oh, S.Y.; Yoo, D.I.; Shin, Y.; Kim, H.C.; Kim, H.Y.; Chung, Y.S.; Park, W.H.; Youk, J.H. Crystalline structure analysis of cellulose treated with sodium hydroxide and carbon dioxide by means of X-ray diffraction and FTIR spectroscopy. Carbohydr. Res. 2005, 340, 2376–2391, doi:10.1016/j.carres.2005.08.007.

33. Shimadzu. Depth of light penetration for ATR measurements. https://www.shimadzu.com/an/ftir/support/faq/2.html (accessed on 30 August 2020).

34. Edwards, D.F.; Ochoa, E. Infrared refractive index of diamond. J. Opt. Soc. Am. 1981, 71, 607, doi:10.1364/JOSA.71.000607.

35. Perotto, G.; Zhang, Y.; Naskar, D.; Patel, N.; Kaplan, D.L.; Kundu, S.C.; Omenetto, F.G. The optical properties of regenerated silk fibroin films obtained from different sources. Appl. Phys. Lett. 2017, 111, 103702, doi:10.1063/1.4998950.

36. Liebner, F.; Potthast, A.; Rosenau, T.; Haimer, E.; Wendland, M. Cellulose aerogels: Highly porous, ultra-lightweight materials. Holzforschung 2008, 62, 129–135, doi:10.1515/HF.2008.051.

37. Pircher, N.; Carbajal, L.; Schimper, C.; Bacher, M.; Rennhofer, H.; Nedelec, J.-M.; Lichtenegger, H.C.; Rosenau, T.; Liebner, F. Impact of selected solvent systems on the pore and solid structure of cellulose aerogels. Cellulose 2016, 23, 1949–1966, doi:10.1007/s10570-016-0896-z.

38. Kuboki, Y.; Jin, Q.; Takita, H. Geometry of carriers controlling phenotypic expression in BMP-induced osteogenesis and chondrogenesis. J. Bone Joint Surg. Am. 2001, 83-A Suppl 1, S105-15.

39. Tsuruga, E.; Takita, H.; Itoh, H.; Wakisaka, Y.; Kuboki, Y. Pore size of porous hydroxyapatite as the cell-substratum controls BMP-induced osteogenesis. J. Biochem. 1997, 121, 317–324, doi:10.1093/oxfordjournals.jbchem.a021589.

40. Karageorgiou, V.; Kaplan, D. Porosity of 3D biomaterial scaffolds and osteogenesis. Biomaterials 2005, 26, 5474–5491, doi:10.1016/j.biomaterials.2005.02.002.

41. DSMZ German Collection of Microorganisms and Cell Cultures GmbH: MC3T3 cell culture data. https://www.dsmz.de/collection/catalogue/details/culture/ACC-210 (accessed on 7 August 2020).

42. Allori, A.C.; Sailon, A.M.; Warren, S.M. Biological basis of bone formation, remodeling, and repair-part II: extracellular matrix. Tissue Eng. Part B Rev. 2008, 14, 275–283, doi:10.1089/ten.teb.2008.0083.

43. Bilezikian, J.P.; Raisz, L.G.; Rodan, G.A. Principles of bone biology, 2nd ed.; Academic Press: San Diego, 2002, ISBN 0-12-098653-1.

44. Oliveira, A.L.; Sun, L.; Kim, H.J.; Hu, X.; Rice, W.; Kluge, J.; Reis, R.L.; Kaplan, D.L. Aligned silk-based 3-D architectures for contact guidance in tissue engineering. Acta Biomater. 2012, 8, 1530–1542, doi:10.1016/j.actbio.2011.12.015.

3. Chapter
Production of recombinant silk fibroin with basic fibroblast growth factor binding affinity

3. Chapter – Production of recombinant silk fibroin with basic fibroblast growth factor binding affinity

3.1. Introduction

Silk Fibroin (SF) is a commonly known material that currently undergoes much research for tissue engineering application. The protein consists of 3 parts, which are 6 subunits of disulfide-linked heavy and light chains and a central peptide called fibrohexamerin [1], which joins the other 6 subunits together by hydrophobic interactions [2].

In order to improve the biological applicability of SF, systems for engineering transgenic silkworms are utilized with the aim to make them express recombinant SF. One such transgenic system is the *piggyBac* Transposase system which allows the random integration of gene cassettes into a TTAA sites in the genome. This way the expression of recombinant silks has been researched and the method has also been used as a means of investigating the effect of gene disruptions [3–5]. Such recombinant SF has been applied for tissue engineering, with the aim of enhancing cell growth by use of a fusion protein of SF and bFGF as scaffold material. This approach was of limited success, as it was not possible to acquire functional, dissolved recombinant SF-bFGF fusion protein from recombinant SF originating from silk cocoons, but only from the posterior silk glands of transgenic silkworms [6].

bFGF is a heparin-binding growth factor with single chain polypeptide produced by a variety of different cell types which possess a specific high affinity receptor for it. It is a fundamental regulator with a broad spectrum of activity comprising but not limited to inducing or delaying differentiation of target cells and stimulating proliferation [7,8] by autocrine and paracrine mechanisms [8]. bFGF elicits potent mitogenic responses from cells of mesodermal or neuroectodermal descent [7,8], particularly for endothelial cells [9]. Applications for bone tissue engineering have shown useful effects of bFGF, which has significant osteoconductivity [10] and supports osteogenic differentiation of mesenchymal stem cells [11]. The use of bFGF was challenged though by its low conformational stability [12], which makes the polypeptide susceptible to denaturation by storage at room temperature, exposition to an alkaline pH or catalytic amounts of Cu^{2+} ions [13].

This property of bFGF is problematic for preservation of function of the polypeptide upon processing the recombinant SF, due to the harsh reaction conditions associated with the degumming step and the dissolution of the SF. This issue had been avoided by renaturation of the bFGF by exposing the recombinant SF to reducing conditions [5,12]. Differently to the application of recombinant SF in cell culture media or films, the application for tissue engineering requires the processing of the material into a 3D scaffold. The renaturation step for bFGF was likely not performed because it requires reducing conditions, which would break the disulfide bonds within the fibroin protein molecule, separating H-chains and L chains, and thereby rendering the L-chain coupled bFGF unable to aggregate with the H-chain, thus excluding it from the scaffold structure.

This work covers an alternate approach for using SF associated bFGF for tissue engineering scaffolds by specifically and non-covalently binding bFGF to a genetically introduced specific binding site in recombinant SF that is processed into a scaffold beforehand. The genetically introduced peptide sequence PLLQATLGGGS, named P7, has been discovered to be bFGF-binding via phage display technology and shows high homology to the immunoglobulin-like domain III of bFGF receptors [14]. The aim of this work is to produce recombinant SF for tissue engineering, which makes use of a recombinant peptide structure that is short enough to not have its functionality be subject to conformational protein structures higher than the primary structure. This results in a functional bFGF-binding SF tissue engineering scaffold that can be loaded with bFGF for variably gradual bFGF release into the surrounding cellular environment.

3.2. Materials and Methods

3.2.1. Experimental animals

The bivoltine strain “Kosetsu” of domestic mulberry silkworm, Bombyx mori, was used to produce transgenic silkworms with expressing recombinant proteins in this study. The larvae were fed on artificial diet with mulberry leaves powder (Kuwano-hana, JA Zennoh Gunma, Takasaki, Japan) and reared at 25°C under a 13-h light/11-h dark cycle (75%–80% relative humidity) [15].

3.2.2. Preparation of vector to produce transgenic silkworm

The *piggyBac* based vector construct for the production of transgenic silkworms to express bFGF-binding peptides (P7) fused with the L chain gene of *Bombyx mori* is shown in Figure 3.1A. A transgene coding oligonucleotide cassette of 91 bp was custom-ordered (Figure S3.1, eurofins, Luxembourg) and inserted into the pLC-MCS plasmid [6], which codes the promoter, the ORF and the polyadenylation sequence of the fibroin L-chain gene. Apart from necessary sequence homologies (Figure S3.1, underlined sequence) for HD Infusion cloning (Takara, Japan), the oligonucleotide cassette coded for the peptide sequence LEVLFQGPLLQATLGGGS (PPP7) in which LEVLFQGP is a recognition site for the PreScission Protease (PP) (GE Healthcare, UK) and PLLQATLGGGS is the desired bFGF-binding sequence (P7) as shown in Figure 3.1B. Transgenic insert and recombinant peptide sequence are hereafter both referred to as P7. The oligonucleotide cassette was introduced into the multiple cloning site (MCS) within the fibroin L-chain coding sequence of the pLC-MCS plasmid via In-Fusion HD Cloning Kit (Takara, Japan) while the *Bam*H I (Takara, Japan) and *Sal* I (Takara, Japan) restriction sites were preserved. The prepared transgene was amplified with PCR while adding the necessary sequence homologies (pB15L primers in Table S3.1, sequence homologies to pBac3xP3-DsRedaf vector are underlined) for subsequent HD Infusion cloning into the pBac3xP3-DsRedaf vector [16] for the transformation of *B. mori*. The pBac3xP3-DsRedaf vector was digested with the restriction enzymes *Asc* I (NEB, USA) and *Fse* I (NEB, USA) and the prepared transgene was inserted via HD Infusion cloning.

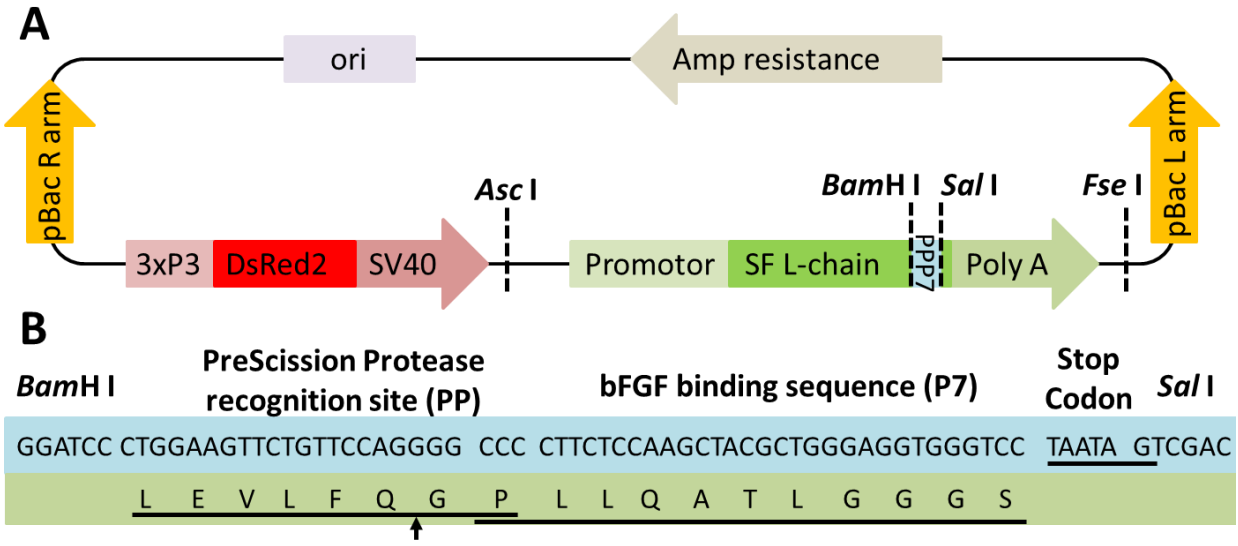

Figure 3.1: *piggyBac* transposon vector for production of transgenic silkworms to express recombinant SF (A) and PPP7 nucleic sequence with the translational amino acid sequence (B). (A) vector with reporter gene (3xP3 promotor, DsRed2 ORF, SV40 Terminator) and SF L-chain transgene (SF L-chain promotor, ORF, PPP7 insert (blue), Polyadenylation signal); (B) bFGF binding sequence P7 (underlined), PreScission Protease recognition site (underlined, cleavage site indicated by arrow), Stop Codon (underlined) and preserved restriction sites (*Bam*H I and *Sal* I); nucleotide sequence with blue background and corresponding amino acid sequence with green background.

3.2.3. Germline transformation and marker detection

In order to break the diapause of embryos for microinjection, the eggs of the bivoltine silkworm Kosetsu were kept in the incubator at 15 °C in the dark until their heads formed and colored to black. After that, the eggs were moved to the incubator of 25 °C and kept until hatching. The larvae were reared to moths, and then non-diapause eggs were prepared for microinjection. The vector with the transgene and the helper plasmid as source of *piggyBac* transposase were microinjected into eggs with a concentration of 0.2 µg/µl respectively [17]. The silkworms derived from microinjection (G0) were grown and the moths were crossed in a single mating manner and G1 eggs were collected. Acid treatment with HCl (specific gravity at 15 °C: 1.11) was performed within 16 h ~ 20 h after egg laying to break the diapause. Transgenic silkworms were detected using a fluorescence microscope (M165FC, Leica Microsystems Ltd., Germany).

3.2.4. Inverse PCR analysis

The genomic insertion loci of the transgene were investigated by inverse PCR. Genomic DNA was extracted from silkworm eggs using the DNeasy Blood & Tissue Kit (Qiagen) and digested by *Sau3*A I (Takara, Japan). After phenol/chloroform extraction and ethanol purification of the digested DNA fragments, self-ligation was performed using T4 ligase (Thermofisher Scientific, USA) at 4 °C for 16 h. The DNA fragments including genomic sequence were amplified by PCR (35 cycles, 58 °C annealing temperature, 15 s annealing, 2 min elongation; Ex Taq® Hot Start Version, Takara, Japan) and *piggyBac* L-arm specific primers (Primers 25 and 31, see Table S3.1 in Supporting information). The PCR products were purified by agarose gel extraction (QIAEX II Gel Extraction Kit, Qiagen, Netherlands) and introduced into a TOPO TA vector (Thermofisher Scientific, USA). After transformation of competent E. coli (C2987H, NEB, USA), positive clones were screened by PCR (Primers 25 and 31, see Table S3.1 in Supporting information). After extracting DNA from the positive clones of E. coli (illustra plasmidPrep Mini Spin Kit, GE Healthcare, UK), it was prepared for sequencing by Big Dye reaction (Thermofisher Scientific, USA) with TOPO TA specific primers (M13 forward and reverse, Thermofisher Scientific, USA) flanking the insertion site. A 3031xl Genetic Analyzer sequencing device (Applied Biosystems, Hitachi Japan) was used for the sequence analysis. The results of sequencing were analyzed with the Silkworm Genome Database (KAIKObase) and the insertion loci were confirmed manually.

3.2.5. Preparation of Silk Fibroin solution

20 g of silk cocoon shells were degummed by cutting them up and sinking them in 2 liters of 2 % $NaCO_3$ solution at 95°C for 30 min. After washing with 95 °C hot reverse osmosis water (ROW) and subsequent drying, 3 g of SF coils were put into 50 ml of 9 M LiBr over night while stirring and the resulting solution was dialyzed (cellulose-based dialysis tube, MWCO 12000-14000, 2-316-02, AS ONE, Japan) against 8 liters of deionized water for 3 days, with 6 solvent changes to remove LiBr and centrifuged at 30,000× g rcf for 5 min to remove impurities. Afterwards the concentration of SF in the solution was determined by drying and weighing of a defined volume.

3.2.6. SDS-PAGE

The samples and control were adjusted to a concentration of 2 mg/ml for SDS-PAGE with ROW. 50 µl of each sample were added to 50 µl of DTT containing 2x loading buffer (AE-1430, EzApply, ATTO, Japan), spun down and kept at 98°C for 5 minutes. After setting up gel chamber (WSE-1100, ATTO, Japan), 1 x electrode buffer (EzRun, ATTO, Japan), and 5-20 % gel (e-PAGEL, E-T520L, ATTO, Japan), samples were loaded (20 µl per well) and run with a protein ladder (Ezprotein ladder, WSE-7020, ATTO, Japan) as marker standard. The electrophoresis was run for 75 min at 20 mA. Afterwards the gel was kept in CBB staining solution (AE-1340 EzStain Aqua, ATTO, Japan) and subsequently washed with ROW.

3.2.7. Western Blotting

In preparation of blotting a SDS-PAGE was performed, without the staining and the following washing step. The separated proteins in the gel were transferred to a blotting membrane (clearBlot Membrane P-Plus, WSE-4051, ATTO, Japan) via a blotting device (WSE-4110, ATTO, Japan) at a voltage of 24V. Phosphate-buffered saline without additional calcium ions (PBS (-)) buffer was used for washing and 1 wt% Casein (Wako, Japan) in PBS (-) buffer was used for blocking. A custom-made rabbit anti-P7 polyclonal antibody (final concentration of 0.53 µg/ml, eurofins, Luxembourg) was used as primary antibody and Anti-Rabbit IgG VHH Single Domain conjugated with horseradish peroxidase (final concentration of 0.05 µg/ml, ab191866, abcam, UK) was used as secondary antibody. Bands were visualized via the reaction of horse raddish peroxidase after adding the staining solution (EZblue, ATTO, Japan).

3.2.8. ELISA

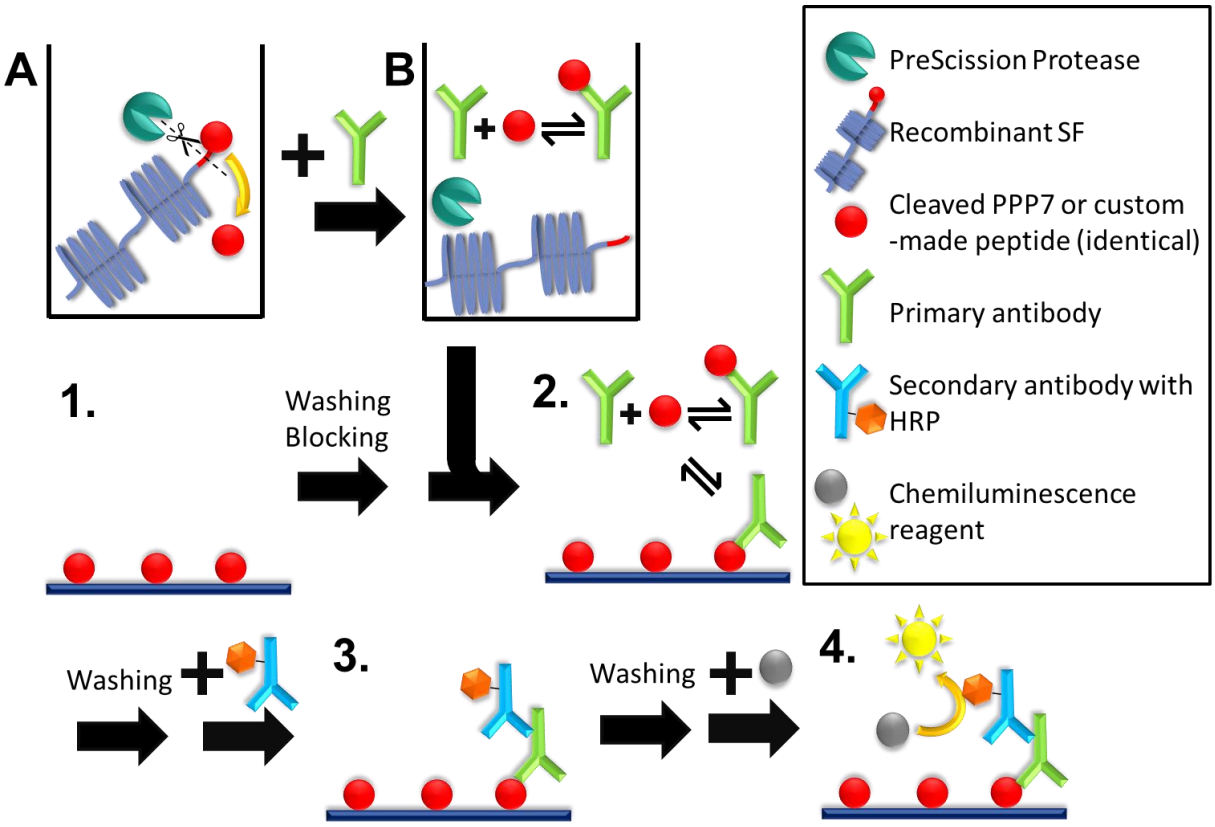

Figure 3.2: ELISA workflow. (A) Digestion of recombinant SF with PreScission Protease. (B) Binding of added primary antibody to free, cleaved PPP7. (Step 1) Coating of ELISA plate wells with custom-made peptide. (Step 2) After washing, blocking and addition of equilibrated solution from (B) competition reaction of primary antibody with wall-coated custom-made peptide and cleaved PPP7 occurs. (Step 3) After washing and addition of secondary antibody, secondary antibody binds to primary antibody. (Step 4) After washing and addition of chemiluminescence reagent, chemiluminescence is ellicited by reaction of the horse raddish peroxidase (HRP) bound to the secondary antibody. Chemiluminescence in each well is measured.

2 mg of dissolved recombinant SF were digested in protease buffer (prepared according to protease protocol) with 10 U of PreScission Protease (GE Healthcare, UK) at 4°C for at least 16 h (Figure 3.2A). Prior to conducting the assay sample solutions were prepared by 1:5 dilution of the enzyme digest with phosphate buffer (Wako, Japan). In order to account for any possible influences of the protease buffer on the assay performance, the standard solutions were prepared with a similar protease buffer content as the samples. Each plate (Nunc no. 437111, Thermofisher Scientific, USA) well was coated with the custom-made

peptide GPLLQATLGGGS (GenScript Japan Inc, Japan), which corresponds to the peptide sequence of PPP7 as shown in Figure 3.1B after cleavage by PreScission protease (Figure 3.2 Step 1). For coating, 100 µl of the peptide (5 µg/ml) were applied per each well, whereas some wells were left uncoated for use as blank. The plate was sealed and put into a shaking incubator at 37 °C for 1 h. Afterwards the wells were washed 2 times for 1 min with 200 µl washing buffer (0.1 v/v% Tween 20 in phosphate buffer) and 2 times for 5 min with 200 µl phosphate buffer. Then 100 µl blocking solution (1 w/v% Casein in phosphate buffer) were added to each well, the plate was sealed and incubated while shaking at 37 °C for 1 h. At the same time standard solutions and sample solutions were diluted 1:1 with primary antibody solution (concentration of 0.4 µg/ml before 1:1 dilution), custom-made rabbit anti-P7 polyclonal antibody, (eurofins, Luxembourg) and preincubated at RT for 1 h (Figure 3.2B). Afterwards the blocking solution was removed, and preincubated standard solutions and sample solutions were added to the wells (Figure 3.2 Step 2). A standard solution without peptide was added to non-coated wells as blank. Each sample, standard and blank was prepared 8-fold. After incubation in the shaking incubator for 1 h at 37 °C the plate was washed as already described and secondary antibody solution was added to each well (concentration of 0.05 µg/ml, ab191866, abcam, UK) and the plate was sealed (Figure 3.2 Step 3). After incubation while shaking at 37 °C for 1 h the solution was removed from each well and the plate was washed as previously described. Then SuperSignal reaction Mix (Thermofisher Scientific, USA) was prepared and 100 µl were added to each well. After gently shaking the plate for 1 min, the plate was inserted into a luminometer (ATTO bioinstrument luminescenser JNRII AB-2300) and the chemiluminescence at 425 nm in each well was measured one time within the first and fifth minute after addition of the reaction mixture (Figure 3.2 Step 4).

The chemiluminescence data obtained was processed into a calibration curve by Origin software (Sigmoidal Boltzmann curve) and the concentration of protease-cleaved PPP7 in recombinant SF was determined. This result was used to calculate the ratio between recombinant and endogenous SF. 1 ml of reaction volume was assumed for all calculations, the molecular weights used are 30 kDa for fibrohexamerin [1], 391.593 kDa for the Fibroin heavy chain (Fib-H) [18],

27.639 kDa for the Fibroin light chain (Fib-L) [19], 1.822 kDa for the recombinant peptide sequence (PPP7), and 1.071 kDa for the cleaved recombinant peptide sequence GPLLQATLGGGS (Cleaved PPP7) used for ELISA (molar mass of P7 containing sequences was calculated by https://web.expasy.org/cgi-bin/peptide_mass/peptide-mass.pl). The SF elementary unit is a hexamer consisting of disulfide-linked heavy and light chains and the glycoprotein fibrohexamerin in a molar ratio of 6:6:1. The calculation was performed as shown below, the used variables are n for the molar amount, c for concentration, M for molar mass and m for mass.

$$n(Cleaved\ PPP7) = \frac{c(Cleaved\ PPP7)}{M\ (Cleaved\ PPP7)} * 1ml$$

$$m(PPP7) = n(Cleaved\ PPP7) * M(PPP7)$$

$$m(SF) = m(sample\ protein) - m(PPP7)$$

$$M(SF\ Hexamer) = 6 * M(SF\ H-chain) + 6 * M(SF\ L-chain) + M(Fibrohexamerin)$$

$$n(SF\ Hexamer) = \frac{m(SF)}{M(SF\ Hexamer)}$$

$$n(SF\ L-chain) = n(SF\ Hexamer) * 6$$

$$Recombinant\ SF\ L-chain\ content = \frac{n(Cleaved\ PPP7)}{n(SF\ L-chain)}$$

3.2.9. Quartz crystal microbalance testing

The method for sample immobilization was selected according to the recommendation of the measurement device maker [20]. Quartz crystal microbalance (QCM) cells were washed with piranha solution (H_2SO_4:H_2O_2 = 1:3). After washing, Lipoamido-dPEG$_8$-acid (1 mmol/l, Quanta BioDesign, Ltd, USA) prepared with Dimethyl sulfoxide (DMSO) was added dropwise to the cell, and the mixture was kept for 1 h at room temperature. After coating, m-dPEG$_8$-Lipoamide (1 mmol/l, Quanta BioDesign, Ltd, USA) prepared in DMSO was added dropwise to the cell, and the mixture was kept for 1 h at room temperature. After washing 3 times with PBS (-) (Wako, Japan), N-Hydroxysulfosuccinimide (0.1 mol/l, Sigma-Aldrich, US) and 1-Ethyl-3-(3-dimethylaminopropyl)-

carbodiimide (0.1 mol/l, Dojindo Molecular Technologies, Japan) were mixed in equal amounts. The mixture was added to the QCM cell and kept at room temperature for 1 h. After washing 3 times, 5 µl of 1 mg/ml aqueous silk fibroin solution were added dropwise to the cell, and the solution was kept at room temperature for 1 h. After washing 3 times with PBS (-), the cell was treated with 1 mg/ml 2-Aminoethanol Hydrochloride (1 mg/ml, Wako, Japan) at room temperature for 1 h. The cell was washed again 3 times with PBS (-) and kept at room temperature until the next day. Then PBS (-) was added to the cell and dissolved bFGF was added 4 times, whereas bFGF was only added after the QCM measurement indicated an equilibrium between surface bound and free bFGF.

3.3. Results and Discussion

3.3.1. Confirmation of successful transgenesis

3.3.1.1. Fluorescent Individuals

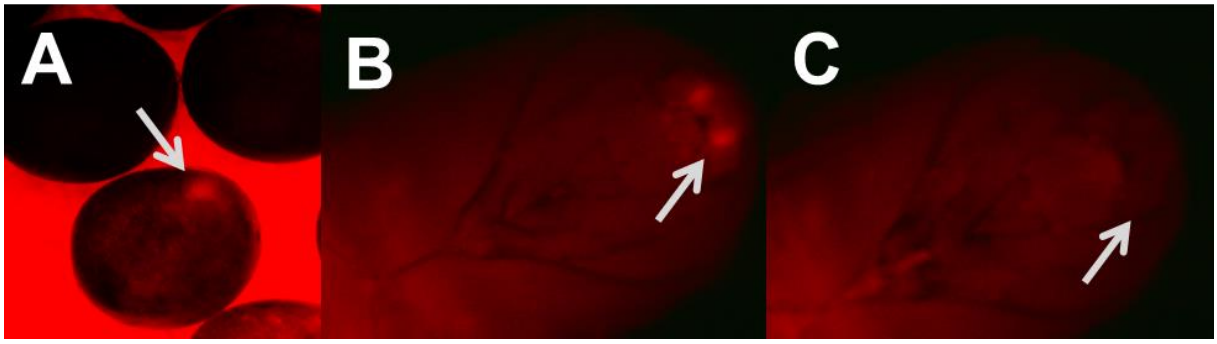

Figure 3.3: The eggs (A) and pupa (B) of transgenic line 2-23 and control pupa (C) during screening by expression of the reporter gene *DsRed2*. Arrows in (A) and (B) indicate fluorescence by *DsRed2* in eyes; Arrow in (C) indicates the absence of fluorescence in eye region.

As shown in Figure 3.1A, the transformation vector contains the SF L-chain transgene as well as the *DsRed2* gene with a 3xP3 promotor which is activated in the nervous system of B. mori [21]. After microinjection the next generation's eggs were screened by expression of the marker gene *DsRed2* driven by the 3xP3 promotor. Figure 3.3A shows how the eggs of our transgenic individuals exhibit fluorescence in the eyes as indicated by the grey arrow, whereas other individuals remain dark. Shown individuals are of transgenic line 2-23; individuals

of line 2-26 and 2-35 show the same phenotype. Transgenic individuals were selected by further breeding which led us to establish the transgenic lines 2-23, 2-26 and 2-35. Before each mating step fluorescence of pupae was confirmed, similar to the transgenic eggs (Figure 3.3B). As indicated by the grey arrow, the fluorescent eyes clearly indicate expression of the reporter gene, while the control shows no fluorescence of eyes (Figure 3.3C).

3.3.1.2. SDS-PAGE and Western Blot

SDS-PAGE was performed to confirm the size of the recombinant protein, the result is shown in Figure 3.4A. The bands show a smear-like morphology in the high molecular weight area, where SF H-chains are located. The significant SF L-chain band (lanes 2-4) is also visible next to the marker band at 25 kDa (lane 1) as indicated by the arrow. The picture shows that no difference in band size is visible between recombinant SF and WT SF (lane 5). This is to be expected as the recombinant peptide (PPP7) only has a molecular weight of approximately 1.8 kDa. Figure 3.4B shows the results of western blotting with a P7 specific antibody. Upon comparison with the recombinant SF and WT SF, the former shows clear bands at 25 kDa but the latter shows no band. This proves that the transgenic silkworm lines 2-23, 2-26 and 2-35 produce recombinant SF.

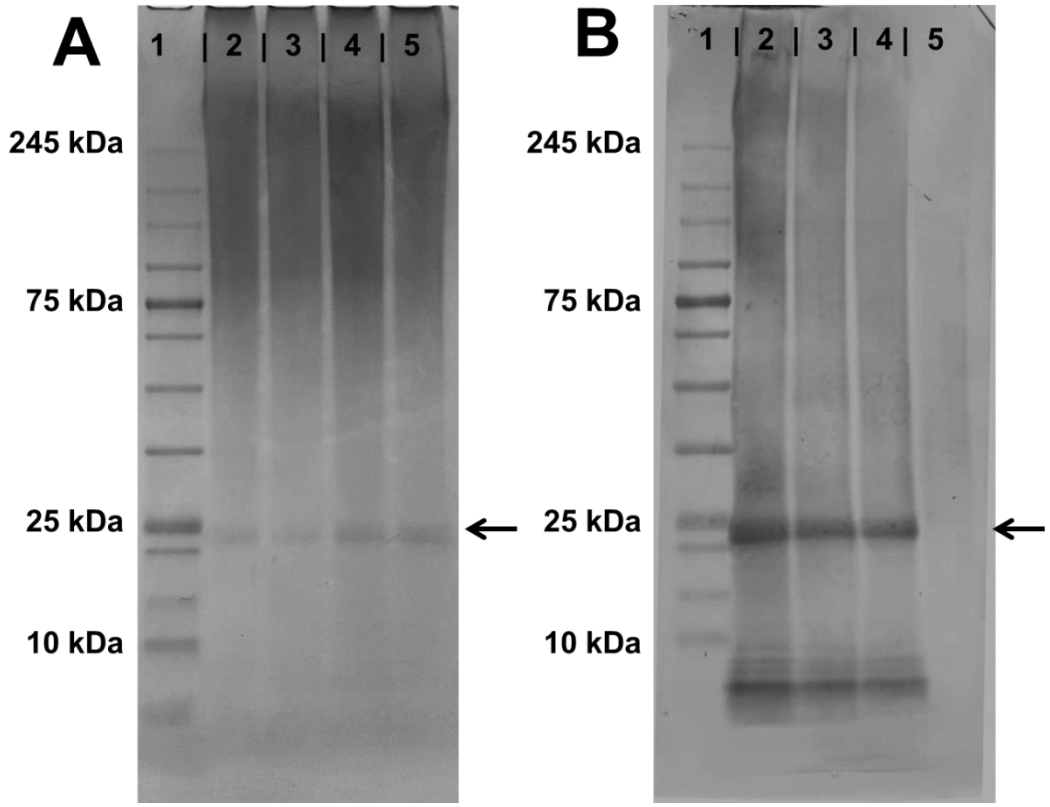

Figure 3.4: SDS-PAGE (A) and Western Blot (B) of recombinant SF and control WT SF with identical lane assignment. Lane 1: marker; lane 2: line 2-23 recombinant SF; lane 3: line 2-26 recombinant SF; lane 4: line 2-35 recombinant SF; lane 5: WT SF. Arrows indicate molecular weight region of recombinant SF L-chain.

3.3.1.3. Inverse PCR

The *piggyBac* Transposon system leads to integration of the transgene into a random TTAA site in the genome.Thus, inverse PCR was performed in order to determine the integration site, whereas results could only be obtained for the sequence flanking the *piggyBac* left arm site of line 2-23. After sequencing the result was inserted into the *B. mori* genome database KAIKObase (https://sgp.dna.affrc.go.jp/KAIKObase/) and the transgene locus in the genome was confirmed. The transgene was inserted into an intron of a cytochrome p450 gene located on chromosome 18 (scaffold 2; Accession number NP_001121192). Figure S3.2 shows the insertion locus and sequence at the insertion site.

3.3.2. Quantification and Binding Affinity

3.3.2.1. Quantification of recombinant Fibroin L-chain by ELISA

As the individuals of the transgenic lines have a normal SF L-chain gene as well as a transgenic SF L-chain gene, both genes are expressed when the silkworm is

spinning its cocoon. This leads to a mixture of recombinant and endogenous SF L-chains in the obtained SF. For estimation of the recombinant P7 efficacy it is necessary to measure the amount of recombinant SF L-chains expressed. In order to measure the amount of recombinant P7 an ELISA was established that was able to measure the P7 peptide concentration after cleavage from recombinant SF by a protease. The same peptide was custom ordered and used for making a standard curve as shown in Figure 3.5. As a result of calculation the percentage of recombinant SF L-chain of SF L-chains was 26.75 % ± 9.46 % in line 2-23, 23.96 % ± 9.58 % in line 2-26 and 16.18 % ± 6.40 % in line 2-35. Four assays were performed for lines 2-23 and 2-26 and three assays for line 2-35. Whereas all samples, standards and blanks were prepared 8-fold for each assay, the 2-35 recombinant SF sample could only be preprared 4-fold for the result shown in Figure 3.5A.

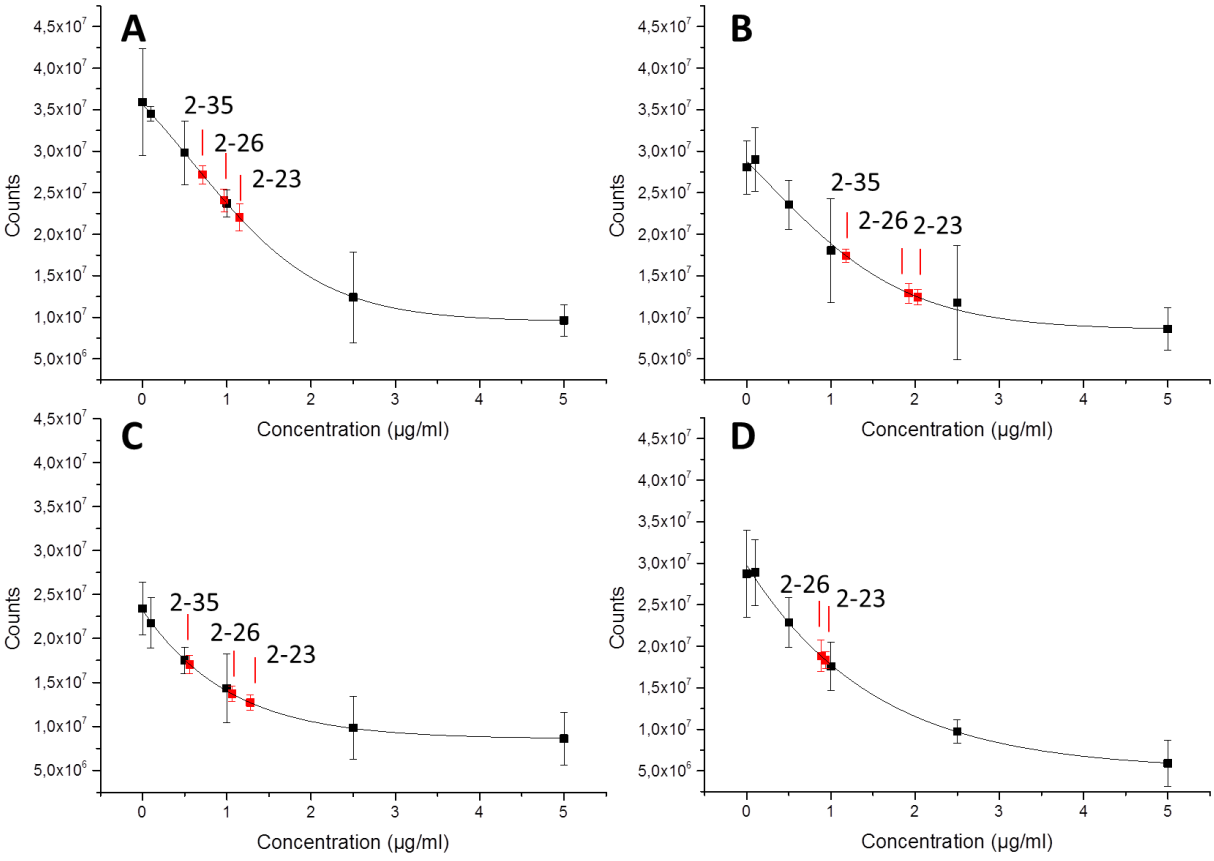

Figure 3.5: ELISA standard curves for determination of P7 content in recombinant SF. Determined P7 concentrations are marked in red.

3.3.2.2. Binding affinity by QCM

The affinity constant of SF to bFGF for WT SF and line 2-23 recombinant SF was successfully determined by QCM. The results showed an affinity constant of 2.92×10^7 for WT SF whereas the recombinant SF had an affinity constant of 3.56×10^7. The measurement could only be conducted sucessfully once, therefore the determined binding affinity should still be considered as preliminary. Nonetheless, the difference in binding affinity indicates an enhanced bFGF binding affinity of our new recombinant SF compared to WT SF.

3.4. Conclusion

In this work we successfully prepared a novel recombinant SF with the ability to specifically bind the growth factor bFGF. The three transgenic lines 2-23, 2-26 and 2-35 could be established, and it was confirmed that the SF from line 2-23 contains the highest amount of recombinant SF L-chains with a content of 26.75 %. The genomic insertion locus for line 2-23 was confirmed and the affinity measurement by QCM indicates an increased binding affinity of our recombinant SF to bFGF compared to wild type SF. This carries great potential for therapeutic application, as SF matrices can be designed to be loadable with bFGF in desirable amounts for timed release. As the SF matrix supplies bound bFGF, the growth factor would be able to elicit its effect to cells in direct proximity immediately upon release. Further, bound bFGF is expected to be stable for a longer period of time than free bFGF. This opens up exciting possibilities for addition of our recombinant SF to scaffolds for tissue engineering or wound healing gels. As such we are looking forward to continue our research and further investigate upon the beneficial properties and applicability of our improved recombinant SF.

3.5. Supporting information

Table S3.1: Primer Data. Sequence homologies for HD infusion are underlined.

Application Primer Name Target	Primer Sequence 5' to 3'
Inverse PCR 25 (Forward) pBac L arm	CGCATTGACAAGCACGCCTC
Inverse PCR 31 (Reverse) pBac L arm	TGACGAGCTTGTTGGTGAGGATTCT
HD infusion pB15L Forward SF Lchain transgene	TACGCGTACGGCGCGTCGATTGGCGCGCCGGTACGGTTC
HD infusion pB15L Reverse SF Lchain transgene	GCCATTCGAATTCGGCGATTGGCCGGCCCATGACAACAG
Sequencing Lseq Forward Lchain before MCS	ATGCAATCTTAGCCAGCAGTGACT
Sequencing pBseq Forward Before *Asc I* site	ATAATCAGCCATACCACATTTGTA
Transformation Check FL-490 F Lchain before MCS	TCATCTTCATTAGAAACTAAACCT
Transformation Check FL-1030 R Lchain before MCS	CTGTGTAAGAGTTAATGACGTTAG
Transformation Check 30ntFL1092F Lchain before MCS	ATCTCTCGGTCCCTTCTTCGGACACGTGGG
Transformation Check 30ntFL1392R Lchain before MCS	TGATTGGTGGAACACTTGAGCAACCGGGGG
Transformation Check 30ntP7R P7 sequence	CTATTAGGACCCACCTCCCAGCGTAGCTTG
Presence Check FL-Forward1 Lchain before MCS	AATCAACTCGTCATCAACCCTGGT
Presence Check P7-Reverse1 P7 sequence	CTATTAGGACCCACCTCCCAGCGTA

***Bam*H I** **PPP7** ***Sal* I**

TAATGACGCGGGATCCCTGGAAGTTCTGTTCCAGGGGCCCCTTCTCCAAGCTACGCTGGGAGGTGGGTCCTAATAGTCGACATCCCCAGGT

Figure S3.1: Oligonucleotide cassette with 91 bp length coding for transgenic insert PPP7 and sequence homologies for the HD infusion protocoll (underlined).

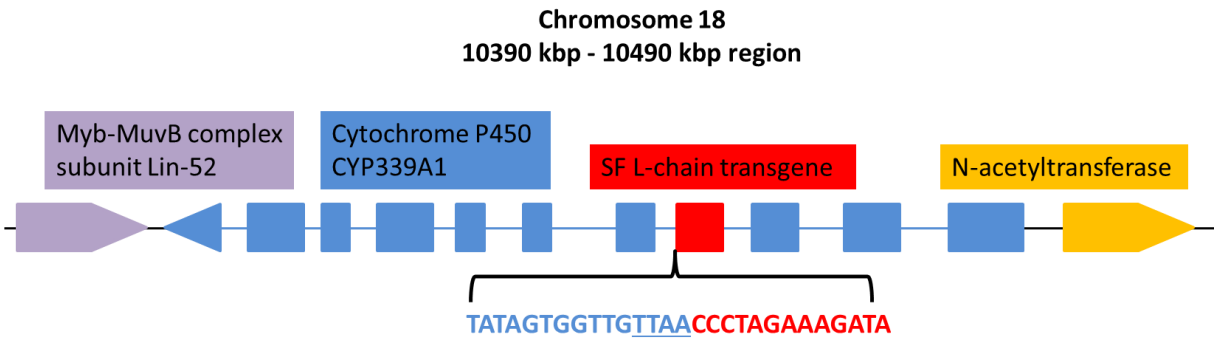

Figure S3.2: Schematic diagram of insertion locus of SF L-chain transgene in chromosome 18, 10390 kbp to 10490 kbp region. The transgene (red) was inserted into an intron of the cytochrome P450 CYP339A1 gene (blue). Exons are shown as boxes, lines inbetween of the same color show introns, the triangle shows an exon and indicates the reading direction. The sequence detected by inverse PCR is shown in a bracket below the transgene: letters in blue show the intron sequence, letters in red show the transgene sequence *(piggyBac* L arm). Adjacent genes (Myb-MuvB complex subunit Lin-52, violet; N-acetyltransferase, yellow) on the chromosome are also indicated. The diagram does not reflect the actual or relative size of gene segments.

3.6. References

1. Inoue, S.; Tanaka, K.; Arisaka, F.; Kimura, S.; Ohtomo, K.; Mizuno, S. Silk fibroin of Bombyx mori is secreted, assembling a high molecular mass elementary unit consisting of H-chain, L-chain, and P25, with a 6:6:1 molar ratio. J. Biol. Chem. 2000, 275, 40517–40528, doi:10.1074/jbc.M006897200.

2. Tanaka, K.; Inoue, S.; Mizuno, S. Hydrophobic interaction of P25, containing Asn-linked oligosaccharide chains, with the H-L complex of silk fibroin produced by Bombyx mori. Insect Biochemistry and Molecular Biology 1999, 29, 269–276, doi:10.1016/S0965-1748(98)00135-0.

3. Feng, X.-B.; Zheng, Z.-W.; Zhang, X.; Gu, J.; Feng, Q.-L.; Huang, L.-H. Discovering genes responsible for silk synthesis in Bombyx mori by piggyBac-based random insertional mutagenesis. Insect science 2019, 26, 821–830, doi:10.1111/1744-7917.12595.

4. Tamura, T.; Thibert, C.; Royer, C.; Kanda, T.; Abraham, E.; Kamba, M.; Komoto, N.; Thomas, J.L.; Mauchamp, B.; Chavancy, G.; et al. Germline transformation of the silkworm Bombyx mori L. using a piggyBac transposon-derived vector. Nat. Biotechnol. 2000, 18, 81–84, doi:10.1038/71978.

5. Hino, R.; Tomita, M.; Yoshizato, K. The generation of germline transgenic silkworms for the production of biologically active recombinant fusion proteins of fibroin and human basic fibroblast growth factor. Biomaterials 2006, 27, 5715–5724, doi:10.1016/j.biomaterials.2006.07.028.

6. Kambe, Y.; Kojima, K.; Tamada, Y.; Tomita, N.; Kameda, T. Silk fibroin sponges with cell growth-promoting activity induced by genetically fused basic fibroblast growth factor. J. Biomed. Mater. Res. A 2016, 104, 82–93, doi:10.1002/jbm.a.35543.

7. Burgess, W.H.; Maciag, T. The heparin-binding (fibroblast) growth factor family of proteins. Annu. Rev. Biochem. 1989, 58, 575–606, doi:10.1146/annurev.bi.58.070189.003043.

8. Gospodarowicz, D.; Ferrara, N.; Schweigerer, L.; Neufeld, G. Structural characterization and biological functions of fibroblast growth factor. Endocr. Rev. 1987, 8, 95–114, doi:10.1210/edrv-8-2-95.

9. Shing, Y.; Folkman, J.; Sullivan, R.; Butterfield, C.; Murray, J.; Klagsbrun, M. Heparin affinity: purification of a tumor-derived capillary endothelial cell growth factor. Science 1984, 223, 1296–1299, doi:10.1126/science.6199844.

10. Li Feng; Li, Y.; Zeng, W.; Xia, B.; Zhou, D.; Zhou, J. Enhancing effects of basic fibroblast growth factor and fibronectin on osteoblast adhesion to bone scaffolds for bone tissue engineering through extracellular matrix-integrin pathway. Exp. Ther. Med. 2017, 14, 6087–6092, doi:10.3892/etm.2017.5320.

11. Wang, R.; Liu, W.; Du, M.; Yang, C.; Li, X.; Yang, P. The differential effect of basic fibroblast growth factor and stromal cell‐derived factor‐1 pretreatment on bone morrow mesenchymal stem cells osteogenic differentiation potency. Mol. Med. Rep. 2018, 17, 3715–3721, doi:10.3892/mmr.2017.8316.

12. ESTAPÉ, D.; van den HEUVEL, J.; RINAS, U. Susceptibility towards intramolecular disulphide-bond formation affects conformational stability and folding of human basic fibroblast growth factor. Biochem. J. 1998, 335, 343–349, doi:10.1042/bj3350343.

13. CACCIA, P.; NITTI, G.; CLETINI, O.; PUCCI, P.; RUOPPOLO, M.; BERTOLERO, F.; VALSASINA, B.; ROLETTO, F.; CRISTIANI, C.; CAUET, G.; et al. Stabilization of recombinant human basic fibroblast growth factor by chemical modifications of cysteine residues. Eur J Biochem 1992, 204, 649–655, doi:10.1111/j.1432-1033.1992.tb16678.x.

14. Li, Q.; Gao, S.; Yu, Y.; Wang, W.; Chen, X.; Wang, R.; Li, T.; Wang, C.; Li, X.; Wu, X. A novel bFGF antagonist peptide inhibits breast cancer cell growth. Mol. Med. Rep. 2012, 6, 210–214, doi:10.3892/mmr.2012.882.

15. Shiomi, K.; Takasu, Y.; Kunii, M.; Tsuchiya, R.; Mukaida, M.; Kobayashi, M.; Sezutsu, H.; Ichida Takahama, M.; Mizoguchi, A. Disruption of diapause induction by TALEN-based gene mutagenesis in relation to a unique neuropeptide signaling pathway in Bombyx. Scientific reports 2015, 5, 15566, doi:10.1038/srep15566.

16. Inoue, S.; Kanda, T.; Imamura, M.; Quan, G.-X.; Kojima, K.; Tanaka, H.; Tomita, M.; Hino, R.; Yoshizato, K.; Mizuno, S.; et al. A fibroin secretion-deficient silkworm mutant, Nd-sD, provides an efficient system for producing recombinant proteins. Insect Biochemistry and Molecular Biology 2005, 35, 51–59, doi:10.1016/j.ibmb.2004.10.002.

17. Toshiki Tamura, Nobuo Kuwabara, Keiro Uchino, Isao Kobayashi, Toshio Kanda. An Improved DNA Injection Method for Silkworm Eggs Drastically Increases the

Efficiency of Producing Transgenic Silkworms. Journal of Insect Biotechnology and Sericology 2007, 155–159.

18. Silk Fibroin H-chain molecular mass. https://www.uniprot.org/uniprot/P05790 (accessed on 12.09.20).

19. Silk Fibroin L-chain molecular mass. https://www.uniprot.org/uniprot/Q7JYG3 (accessed on 12 September 2020).

20. Immobilization methods for QCM. http://www.initium2000.com/en/method/ (accessed on 27 December 2020).

21. Berghammer, A.J.; Klingler, M.; Wimmer, E.A. A universal marker for transgenic insects. Nature 1999, 402, 370–371, doi:10.1038/46463.

4. Chapter
A Facile and Sustainable Pathway to Functional Cellulose Nanofibers with Flame-retardant and Catalytic Properties

4. Chapter – A Facile and Sustainable Pathway to Functional Cellulose Nanofibers with Flame-retardant and Catalytic Properties

4.1. Introduction

In chapter 2 the improvement of mechanical properties of a SF-based scaffold for BTE was demonstrated by composition of SF with cellulose. Though the properties of the composite were well suited for BTE application, the production method required a harmful, organic solvent. In order to establish a safer solvent system for making SF/cellulose composites a $ZnCl_2$-based solvent was investigated, whereas coprecipitation did unfortunately not yield desirable material properties. Nonetheless, after the $ZnCl_2$-treatment the used cellulose pulp was very finely fibrillated. With this finding the initial focus was adjusted to investigate the use of $ZnCl_2$ for the production of cellulose nanofibers. As $ZnCl_2$ pretreatment seemed promising as an energy-saving measure for fibrillation, this work aimed to improve the general feasibility of cellulose nanofiber application, in particular the use of cellulose nanofibers as structural compound for BTE scaffolds.

Nano-structured cellulose is a term for cellulosic materials with the size of at least one dimension being in the nanometer range [1], whereas nanofibrillar and nanocrystalline cellulose are the two most known subforms. Commercial uses for nanocellulose include the use as absorbent in diapers and rheology modifier in pen inks (cellulose nanofibrils) [2,3], or as food product by the name “nata de coco” (cellulose of bacterial origin) [4]. The application of cellulose nanofibrils and nanocrystals is also considered for use in composites, whereas the high aspect ratio of nanofibrils [5,6], and the high crystallinity and strength of nanocrystals [7] are both useful for enhancing composite properties. An example for this is the use of nanocellulose together with brittle, silica-based materials for bone tissue engineering, with the nanocellulose component aiding the stability of the material [8]. Cellulose nanofibrils and nanocrystals also exhibit osteoconductive behavior [9] and many methods have been established to form tissue engineering scaffolds with varying elastic modulus, pore size and interconnectivity [10]. The defibrillation of fibers to nanocellulose requires energy-intensive - and thus costly

- mechanical treatments. Therefore to reduce the energy demand and increase the economic viability, biotechnological, chemical or physical treatments are often performed [11,12]. Such pretreatments commonly augment the accessibility of hydroxyl groups, break physical inter-fibrillar interactions and reduce crystallinity [13]. One group of solvents used for cellulose pretreatment are molten salt hydrates which are non-derivatizing, though they can be used as media for chemical derivatization [14–16]. $ZnCl_2$ hydrate is the inorganic molten salt hydrate [16] most widely used for dissolution of cellulose and as a medium for hydrolysis and derivatization [17]. The latter use is related to the catalytic ability of $ZnCl_2$ to act as a Lewis acid and to promote esterification reactions [18,19]. $ZnCl_2$ is a low-cost chemical with low risk of volatilization and ignition [20], which is a plus against ordinary organic solvents. Cellulose recovery and regeneration processes from $ZnCl_2$ solutions have also been established [21]. $ZnCl_2$ has also been shown to be recyclable [22], even from a complex biomass mixture [23]. Whether $ZnCl_2$ hydrate is able to dissolve cellulose or only swell it greatly depends on the amount of water present: Cellulose can be only dissolved in the trihydrate ($ZnCl_2$•$3H_2O$), whereas swelling occurs in the cases of the dihydrate or tetrahydrate salt [24,25]. The occurrence of structural changes within the celluloses' crystal lattice is dependent on whether the cellulose has only been swollen by $ZnCl_2$ hydrate or had been dissolved. The swelling of cellulose with this salt hydrate has been described to affect the cellulose I crystal structure only slightly or not at all [26,27], while dissolution and subsequent regeneration of cellulose obviously yields a cellulose II crystal lattice [24].

$ZnCl_2$ hydrate melts are used to obtain vulcanized fibers. This process works by swelling and subsequent gelation of the cellulose fiber exterior, which increases inter-fibrillar adhesion, preserving the native cellulose I structure [21]. The presence of $ZnCl_2$ in the end product can often be desirable due to various beneficial properties of $ZnCl_2$. It acts as an excellent flame retardant which is of obvious use in particular for cellulosic materials [28]. The antimicrobial and antifungal [29] properties of $ZnCl_2$ have also been reported, which led to numerous commercial applications in mouth rinses and dentifrices, as well as considerations as a food preservative [30–32]. The application as preservative might also offer great potential regarding the storage of cellulose nanofibers: this

material is usually stored in never-dried form which is highly susceptible to microbial growth. $ZnCl_2$ was also shown to impose increased freeze tolerance, ion conductivity and temperature dependent shape reversibility properties in cellulose hydrogels when used with $CaCl_2$ [33].

As cellulose nanofibers are investigated for use in bone tissue engineering scaffolds, this work aims to promote the feasibility of cellulose nanofiber application by establishing an environmentally friendly, energy-saving method for their production. To expand on the scope of applications for these nanofibers possible functionalization via $ZnCl_2$ hydrate melt as physical and mild pretreatment was investigated. It met all our prerequisites, offering established recovery procedures, chemical innocuousness, and the plus of simultaneously introducing new advantageous properties. The swelling of the cellulose fibrils by the salt hydrate melt evidently also reduces the amount of energy necessary for homogenization of the fibrils to nanocellulose. This paper demonstrates these advantages and studies the functionalization of these nanocelluloses with regard to their increased thermal stability and catalytic activity.

4.2. Materials and Methods

Dry cellulose fibers in the form of a beech dissolving pulp was provided by Lenzing AG (Lenzing, Austria) and was used for all related experiments. All chemicals were from Sigma-Aldrich Handels GmbH (Vienna, Austria).

4.2.1. $ZnCl_2$ treatment

The dried pulp was blended for 2 min (DeLonghi Blade KG49) in dry state. Then the pulp was added to 20 wt% or 65 wt% aqueous $ZnCl_2$ solutions at a concentration of 4 % (mass cellulose per volume $ZnCl_2$ hydrate). For comparison, a blank sample was produced with the same volume of deionized (DI) water. Upon addition of $ZnCl_2$ solutions or DI water, the samples were mixed using a stirrer and afterwards kept on a shaker for approximately 16 h at room temperature. Finally, the suspensions were diluted with DI water to 0.5 wt%, washed and filtered. The celluloses were dispersed with a magic LAB® UTC dispersion unit (IKA®-Werke GmbH & Co, Staufen, Germany) in DI water (0.4 wt%) at 10000 rpm for 10 min, 15000 rpm for 25 min and 20000 rpm for 10 min. Finally, the dispersions were passed 5 times through a high-pressure

homogenizer (AVP-1000, SPX FLOW, Inc., Charlotte, United States) at a pressure of 800-900 bar. The obtained suspensions ($ZnCl_2$-CNF and blank) were analyzed by rheological measurements and used to prepare cellulose films.

The amount of $ZnCl_2$ in the sample was approximated by thermogravimetric analysis (see TGA section for more information) from the residual mass value at 400 °C, with $ZnCl_2$-pulp and CNF containing approx. 20 wt% (Figure 4.4). This was repeated at different washing stages to produce $ZnCl_2$-CNF-h with 33 wt% $ZnCl_2$.

4.2.2. Film preparation

Films were prepared from fibrillated celluloses by filtration through a filter sandwich composed of a glass fiber filter (grade 696, porosity of 1.2 µm, VWR International GmbH, Vienna, Austria) topped with a paper filter. The wet film was dried in a hot press at 80°C and 1 bar pressure.

4.2.3. Flammability test

Flammability tests were performed with paper strips produced from CNF-$ZnCl_2$, CNF-$ZnCl_2$-h and non-$ZnCl_2$-treated sample (blank), having the same dimension (7.4 cm x 1.5 cm and a thickness of approx. 0.02 cm), produced analogously to the “film preparation”.

All samples and the reference were fixed at the same distance from the flame source (lighter) (see Figure 4.6 and Figure 4.7). The flame source was switched on for a total of 20 s to ignite the respective samples. Pictures of the sample were taken sequentially to estimate the flame resistance of the samples. The residual mass percentage after the test (mass of sample after 20 s ignition / mass of sample at t_0 *100) was measured in duplicate and averaged values are reported.

4.2.4. Fiber acetylation

The catalytic activity of $ZnCl_2$-CNF50 in acetylation was studied by comparison to the same reference material as in the flammability test. The sample was immersed in acetic anhydride for 10 s, removed and transferred into a 20 ml glass vial. The sample was then heated at 60 °C in an oven for 4 h and finally analyzed by IR to qualitatively evaluate the acetylation efficiency.

4.2.5. Sample preparation for gel permeation chromatography (GPC) and nuclear magnetic resonance spectroscopy (NMR)

The 0.5 % cellulose dispersion was washed extensively and dried with a suction filter. Part of the dried cellulose was used for NMR analysis as it was. The remaining cellulose was washed with DI water, ethanol and DMAc, before being dissolved in DMAc/9% LiCl. The dissolved sample was analyzed by GPC.

The solid-state NMR experiments were performed by using a Bruker Avance III HD 400 spectrometer with a resonance frequency of ^{1}H of 400.13 MHz, and ^{13}C of 100.61 MHz, respectively. A 4 mm dual broadband CP-MAS probe was equipped. ^{13}C spectra were measured by using the TOSS (total sideband suppression) sequence at ambient temperature with a spinning rate of 5 kHz. Other measurement settings were a cross polarization (CP) contact time of 2 ms, a recycle delay of 2 s, SPINAL-64 ^{1}H decoupling, an acquisition time of 49 ms, and a spectral width set to 250 ppm. The chemical shifts were externally referenced against the carbonyl signal of glycine with δ = 176.03 ppm. Before Fourier transformation the acquired FIDs were apodized with an exponential function (lb = 11 Hz). Crystallinity was estimated by the area of the crystalline C4 peak divided by the areas of the amorphous and crystalline contribution of the C4 peak. All materials for solid-state NMR were air-dried at room temperature before measurement.

The GPC measurement setup comprised an online degasser Dionex (Sunnyvale, California, United States) DG-2410; a Kontron (Augsburg, Germany) 420 pump, pulse damper; and an auto sampler, HP 1100. Further, a column oven, Gynkotek (Munich, Germany) STH 585; and a MALLS detector, Wyatt (Santa Barbara, California, United States) Dawn DSP with argon ion laser (λ_0= 488 nm); as well as a RI detector, Showa Denko (Tokyo, Japan) Shodex RI-71 were used. The data was evaluated with Wyatt ASTRA software. The measurement settings were as follows: a flowrate of 1.00 ml/min was set; and four columns from Agilent Technologies (Santa Clara, California, United States) PLgel mixed-A LS, 20 µm, 7.5 × 300 mm were used. Furthermore the injection volume was set at 100 µl (sample concentration: 10-20 mg/ml); the run time was 45 min and DMAc/LiCl (0.9 % w/v) was used as mobile phase.

4.2.6. Rheology measurements

The rheological properties of the fibrillated celluloses (blank and $ZnCl_2$-CNF) were studied with a Bohlin Instruments (Gloucester, England) CVO 50 rheometer. All measurements were performed at 25°C using a cone-plate measuring system (4°/40 mm) with a gap size of 150 µm. The shear viscosity was measured at shear rates from 0.1 s^{-1} to 100 s^{-1}.

4.2.7. SEM

Scanning electron microscopy (SEM) was performed to examine the microstructure and surface morphology of cellulose samples. High vacuum secondary electron imaging was performed using an Apreo VS SEM (Thermo Scientific, The Netherlands) at 500 V. Samples were not coated with conductive layers.

4.2.8. TGA

A thermogravimetric analyzer (TG 209 F1, Netzsch, Selb, Germany) was used to monitor the combustion kinetics of the different variations. An Al_2O_3 crucible was loaded with a minimum sample mass of 8 mg. The heating range was defined from 25 °C to 650 °C, with a linear increase of 10 K/min. The whole experiment was performed under atmospheric pressure with an air to nitrogen ratio of 80 to 20, respectively. The flow rate was set to 20 ml/min. As comparison, an analogue experiment was conducted under pure nitrogen atmosphere (Figure 4.4). Two samples per variant were recorded.

4.2.9. Tensile test

For the mechanical characterisation, six samples per variant with a length of 60 mm and a width of 5 mm were prepared. The samples were preconditioned at 45 % r.h. and 21 °C for 24 h. The tensile test was conducted with a universal testing machine (Z20, Zwick-Roell, Ulm, Germany) equipped with a 500 N load cell. The preload was set to 0.2 N and the testing was performed at a displacement rate of 1.5 mm/min. The extension was measured indirectly via the crosshead travel and the modulus of elasticity in the linear-elastic range was adjusted by a linear regression.

4.2.10. NMR measurements

Freeze-dried samples were used for NMR analysis according to Beaumont et al. [34]. The crystallinity index was determined by the peak separation method of the cellulose C4 peaks according to Park et al. [35]. The ratio of cellulose allomorphs I and II was determined by integration of characteristic cellulose I and cellulose II regions identified from literature [36]. A comparison of characteristic regions is shown in Figure S4.5.

4.3. Results and Discussion

4.3.1. Fibrillation to Nanofibers

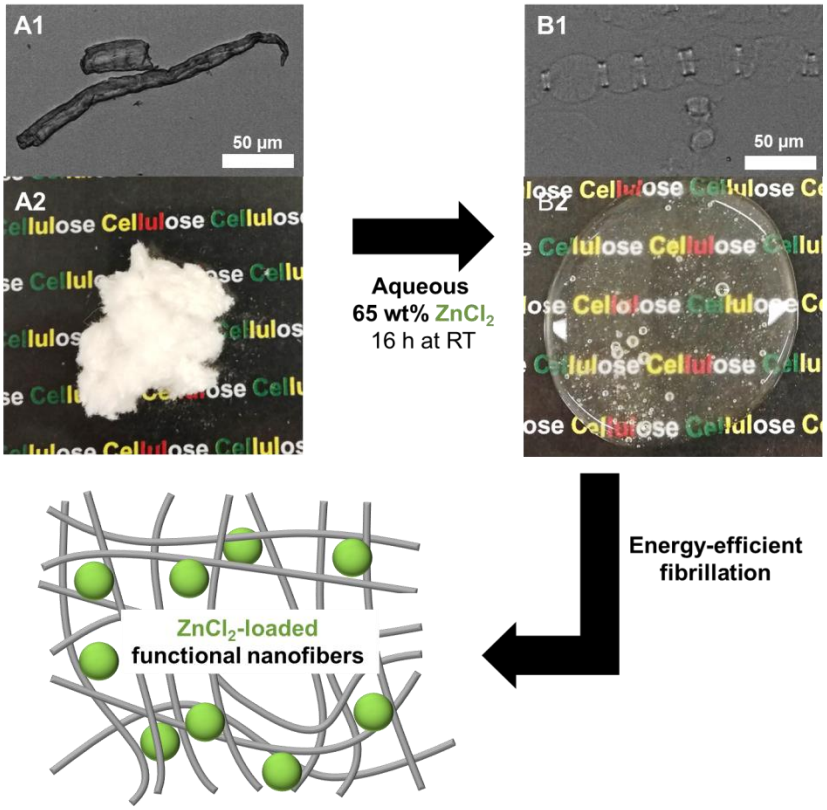

Figure 4.1: Schematic workflow for production of $ZnCl_2$-CNF. Dried cellulose pulp was added to aqueous 65 wt% $ZnCl_2$ solution for 16 h at room temperature. The swelling of the pulp fiber in the melt hydrate is clearly shown by comparison of images of the non-treated (A1-2) and treated fibers (B1-2). The treatment facilitated greatly the necessary energy to defibrillate into nanofibers.

As illustrated in Figure 4.1, the $ZnCl_2$-treatment is simple and straightforward: Dried cellulose dissolving pulp, with a hemicellulose content of only 3.7 % [37], was suspended and equilibrated in an aqueous 65 wt% $ZnCl_2$ solution for 16 h.

This treated pulp ($ZnCl_2$-pulp) was subsequently washed and homogenized by only 5 passes through a high-pressure homogenizer yielding cellulose nanofibers ($ZnCl_2$-CNF). Conventional fibrillation of the same pulp in never-dried state, i.e. without $ZnCl_2$ treatment, has been reported to require approx. 20 passes [38,39], to yield cellulose nanofibers. Please note that comparable fibrillation of dried pulp, which we used in our work, would most likely require an even higher number of passes [40], due to irreversible drying effects, i.e. hornification [41].

Figure 4.1A and 4.1B show the difference in sample condition before and after $ZnCl_2$-treatment, respectively. A distinct change was evident: $ZnCl_2$ induced swelling and ballooning of the fibers (Figure 4.1B1). This is attributed to the interactions of the cellulose surface with the $ZnCl_2$ molten salt hydrate. To better assess the effect of the $ZnCl_2$-treatment on the material properties, all studies were conducted in parallel with the $ZnCl_2$ samples and with blanks treated with water instead but otherwise handled the same. Both sample and blank had the same processing time and received the same mechanical energy input. Other samples were also prepared using 40 wt% and 20 wt% $ZnCl_2$ solutions (Figure S4.2), but notable effects were only observed upon treatment with the 65 wt% $ZnCl_2$ solution.

4.3.2. Mechanical, morphological and molecular properties of cellulose nanofibers

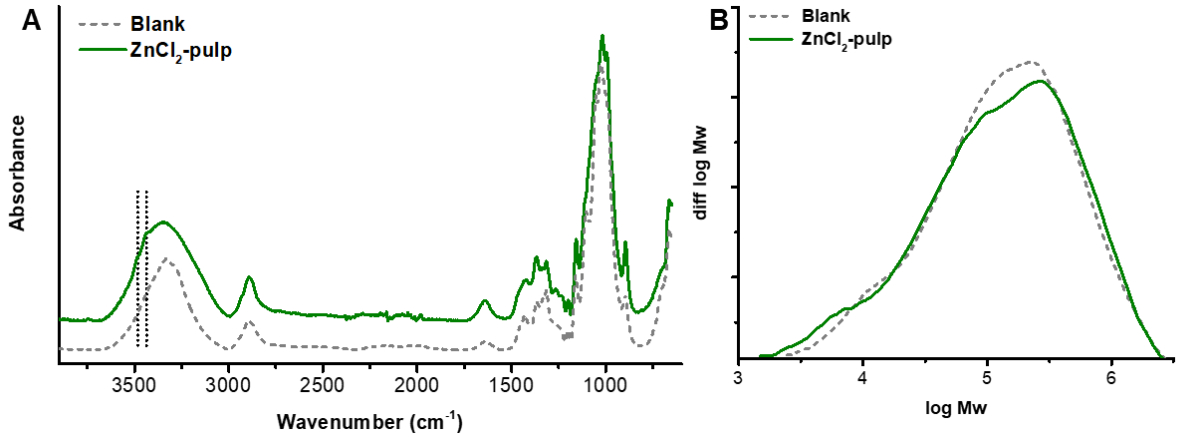

Figure 4.2: Effect of the $ZnCl_2$-treatment on the cellulose structure: infrared spectroscopy (A) and gel permeation chromatography (B). Part of the native cellulose I allomorph was transformed into cellulose II, i.e. regenerated cellulose, as shown in the appearance of characteristic cellulose II bands in the IR spectrum (3491 cm^{-1} and 3447 cm^{-1}). The molar mass distribution was largely unaffected by the treatment.

The $ZnCl_2$-pulp was analyzed by IR spectroscopy (Figure 4.2A), gel permeation chromatography (GPC, Figure 4.2B) and solid-state nuclear magnetic resonance spectroscopy (NMR, Figure 4.3 and Table 4.1) to study the effect of the treatment on the fibers crystalline structure and their molar mass. In all studies, the $ZnCl_2$-treated sample was compared to the blank sample.

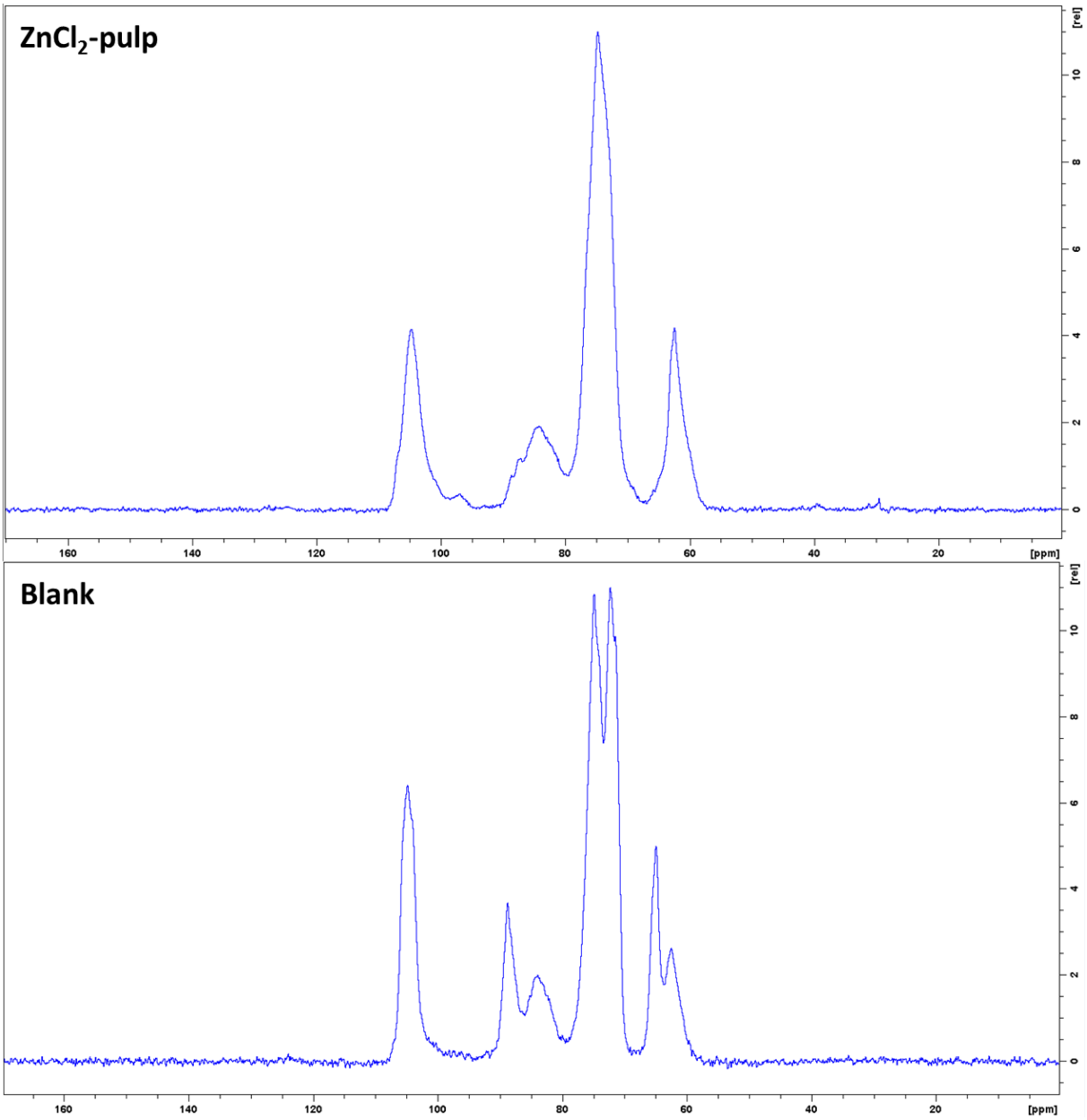

Figure 4.3: ^{13}C Solid-state NMR spectra of $ZnCl_2$-pulp and blank.

The IR spectrum in Figure 4.2A shows clearly that the crystal structure of the fiber was affected by the $ZnCl_2$-treatment and the characteristic cellulose II bands are highlighted [42]. In addition, the OH-stretching bands in between 3600 cm^{-1} and 3000 cm^{-1} and the band at 1600 cm^{-1} related to the adsorbed water on the cellulose fiber, are more pronounced in $ZnCl_2$-pulp. This indicates that the treated samples feature a more accessible structure. More detailed examination of the crystalline structure with solid-state NMR (Figure 4.3 and Table 4.1) showed that the more pronounced water interaction is primarily caused by partial amorphization of the cellulose structure. The crystallinity was significantly

reduced from 47% to only 20%; the resulting crystallites interestingly being a cellulose I/cellulose II mix. This is in contrast to recent publications, which did not show any effect on the crystal structure, although using a short treatment of cellulose with 65 wt% $ZnCl_2$ solution [21]. With regard to allomorph transition, the treatment time seems to be crucial; and our prolonged treatment enabled $ZnCl_2$ interactions not only with cellulose chains in accessible, but also non-accessible, crystalline cellulose regions. Similar observations were made upon $ZnCl_2$-treatments of cotton fibers, which showed that the effect of $ZnCl_2$ on the crystal structure is rather slow in comparison to sodium hydroxide treatments and hence strongly dependent on the impregnation time [43]. The $ZnCl_2$ interaction with the cellulose's hydroxyl groups break the inter- and intra-chain hydrogen bonds [44], resulting in a more accessible (amorphous) cellulose structure of the $ZnCl_2$-treated samples. The fact that remaining crystalline regions after the treatment are both of cellulose I and II indicates that a process similar to the mercerization with NaOH occurs as well with $ZnCl_2$, and similar to NaOH aqueous 65 wt% $ZnCl_2$ solution is not able to solubilize cellulose [25]. Although the changes on the crystalline cellulose structure are rather severe, the molar mass distribution of cellulose is hardly affected by the treatment. This was shown by gel permeation chromatography; the so-obtained molar mass distribution is shown in Figure 4.2B. The weight-averaged molar mass is not influenced by the treatment, but it seems that the low-molar mass fraction (mostly associated with hemicelluloses) is slightly degraded or lost by the treatment. This hemicellulose-specific $ZnCl_2$-mediated degradation has been reported in the literature [45]. As the hemicellulose content of the pulp used in this work was 3.7% [37], this is also approximately the mass loss experienced by $ZnCl_2$ treatment and subsequent washing. The amount of $ZnCl_2$ in the samples ($ZnCl_2$-pulp and $ZnCl_2$-CNF) was approximated to be 20 wt%, by thermogravimetric analysis (Figure 4.4).

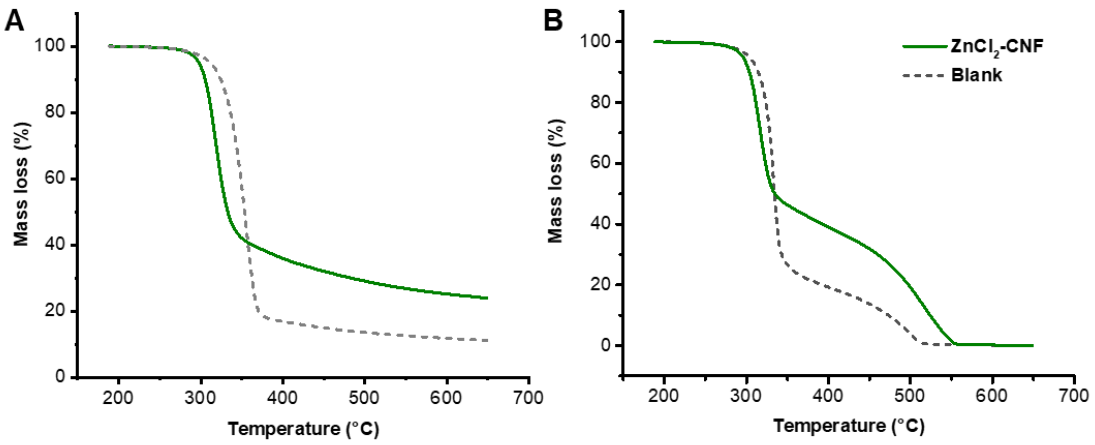

Figure 4.4: Thermal gravimetric analysis in nitrogen atmosphere (A) and oxygen-rich atmosphere (B), weight mass differences at 400 °C can be used to estimate the remaining $ZnCl_2$ in the sample. The onset temperature for the thermal degradation of the $ZnCl_2$-containing sample experiences a minor decrease compared to the cellulose blank sample, which is in accordance with similar results by other authors [25]. $ZnCl_2$ vaporizes above 400 °C in oxygen-rich atmosphere [46], which we observed as well (B).

$ZnCl_2$-pulp was homogenized to obtain a stable dispersion of cellulose nanofibers ($ZnCl_2$-CNF). After the homogenization, the $ZnCl_2$-CNF featured an increased viscosity and a more pronounced shear-thinning effect (Figure 4.5F). As the viscosity depends on the aspect-ratio, a higher degree of fibrillation causes higher viscosity [47,48]. This proved that the $ZnCl_2$-treatment significantly increased the fibrillation tendency of the cellulose fiber. This is also clearly shown in the SEM and light microscopy images (Figure 4.5). $ZnCl_2$-CNF was well fibrillated into a nanofibrous structure, whereas the blank was only partially fibrillated and contained intact fiber residues. The fiber diameter also affects the optical properties of CNF films and explains the higher transparency of the $ZnCl_2$-CNF in comparison to the blank, shown in the insets of Figure 4.5D. The fibrillar morphology of $ZnCl_2$-CNF stays in contrast to spherical cellulose II nanocelluloses extracted from previously dissolved cellulose fibers [34,49–51].

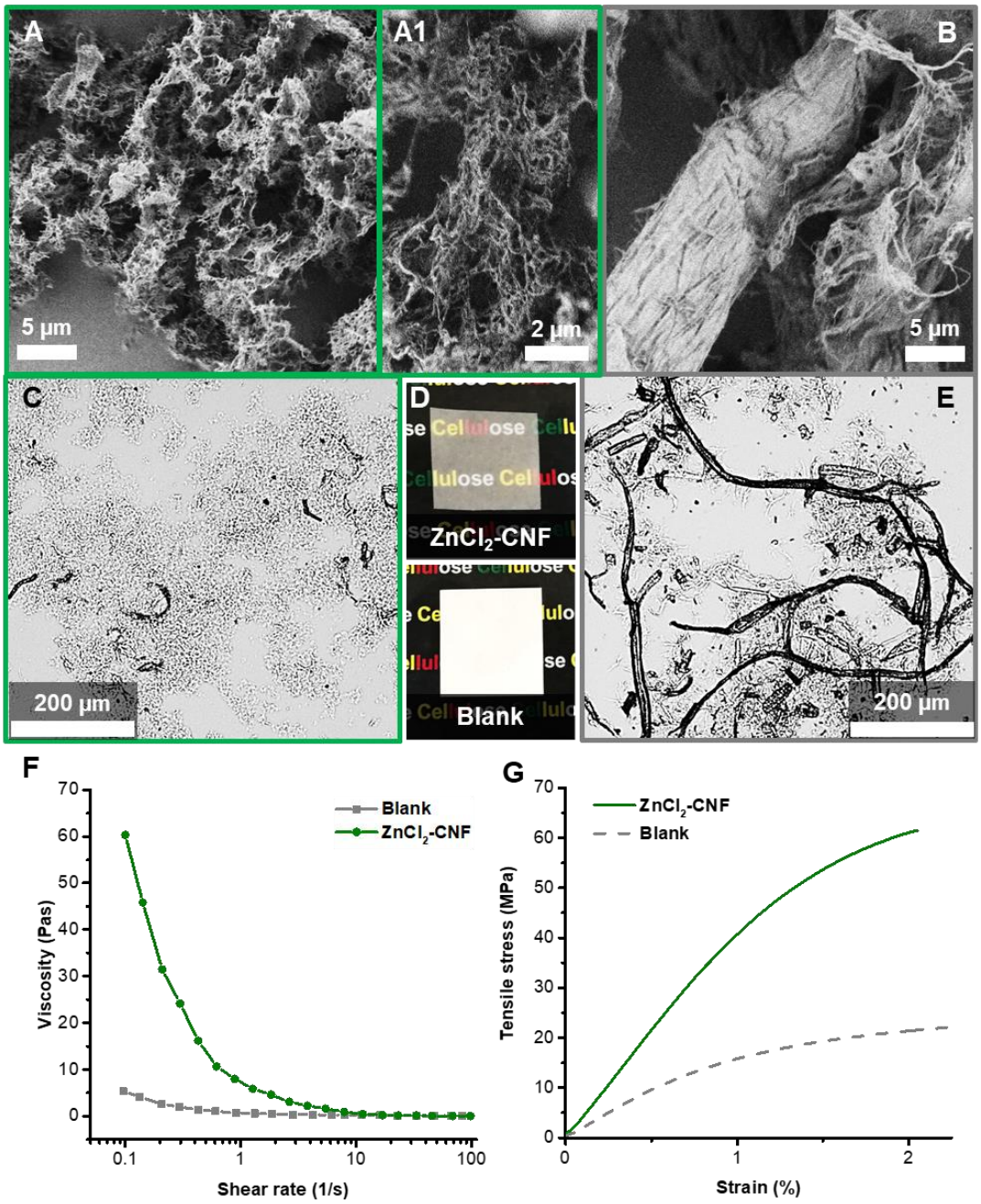

Figure 4.5: $ZnCl_2$-treatment significantly increased the fibrillation tendency of the cellulose fibers. Scanning electron microscopy images (A, A1, B) and light microscopy images (C,E). The films (D) made from $ZnCl_2$-CNF are more transparent due to its mostly nanosized fibrous structure than the paper-like films from the non-$ZnCl_2$-treated, homogenized blank sample (note that both samples were homogenized with the same processing time and energy input). The higher fibrillation degree accounts as well for the higher viscosity (F), the stronger shear-thinning effect and the higher tensile strength (G) of $ZnCl_2$-CNF.

Table 4.1: Effect of $ZnCl_2$-treatment on crystal structure and mechanical properties of the produced films in comparison to non-treated cellulose. Crystalline structure and crystallinity indices were investigated with solid-state ^{13}C NMR spectroscopy.

	Cellulose allomorph	Crystallinity	Young's Modulus (MPa)	Tensile Strength (MPa)
$ZnCl_2$	Cellulose I/II	20 %	4296 ± 533	61 ± 6
Blank	Cellulose I	47 %	1945 ± 118	24 ± 2

Tensile strength and Young's modulus were measured from films of $ZnCl_2$-CNF in comparison to those of a homogenized blank sample (Figure 4.5G and Table 4.1). It was obvious that both tensile strength and young modulus increased more than twofold through the $ZnCl_2$-treatment, namely to 61 MPa and 4.3 GPa, respectively. This remarkable increase is a result of the higher fibrillation degree of the $ZnCl_2$-treated sample. The mechanical properties of $ZnCl_2$-CNF films are in the lower range of CNF literature values [52–54], which is likely due to the low crystallinity of the $ZnCl_2$-treated samples.

4.3.3. Additional functionality of cellulose nanofibers

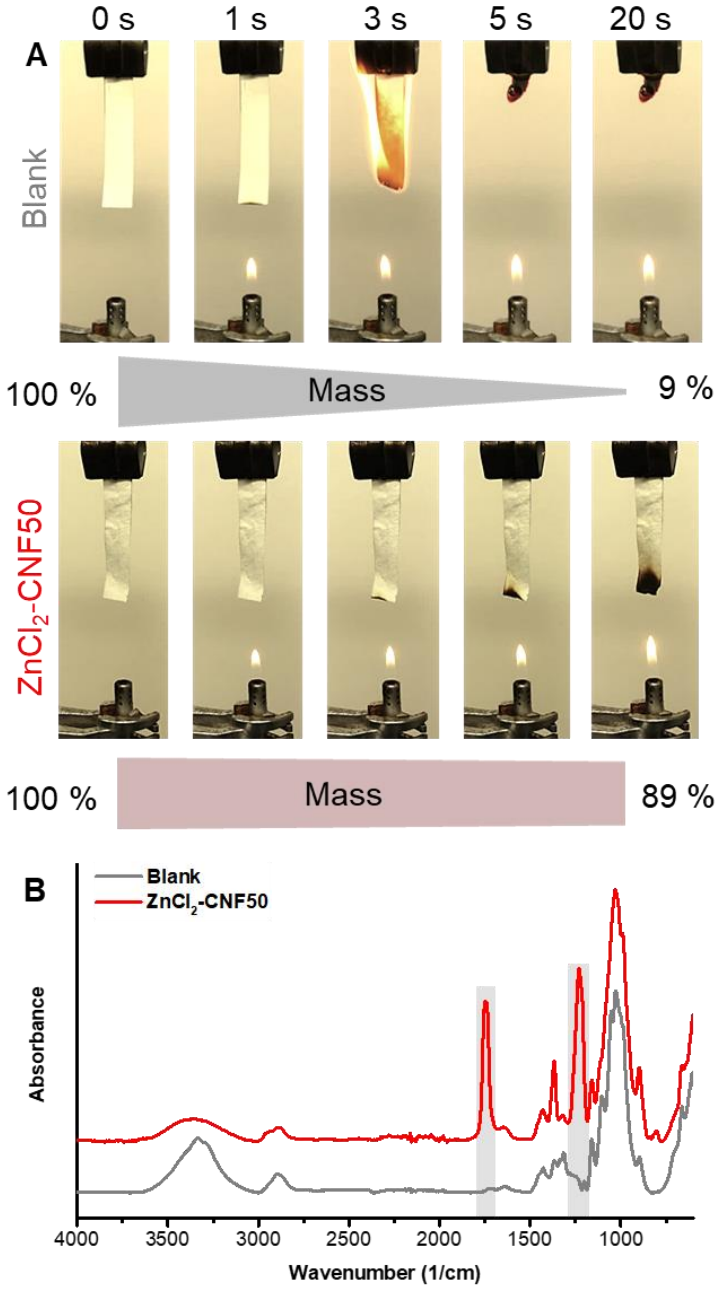

Figure 4.6: The fire-retardant properties of the $ZnCl_2$-treated cellulose nanofibres are demonstrated by a flammability test (A) of $ZnCl_2$-CNF-h (containing 33 wt% $ZnCl_2$) in comparison to the non-$ZnCl_2$-treated blank papers (7.4 cm x 1.5 cm specimen). $ZnCl_2$-CNF featured a 10 times higher residual mass than the blank. The IR spectra (B) prove the catalytic activity of $ZnCl_2$-CNF-h treated with acetic anhydride. Characteristic acetyl group-related bands are indicated in the IR spectrum and show a distinctly higher degree of acetylation of the $ZnCl_2$ sample compared to the blank.

$ZnCl_2$-CNF with a higher $ZnCl_2$ content of 33 wt% ($ZnCl_2$-CNF-h) was prepared and used to identify the functional properties of the $ZnCl_2$-loaded nanocellulose. As shown in the flammability test in Figure 4.6A, non-$ZnCl_2$-treated CNF almost completely combusted under test conditions (mass loss > 90 wt%). Although, $ZnCl_2$ shifted the onset temperature of the combustion to slightly lower temperatures (Figure 4.4A), the sample $ZnCl_2$-CNF-h was only little affected under the flammability test conditions, with only 10 wt% mass loss after the test. We performed a test with the $ZnCl_2$-CNF sample (with 20 wt% $ZnCl_2$) as well, at this lower salt content, combustion of the sample occurred but was delayed, and we noticed an increased char formation (Figure 4.7).

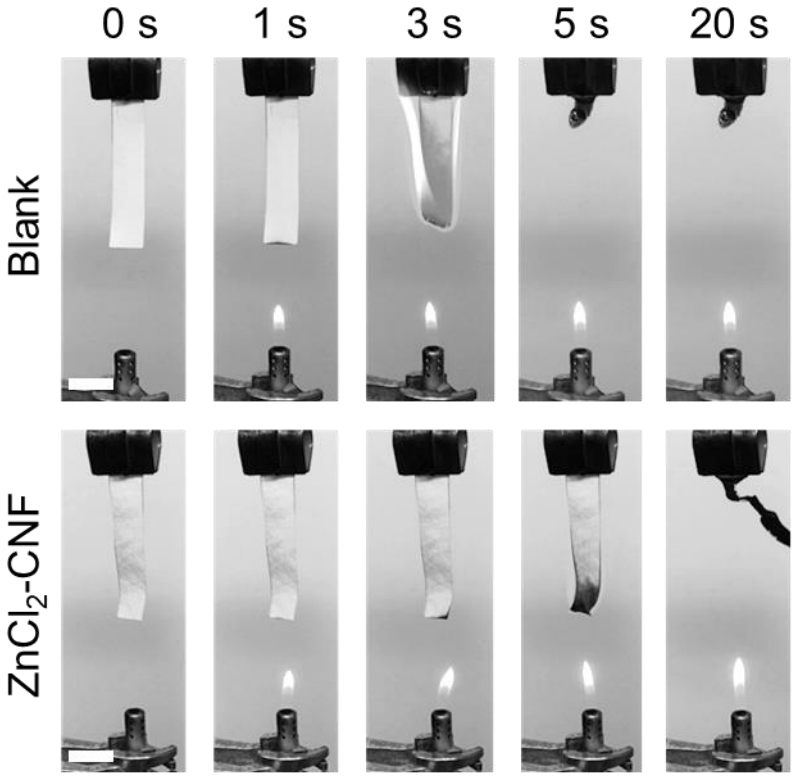

Figure 4.7: Flammability test of $ZnCl_2$-CNF in comparison to the blank sample, the combustion of the sample is delayed in the former and a higher char formation is noticed. The remaining sample mass was 37 % and 9 % in the case of $ZnCl_2$-CNF and blank, respectively.

$ZnCl_2$-CNF showed a catalytic activity in esterification reactions due to the $ZnCl_2$ located at the fiber surface, which due to its Lewis-acid character caused

increased acetylation efficiency in a test reaction with acetic anhydride, as proven by the pronounced acetyl group-related bands (C=O at 1744 cm^{-1} and C-O band at 1229 cm^{-1}) [55] in the IR spectrum in Figure 4.6B. The reference was acetylated only to a hardly traceable degree.

4.4. Conclusion

An easy, environmentally friendly and energy-saving method for processing cellulose pulp into nanocellulose has been established. Cellulose samples were pretreated with a readily recyclable, aqueous 65 wt% $ZnCl_2$ solution, which swells the fiber structure by ballooning. Although the molar mass of the treated cellulose was very little affected, there were significant changes in the cellulose´s crystal structure. After a 16 h treatment, the crystallinity was reduced to 20 % and solid-state NMR showed the remaining crystallites to be of both cellulose I and cellulose II allomorph. The treatment thus effected a partial phase transition from cellulose allomorph I into II. Rheology measurements and SEM showed that the $ZnCl_2$-treatment strongly augmented the fibrillation tendency allowing for an energy-saving CNF production. The obtained CNF was processed into translucent films with an elastic modulus of 4.3 GPa. Remaining $ZnCl_2$ in the samples introduced fire retardant properties as demonstrated by flammability tests. Surface acetylation in the $ZnCl_2$-CNF was pronouncedly increased compared to the blank counterpart. Possible antimicrobial and antifungal properties the $ZnCl_2$-treated specimens can be deduced from established knowledge but have not been tested for our samples. A beneficial effect in preventing growth of bacterial and fungi during CNF storage can be reasonably expected.

In summary, we would like to promote the usage of the $ZnCl_2$-method for cellulose nanofiber production, since it allows not only for increased energy-efficiency but can be simultaneously used to yield materials with special properties that are otherwise achieved not that conveniently.

4.5. Supporting Information

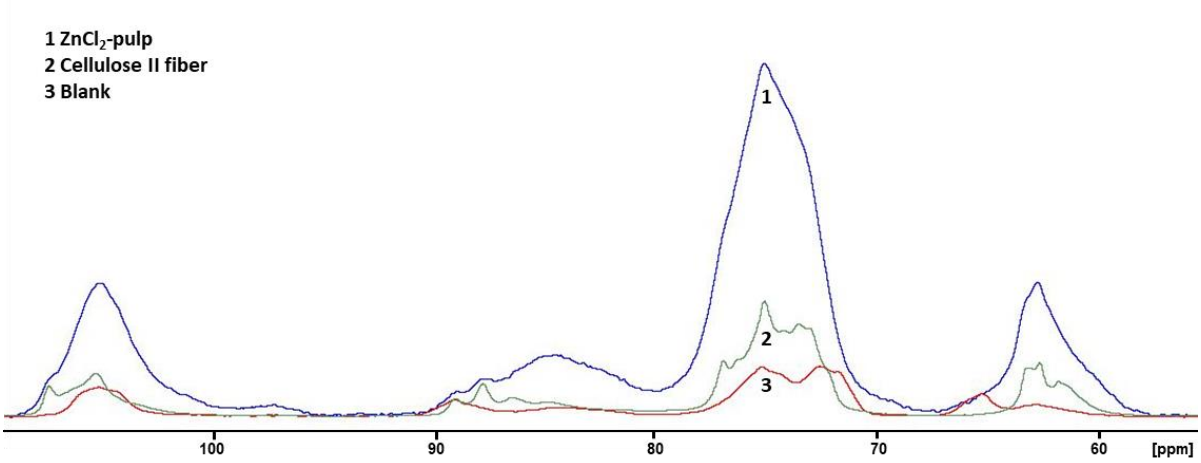

Figure S4.1: ^{13}C Solid state NMR Comparison of $ZnCl_2$-pulp in comparison to a cellulose II fiber and the blank sample. Characteristic peaks of cellulose I and cellulose II allomorph in C4 peak region (80-92 ppm) and C6 region (58-68 ppm) were used to approximate the allomorph ratio.

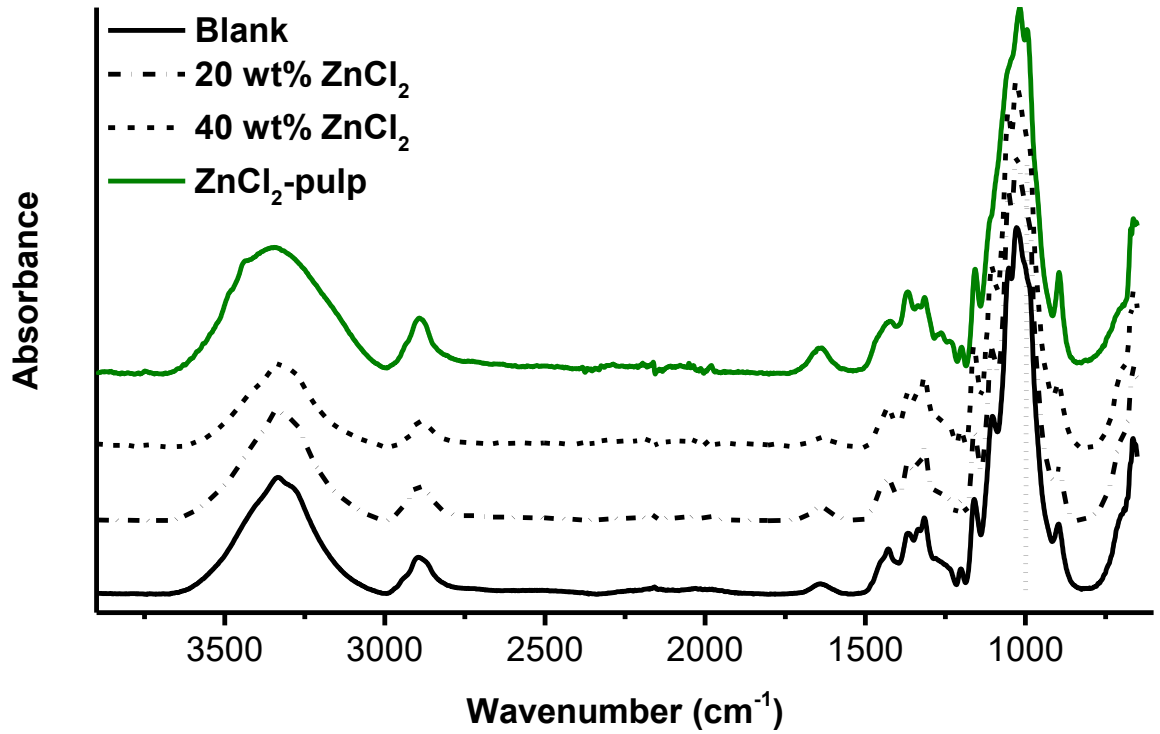

Figure S4.2: Comparison of IR spectra of samples from different $ZnCl_2$-treatments and blank sample. Structural changes were only observed at 65 wt% $ZnCl_2$ ($ZnCl_2$-pulp). This agrees with observations made in GPC analyses and tensile tests (data not included).

4.6. References

1. Abdul Khalil, H.; Davoudpour, Y.; Islam, M.N.; Mustapha, A.; Sudesh, K.; Dungani, R.; Jawaid, M. Production and modification of nanofibrillated cellulose using various mechanical processes: A review. Carbohydrate Polymers 2014, 99, 649–665, doi:10.1016/j.carbpol.2013.08.069.

2. Nagasawa T. The Promise of Cellulose Nanofibers. http://www.nippon.com/en/genre/economy/l00151/ (accessed on accessed on 16 December 2020).

3. Nagata K. Japan pins tech hopes on game-changing nanofiber. http://www.japantimes.co.jp/news/2016/04/11/business/tech/japan-pins-tech-hopes-game-changing-nanofiber/ (accessed on accessed on 16 December 2020).

4. Sanchez, P.C. Philippine fermented foods. Principles and technology; University of the Philippines Press: Diliman, Quezon City, 2008, ISBN 9789715425544.

5. Eichhorn, S.J.; Dufresne, A.; Aranguren, M.; Marcovich, N.E.; Capadona, J.R.; Rowan, S.J.; Weder, C.; Thielemans, W.; Roman, M.; Renneckar, S.; et al. Review: current international research into cellulose nanofibres and nanocomposites. J Mater Sci 2010, 45, 1–33, doi:10.1007/s10853-009-3874-0.

6. an Nakagaito; Kondo, H.; Takagi, H. Cellulose nanofiber aerogel production and applications. Journal of Reinforced Plastics and Composites 2013, 32, 1547–1552, doi:10.1177/0731684413494110.

7. Habibi, Y.; Lucia, L.A.; Rojas, O.J. Cellulose nanocrystals: chemistry, self-assembly, and applications. Chem. Rev. 2010, 110, 3479–3500, doi:10.1021/cr900339w.

8. Ferreira, F.V.; Souza, L.P.; Martins, T.M.M.; Lopes, J.H.; Mattos, B.D.; Mariano, M.; Pinheiro, I.F.; Valverde, T.M.; Livi, S.; Camilli, J.A.; et al. Nanocellulose/bioactive glass cryogels as scaffolds for bone regeneration. Nanoscale 2019, 11, 19842–19849, doi:10.1039/C9NR05383B.

9. Osorio, D.A.; Lee, B.E.J.; Kwiecien, J.M.; Wang, X.; Shahid, I.; Hurley, A.L.; Cranston, E.D.; Grandfield, K. Cross-linked cellulose nanocrystal aerogels

as viable bone tissue scaffolds. Acta Biomater. 2019, 87, 152–165, doi:10.1016/j.actbio.2019.01.049.

10. Ferreira, F.V.; Otoni, C.G.; France, K.J. de; Barud, H.S.; Lona, L.M.; Cranston, E.D.; Rojas, O.J. Porous nanocellulose gels and foams: Breakthrough status in the development of scaffolds for tissue engineering. Materials Today 2020, 37, 126–141, doi:10.1016/j.mattod.2020.03.003.

11. Henriksson, M.; Henriksson, G.; Berglund, L.A.; Lindström, T. An environmentally friendly method for enzyme-assisted preparation of microfibrillated cellulose (MFC) nanofibers. European Polymer Journal 2007, 43, 3434–3441, doi:10.1016/j.eurpolymj.2007.05.038.

12. V.S. Chauhan, S.C. Use of nanotechnology for high performance cellulosic and papermaking products. Cellulose Chemistry and Technology 2012, 46, 389–400.

13. M. Szczesna-Antczak, J. Kazimierczak, T. Antczak. Nanotechnology - Methods of Manufacturing Cellulose Nanofibres. Fiber and Textile in Eastern Europe 2012, 20, 8–12.

14. Fischer, S.; Leipner, H.; Thümmler, K.; Brendler, E.; Peters, J. Inorganic molten salts as solvents for cellulose: Inorganic molten salts as solvents for cellulose. Cellulose 2003, 10, 227–236, doi:10.1023/a:1025128028462.

15. Sen, S.; Martin, J.D.; Argyropoulos, D.S. Review of Cellulose Non-Derivatizing Solvent Interactions with Emphasis on Activity in Inorganic Molten Salt Hydrates. ACS Sustainable Chem. Eng. 2013, 1, 858–870, doi:10.1021/sc400085a.

16. Cellulose Solvents: For Analysis, Shaping and Chemical Modification.; Liebert, T.F.; Heinze, T.J.; Edgar, K.J.; Liebert, T.; Heinze, T., Eds.; American Chemical Society: Washington, DC, 2010, ISBN 9780841200067.

17. de Almeida, R.M.; Li, J.; Nederlof, C.; O'Connor, P.; Makkee, M.; Moulijn, J.A. Cellulose Conversion to Isosorbide in Molten Salt hydrate Media. ChemSusChem 2010, 3, 325–328, doi:10.1002/cssc.200900260.

18. Abbott, A.P.; Bell, T.J.; Handa, S.; Stoddart, B. O-Acetylation of cellulose and monosaccharides using a zinc based ionic liquid. Green Chem. 2005, 7, 705–707, doi:10.1039/b511691k.

19. Solhy, A.; Clark, J.H.; Tahir, R.; Sebti, S.; Larzek, M. Transesterifications catalysed by solid, reusable apatite–zinc chloride catalysts. Green Chem 2006, 8, 871–874, doi:10.1039/B605835N.

20. National Center for Biotechnology Information. PubChem Database. Zinc chloride, CID=5727. https://pubchem.ncbi.nlm.nih.gov/compound/Zinc-chloride (accessed on 11 May 2020).

21. Nemoto, J.; Fukushima, S.; Kobayashi, A.; Tagawa, M.; Saito, T.; Isogai, A. All-cellulose Materials Adhered with Cellulose Nanofibrils. JAPAN TAPPI JOURNAL 2018, 72, 1050–1058, doi:10.2524/jtappij.72.1050.

22. Cao, N.-J.; Xu, Q.; Chen, C.-S.; Gong, C.S.; Chen, L.F. Cellulose hydrolysis using zinc chloride as a solvent and catalyst. Appl Biochem Biotechnol 1994, 45-46, 521–530, doi:10.1007/BF02941827.

23. Bi, Z.; Lai, B.; Zhao, Y.; Yan, L. Fast Disassembly of Lignocellulosic Biomass to Lignin and Sugars by Molten Salt Hydrate at Low Temperature for Overall Biorefinery. ACS Omega 2018, 3, 2984–2993, doi:10.1021/acsomega.8b00057.

24. Lu, X.; Shen, X. Solubility of bacteria cellulose in zinc chloride aqueous solutions. Carbohydrate Polymers 2011, 86, 239–244, doi:10.1016/j.carbpol.2011.04.042.

25. Sen, S.; Losey, B.P.; Gordon, E.E.; Argyropoulos, D.S.; Martin, J.D. Ionic Liquid Character of Zinc Chloride Hydrates Define Solvent Characteristics that Afford the Solubility of Cellulose. J. Phys. Chem. B 2016, 120, 1134–1141, doi:10.1021/acs.jpcb.5b11400.

26. Pandey, S.N.; Nair, P. Studies on chemically modified cotton. V. Effect of zinc chloride solutions on swelling and other properties of cotton. J. Appl. Polym. Sci. 1976, 20, 525–542, doi:10.1002/app.1976.070200223.

27. Modi, J.R.; Trivedi, S.S.; Mehta, P.C. Heterogeneous hydrolysis of cotton cellulose treated with different swelling agents. J. Appl. Polym. Sci. 1963, 7, 15–26, doi:10.1002/app.1963.070070102.

28. LEVAN, S.L. Chemistry of Fire Retardancy. In The Chemistry of Solid Wood; Rowell, R., Ed.; American Chemical Society: Washington, DC, 1984; pp 531–574, ISBN 0-8412-0796-8.

29. United Staes Environmental Protection Agency. EPA R.E.D. FACTS: Zinc salts. https://archive.epa.gov/pesticides/reregistration/web/pdf/zinc_salt.pdf (accessed on 2020).

30. Bautista-Gallego, J.; Arroyo-López, F.N.; Romero-Gil, V.; Rodríguez-Gómez, F.; Garrido-Fernández, A. Evaluating the effects of zinc chloride as a preservative in cracked table olive packing. J. Food Prot. 2011, 74, 2169–2176, doi:10.4315/0362-028X.JFP-11-201.

31. Gu, H.; Fan, D.; Gao, J.; Zou, W.; Peng, Z.; Zhao, Z.; Ling, J.; LeGeros, R.Z. Effect of ZnCl2 on plaque growth and biofilm vitality. Arch. Oral Biol. 2012, 57, 369–375, doi:10.1016/j.archoralbio.2011.10.001.

32. LISTERINE. Share LISTERINE® ULTRACLEAN® ARCTIC MINT® Antiseptic Mouthwash. https://www.listerine.com/mouthwash/listerine-ultraclean-arctic-mint-antiseptic-mouthwash (accessed on 11 May 2020).

33. Zhang, X.-F.; Ma, X.; Hou, T.; Guo, K.; Yin, J.; Wang, Z.; Shu, L.; He, M.; Yao, J. Inorganic Salts Induce Thermally Reversible and Anti‐Freezing Cellulose Hydrogels. Angew. Chem. 2019, 131, 7444 – 7448, doi:10.1002/ange.201902578.

34. Beaumont, M.; Rennhofer, H.; Opietnik, M.; Lichtenegger, H.C.; Potthast, A.; Rosenau, T. Nanostructured Cellulose II Gel Consisting of Spherical Particles. ACS Sustainable Chem. Eng. 2016, 4, 4424–4432, doi:10.1021/acssuschemeng.6b01036.

35. Park, S.; Baker, J.O.; Himmel, M.E.; Parilla, P.A.; Johnson, D.K. Cellulose crystallinity index: measurement techniques and their impact on interpreting

cellulase performance. Biotechnol. Biofuels 2010, 3, 10, doi:10.1186/1754-6834-3-10.

36. Maunu, S.; Liitiä, T.; Kauliomäki, S.; HORTLING, B.O.; SUNDQUIST, J. 13C CPMAS NMR investigations of cellulose polymorphs in different pulps. Cellulose 2000, 7, 147–159, doi:10.1023/A:1009200609482.

37. Sixta, H. Pulp Properties and Applications. In Handbook of Pulp; Sixta, H., Ed.; Wiley-VCH Verlag GmbH: Weinheim, Germany, 2006; pp 1009–1067, ISBN 9783527619887.

38. Hettegger, H.; Beaumont, M.; Potthast, A.; Rosenau, T. Aqueous Modification of Nano- and Microfibrillar Cellulose with a Click Synthon. ChemSusChem 2016, 9, 75–79, doi:10.1002/cssc.201501358.

39. Beaumont, M.; Bacher, M.; Opietnik, M.; Gindl-Altmutter, W.; Potthast, A.; Rosenau, T. A General Aqueous Silanization Protocol to Introduce Vinyl, Mercapto or Azido Functionalities onto Cellulose Fibers and Nanocelluloses. Molecules 2018, 23, doi:10.3390/molecules23061427.

40. Iwamoto, S.; Abe, K.; Yano, H. The effect of hemicelluloses on wood pulp nanofibrillation and nanofiber network characteristics. Biomacromolecules 2008, 9, 1022–1026, doi:10.1021/bm701157n.

41. Beaumont, M.; König, J.; Opietnik, M.; Potthast, A.; Rosenau, T. Drying of a cellulose II gel: effect of physical modification and redispersibility in water. Cellulose 2017, 24, 1199–1209, doi:10.1007/s10570-016-1166-9.

42. Hishikawa, Y.; Togawa, E.; Kondo, T. Characterization of Individual Hydrogen Bonds in Crystalline Regenerated Cellulose Using Resolved Polarized FTIR Spectra. ACS Omega 2017, 2, 1469–1476, doi:10.1021/acsomega.6b00364.

43. N. B. Patil, N. E. Dweltz. Studies on Decrystallization of Cotton. Textile Research Journal 1965, 35, 517–523, doi:10.1177/004051756503500605.

44. Rosenau, T.; Potthast, A.; Hofinger, A.; Bacher, M.; Yoneda, Y.; Mereiter, K.; Nakatsubo, F.; Jäger, C.; French, A.D.; Kajiwara, K. Toward a Better

Understanding of Cellulose Swelling, Dissolution, and Regeneration on the Molecular Level. In Cellulose Science and Technology; Rosenau, T., Potthast, A., Hell, J., Eds.; John Wiley & Sons, Inc: Hoboken, NJ, USA, 2018; pp 99–125, ISBN 9781119217619.

45. Cao, N.J.; Xu, Q.; Chen, L.F. Xylan hydrolysis in zinc chloride solution. Applied Biochemistry and Biotechnology 1995, 51, 97–104, doi:10.1007/BF02933414.

46. Jones, F.; Tran, H.; Lindberg, D.; Zhao, L.; Hupa, M. Thermal Stability of Zinc Compounds. Energy Fuels 2013, 27, 5663–5669, doi:10.1021/ef400505u.

47. Rezayati Charani, P.; Dehghani-Firouzabadi, M.; Afra, E.; Shakeri, A. Rheological characterization of high concentrated MFC gel from kenaf unbleached pulp. Cellulose 2013, 20, 727–740, doi:10.1007/s10570-013-9862-1.

48. Pääkkö, M.; Ankerfors, M.; Kosonen, H.; Nykänen, A.; Ahola, S.; Österberg, M.; Ruokolainen, J.; Laine, J.; Larsson, P.T.; Ikkala, O.; et al. Enzymatic Hydrolysis Combined with Mechanical Shearing and High-Pressure Homogenization for Nanoscale Cellulose Fibrils and Strong Gels. Biomacromolecules 2007, 8, 1934–1941, doi:10.1021/bm061215p.

49. Beaumont, M.; Nypelö, T.; König, J.; Zirbs, R.; Opietnik, M.; Potthast, A.; Rosenau, T. Synthesis of redispersible spherical cellulose II nanoparticles decorated with carboxylate groups. Green Chem 2016, 18, 1465–1468, doi:10.1039/C5GC03031E.

50. Beaumont, M.; Rosenfeldt, S.; Tardy, B.L.; Gusenbauer, C.; Khakalo, A.; Nonappa; Opietnik, M.; Potthast, A.; Rojas, O.J.; Rosenau, T. Soft cellulose II nanospheres: sol-gel behaviour, swelling and material synthesis. Nanoscale 2019, 11, 17773–17781, doi:10.1039/C9NR05309C.

51. Wang, H.-Q.; Tan, H.; Hua, S.; Liu, Z.-Y.; Yang, W.; Yang, M.-B. High Efficiency Conversion of Regenerated Cellulose Hydrogel Directly to Functionalized Cellulose Nanoparticles. Macromol. Rapid Commun. 2017, 38, doi:10.1002/marc.201700409.

52. Spence, K.L.; Venditti, R.A.; Rojas, O.J.; Habibi, Y.; Pawlak, J.J. A comparative study of energy consumption and physical properties of microfibrillated cellulose produced by different processing methods. Cellulose 2011, 18, 1097–1111, doi:10.1007/s10570-011-9533-z.

53. Zimmermann, T.; Bordeanu, N.; Strub, E. Properties of nanofibrillated cellulose from different raw materials and its reinforcement potential. Carbohydrate Polymers 2010, 79, 1086–1093, doi:10.1016/j.carbpol.2009.10.045.

54. Prakobna, K.; Galland, S.; Berglund, L.A. High-performance and moisture-stable cellulose-starch nanocomposites based on bioinspired core-shell nanofibers. Biomacromolecules 2015, 16, 904–912, doi:10.1021/bm5018194.

55. Tserki, V.; Panayiotou, C.; Zafeiropoulos, N.E. A Study of the Effect of Acetylation and Propionylation on the Interface of Natural Fibre Biodegradable Composites. Advanced Composites Letters 2005, 14, 65-71, doi:10.1177/096369350501400202.

5. Chapter
Conclusion

5. Chapter – Conclusion

Nowadays the use of autografts, allografts and BMPs to treat atrophic or hypothrophic bone non-unions is common. However, unfortunately these methods have several drawbacks: While autografts show the best performance of bone growth in non-unions, their harvest is quite problematic as significant donor site morbidity ensues, which may lead to chronic pain and even sensory loss at the donor site. Allografts are easier to acquire and even though they are not osteogenic because of decellularization, they retain a certain degree of osteoinductivity and offer a very good osteoconductive template. Regrettably, they carry a high infection risk of 5% to 12.2%, which poses a danger, particularly to elderly patients. BMPs are an elegant solution to promoting bone growth in non-unions, but as pharmaceuticals, they are only admitted for select procedures, which strongly limits their application. Widely applicable, safe alternatives to the current methods are needed. For this reason the aim of this dissertation was the innovation of silk fibroin based bone tissue engineering scaffold materials for use as alternatives to autografts and allografts.

As described in the second chapter, SF/cellulose hydrogels with a defined porous structure were successfully developed by a new approach that uses a binary solution of predissolved degummed SF and cellulose in DMAc/LiCl and NaCl powder as a porogen. The pore size and the porosity of the SF/cellulose hydrogels were 340 µm to 370 µm and 73% to 74%, respectively. They did not change with the cellulose contents in the hydrogels. The presence of cellulose improved the mechanical stiffness and strength of the SF material. The sequential regeneration favors the formation of a reinforcing cellulose framework, regenerated first by atmospheric humidity, upon which, in a second step, SF is assembled by the action of methanol as the antisolvent. This causes the formation of a reinforcing cellulose framework structure embedded in a SF matrix. In surface-near layers, the secondary structure of SF in the hydrogels assumed abundant β-sheet conformation, whereas deeper layers of the scaffold show decreased β-sheet contents. As *in vivo* SF degradation inversely scales with β-sheet content, this offers great potential for resorption of the material upon sufficient bone regeneration by the body. The cellulose framework/SF matrix structure maximized material dependent improvement of hydrogel properties, as

the cellulose framework mainly contributed to mechanical property enhancement, while the SF matrix supported cell growth. Osteocyte differentiation of MC3T3-E1 cells cultured on the hydrogels was observed. Even more, the good differentiation properties of SF materials were not impaired by the incorporation of cellulose, and the osteocyte differentiation was accelerated compared to other SF substrates. These results show SF/cellulose hydrogels to be a suitable scaffold for BTE.

An important reason that contributes to the bone healing results achieved by autografts is the presence of growth factors that are endogenous to bone tissue. The project described in the third chapter aimed at making a recombinant SF based scaffold material with the ability to release basic fibroblast growth factor (bFGF) and thereby imitate natural bone tissue. In the project a novel recombinant SF with the ability to specifically bind bFGF was successfully prepared. This has great potential for therapeutic application, as SF matrices can be designed to be loadable with bFGF in desirable amounts for timed release. As the SF matrix supplies bound bFGF, the growth factor would be able to elicit its effect to cells in direct proximity immediately upon release. Further bound bFGF is expected to be stable for a longer period of time than free bFGF. Addition of the recombinant SF to scaffolds for tissue engineering would allow a tailorable supply of bFGF for tissue regeneration.

In another approach for making SF/cellulose composites for BTE, both materials were dissolved in $ZnCl_2$ hydrate solution. While this process yielded cellulose fibers of a very small size upon precipitation of cellulose, the method was not adequate for making composites. Upon further investigation of the small, fibrous cellulose obtained and as the application of nanocellulose for BTE has already been investigated, the previous research goal was adjusted to improve the production process of cellulose nanofibers and thereby promote their application for BTE and in general. By taking advantage of the constitution of the $ZnCl_2$-treated cellulose fibers, an easy, environmentally friendly and energy-saving method for processing cellulose pulp into nanocellulose has been established. Cellulose samples were pretreated with a readily recyclable, aqueous 65 wt% $ZnCl_2$ solution, which swells the fiber structure by ballooning. Although the molar mass of the treated cellulose was very little affected, there were significant

changes in the cellulose´s crystal structure. After a 16 h treatment, the crystallinity was reduced to 20 % and solid-state NMR showed the remaining crystallites to be of both cellulose I and cellulose II allomorph. The treatment thus effected a partial phase transition from cellulose allomorph I into II. Rheology measurements and SEM showed that the $ZnCl_2$-treatment strongly augmented the fibrillation tendency allowing for an energy-saving cellulose nanofiber (CNF) production. The obtained CNF was processed into translucent films with an elastic modulus of 4.3 GPa. Deliberately retained $ZnCl_2$ in the samples introduced fire retardant properties as demonstrated by flammability tests, and elicited pronouncedly increased surface acetylation compared to the blank counterpart. Possible antimicrobial and antifungal properties of the $ZnCl_2$-treated specimens can be deduced from established knowledge but have not been tested for our samples. A beneficial effect in preventing growth of bacteria and fungi during CNF storage can be reasonably expected. In summary, the usage of the $ZnCl_2$-method for cellulose nanofiber production, allows not only for increased energy-efficiency but simultaneously yields materials with special properties that are otherwise achieved not that conveniently.

Bone restoration in non-unions depends on the mechanical environment, the use of growth factors, mesenchymal stem cells and scaffolds. In this dissertation silk fibroin was strengthened with cellulose for use as scaffold material and genetically modified to allow silk fibroin to supply growth factors. By fulfilling two of the prerequisites for bone restoration, the established methods and materials will hopefully contribute to the substitution of autologous and allogeneic bone grafts with more patient-friendly alternatives.

Acknowledgement

Acknowledgement

I would like to express my deepest gratitude to Professor Yasushi Tamada, who allowed me much freedom in pursuing the research I was interested in and always supported me with his guidance and insight. He also introduced me to Professor Kunihiro Shiomi who gave me the means of conducting research with transgenic silkworms. I am very grateful for his support as the work with transgenic animals was one of my main aspirations when I started my doctoral course.

I want to thank Professor Thomas Rosenau and Dr. Marco Beaumont for hosting me during my academic internship in Vienna, Austria and for their introduction to cellulose and their help and guidance in all cellulose related matters, which was invaluable.

I am thankful to all co-authors of my papers, to the technicians and lab mates that helped me with my experiments, without which this dissertation would have been impossible.

The monetary support of the Global Leader Program for Fiber Renaissance enabled me to focus on my projects, which I am very grateful for. Further, I would like to thank the people in the student and program administration who organized various excursions, factory tours and internships and thereby gave me opportunities to make experiences that I would have not had otherwise.

Finally, I express my thanks to my partner, friends and family who encouraged and supported me throughout my doctoral course and particularly to all the people I met who took the time to guide and direct me through the cultural differences in Japan.